Published OnlineFirst November 18, 2014; DOI: 10.1158/0008-5472.CAN-13-3131

Tumor and Stem Cell Biology

Cancer Research

Contributions to Drug Resistance in Glioblastoma Derived from Malignant Cells in the Sub-Ependymal Zone

Sara G.M. Piccirillo[1], Inmaculada Spiteri[2], Andrea Sottoriva[2,3], Anestis Touloumis[2,4], Suzan Ber[1], Stephen J. Price[5], Richard Heywood[1], Nicola-Jane Francis[6], Karen D. Howarth[7], Vincent P. Collins[8], Ashok R. Venkitaraman[6], Christina Curtis[3], John C. Marioni[4], Simon Tavaré[2], and Colin Watts[1,5]

Abstract

Glioblastoma, the most common and aggressive adult brain tumor, is characterized by extreme phenotypic diversity and treatment failure. Through fluorescence-guided resection, we identified fluorescent tissue in the sub-ependymal zone (SEZ) of patients with glioblastoma. Histologic analysis and genomic characterization revealed that the SEZ harbors malignant cells with tumor-initiating capacity, analogous to cells isolated from the fluorescent tumor mass (T). We observed resistance to supramaximal chemotherapy doses along with differential patterns of drug response between T and SEZ in the same tumor. Our results reveal novel insights into glioblastoma growth dynamics, with implications for understanding and limiting treatment resistance. *Cancer Res; 75(1); 194–202. ©2014 AACR.*

Introduction

The basis of phenotypic diversity and treatment failure in human glioblastoma is poorly understood. Murine models of gliomagenesis point to sub-ependymal neural stem cells (NSC) as a putative cell of origin for astrocytic tumors. The stepwise premalignant loss of tumor suppressors *p53*, *NF1*, and *PTEN* (1, 2) has been shown to lead to the development of an aggressive disease characterized by resistance to genotoxic injury (3).

In addition, stratifying patients using transcriptional profiles derived from a large cohort of glioblastoma single-tumor samples (4) has identified multiple disease subtypes, which may have prognostic significance (5, 6). However, emerging data on genomic intratumor heterogeneity in glioblastoma indicate spatial segregation of genetically distinct clones in the same tumor (7), making the interpretation of single-sample tumor data challenging. Importantly, this may contribute to the pervasive failure of treatment in patients with glioblastoma.

Clinical trials have established that use of a fluorescence biomarker, 5-aminolevulinic acid (5-ALA), can enhance the surgical resection of glioblastoma (8). We have demonstrated the use of 5-ALA in a fluorescence-guided multiple sampling (FGMS) strategy that permits real-time spatially segregated tumor sampling during surgery (7, 9). Combining visible fluorescence with neuroanatomy allows for the objective distinction of the tumor mass T (visible fluorescent). Importantly, a spatially distinct and visibly fluorescent sub-ependymal zone (SEZ) can also be identified in a subset of patients with glioblastoma.

Here, we report an integrated genomic analysis of SEZ and T samples, obtained by FGMS, which reveals that malignant cells in the SEZ contribute to tumor growth. Functional characterization confirms that the SEZ contains tumor-initiating cells (TIC) that can recapitulate the disease in orthotopic patient-derived xenogeneic models in a manner similar to TICs isolated from the corresponding T. TICs in the SEZ contribute to resistance to chemotherapy and show differential patterns of response when compared with T of the same patients.

Materials and Methods

Glioblastoma sample collection

Patient informed consent was obtained through our research clinic (10). Tissue collection protocols were compliant with the UK Human Tissue Act 2004 (HTA Licence ref 12315) and approved by the Local Regional Ethics Committee (LREC ref. 04/Q0108/60). No difference in 5-ALA labeling capacity was observed among patients. See Supplementary Experimental

[1]John van Geest Centre for Brain Repair, Department of Clinical Neurosciences, University of Cambridge, Cambridge, United Kingdom. [2]Cancer Research UK Cambridge Institute, Li Ka Shing Centre, Cambridge, United Kingdom. [3]Department of Preventive Medicine, Keck School of Medicine, University of Southern California, Los Angeles, California. [4]European Bioinformatics Institute (EMBL-EBI), Wellcome Trust Genome Campus, Hinxton, Cambridge, United Kingdom. [5]Division of Neurosurgery, Department of Clinical Neurosciences, University of Cambridge, Addenbrooke's Hospital, Cambridge, United Kingdom. [6]Medical Research Council Cancer Unit, University of Cambridge, Cambridge, United Kingdom. [7]Hutchison/MRC Research Centre and Department of Pathology, University of Cambridge, Cambridge, United Kingdom. [8]Division of Molecular Histopathology, Department of Pathology, University of Cambridge, Addenbrooke's Hospital, Cambridge, United Kingdom.

Note: Supplementary data for this article are available at Cancer Research Online (http://cancerres.aacrjournals.org/).

I. Spiteri and A. Sottoriva contributed equally to this article.

Corresponding Authors: Sara G.M. Piccirillo, University of Cambridge, Forvie Site, Robinson Way, Cambridge CB2 0PY, UK. Phone: 44-1223-334121; Fax: 44-1223-331174; E-mail: sp577@cam.ac.uk; and Colin Watts, cw209@cam.ac.uk

doi: 10.1158/0008-5472.CAN-13-3131

Published OnlineFirst November 18, 2014; DOI: 10.1158/0008-5472.CAN-13-3131

Procedure for details on 5-ALA administration and sample collection.

Quantitative real-time PCR analysis

Total RNA was extracted from T and SEZ tissues using TRIzol (Invitrogen) according to the manufacturer's instructions. RNA was treated with DNase (Qiagen) and cDNA was synthesized from 5 μg of total RNA using Random Primers (Invitrogen), and a Superscript III First-Strand Synthesis System for real-time PCR (RT-PCR; Invitrogen). The RT-PCR for *Nestin*, *Gfap*, *Sox2*, and *MIB1* transcripts was performed using CFX96 RT-PCR (Bio-Rad), RT^2 qPCR Primer Assay and SYBR Green Master Mix (Qiagen) according to the manufacturer's instructions. 18S was used as the housekeeping reference. Relative expression quantification was performed by the $\Delta\Delta C_t$ method. Experiments were performed in triplicate and each experiment was repeated three times.

Cell line derivation and implantation

Cell cultures from T and SEZ of 42 patients were established from patients with glioblastoma undergoing surgery at Addenbrooke's Hospital, Cambridge, in 2010 to 2012. The cells were isolated as described previously (9, 11, 12) and used either uncultured (primary) or propagated *in vitro* for two passages (briefly cultured) in serum-free medium. The U87 cell line was obtained from the ATCC, cultured according to the supplier's recommendations and used just after resuscitation. Tissue collection to establish HFNSCs was approved by the Local Regional Ethics Committee. Cells were established in 2011 and grown in serum-free medium to form neurospheres and used at early passage. All the cell cultures have been tested for *Mycoplasma* contamination by PCR before use. See Supplementary Experimental Procedure for details on cell propagation, immunofluorescence, and *in vivo* experiments.

DNA and RNA extraction

DNA from T and SEZ tissues of 14 patients with glioblastoma was extracted for copy-number analysis using the DNeasy Blood and Tissue Kit (Qiagen). RNA from T and SEZ tissues of 15 patients with glioblastoma was extracted for gene-expression analysis using TRIzol (Invitrogen) and cleaned up using MiniElute columns (Qiagen). See Supplementary Experimental Procedure for details on copy-number and gene-expression analysis. Copy-number results were validated by FISH as described in the Supplementary Experimental Procedure.

Drug treatment assay

Treatment with temozolomide, cisplatin, and cediranib was evaluated using the *in vitro* BrdUrd cell proliferation assay (Millipore). A total of 3×10^3 cells were plated in triplicate per treatment condition. Control wells for temozolomide, cisplatin, and cediranib are shared as these treatments have been applied in the same experiments. One day after plating, the treatment was applied for 3 days. BrdUrd was applied in the final 24 hours of the treatment. Each experiment was repeated three times. See Supplementary Experimental Procedure for details on drug concentration.

MGMT promoter methylation

Analysis of *MGMT* promoter methylation was performed by PCR (13) and by pyrosequencing (14). In brief, DNA was bisulfite converted and subsequently subjected to PCRs using specific primer pairs for the methylated or the modified unmethylated DNA. PCR products were resolved in a 2% agarose gel stained with SybrSafe. See Supplementary Experimental Procedure for further details.

Phylogenetic reconstruction

Multiple spatially separated samples taken from each glioblastoma were collected to reconstruct the phylogenetic relationship between the tumor and the SEZ using copy number profiles and molecular clock analysis. See Supplementary Experimental Procedure for further details.

Statistical analysis

For *in vivo* experiments using Nod/Scid animals, we performed Kaplan–Meier survival analysis using the log-rank test for hypothesis testing.

For drug response analysis using BrdUrd, a one-way ANOVA was performed for each patient.

The *P* values for the pairwise mean comparisons of each treatment with the corresponding control were calculated using the Tukey Honestly Significant Difference test. In the related figures and for each patient, we plotted the normalized mean treatment response using the corresponding mean control as a reference, except in Supplementary Fig. S12, where we normalized to the mean of the 50 μmol/L temozolomide treatment response. The minimum and maximum normalized values are provided to present the dispersion of the normalized data.

Results

SEZ harbors residual disease in patients with glioblastoma

We screened 65 patients with glioblastoma given 5-ALA, and confirmed that visibly fluorescent disease extended to the SEZ in 65% (42/65) of the cases. Multiple samples were obtained from 14 patients. Histologic features of high-grade glioma (15) were detected in SEZ and T of the patients (Fig. 1A; additional two representative glioblastomas are shown in Supplementary Fig. S1A and S1B). SEZ tissue was also used to identify the ependymal layer and confirm correct sampling (Supplementary Fig. S2).

Glioblastoma has been shown to heterogeneously express glial fibrillary acidic protein (Gfap; ref. 16), and consistent with this, we noted high expression of Gfap in SEZ samples compared with matched T samples (Fig. 1B and C top, and Supplementary Fig. S1C). Expression of the precursor marker Nestin was detected both in T and SEZ tissues (Fig. 1B and C middle, and Supplementary Fig. S1C). The SEZ showed increased vascularization in comparison with T, as determined by CD31 expression (Fig. 1B and C, bottom). Weak expression of the neuronal marker Tuj1 was observed in both areas (Supplementary Fig. S1C). One of the histologic hallmarks of glioblastoma is a high proliferative activity (17), and we observed similar numbers of mitotic cells in T and SEZ (MIB1 index 20.5 ± 2.8 and 18.1 ± 1.9, respectively; Supplementary Fig. S1C). The extent of focal necrosis was similar in T and SEZ of the same patients (except for sp40; Supplementary Table S1). Consistent with immunohistochemical analysis, T and SEZ contained similar amounts of tumor tissue (except for sp54; Supplementary Table S1). Together, these data suggest that regulatory mechanisms promoting proliferation and vascularization are common to the T and the SEZ tissues.

To confirm these findings, we performed real-time analysis of gene expression for markers of glial and precursors cells (*Gfap* and

Published OnlineFirst November 18, 2014; DOI: 10.1158/0008-5472.CAN-13-3131

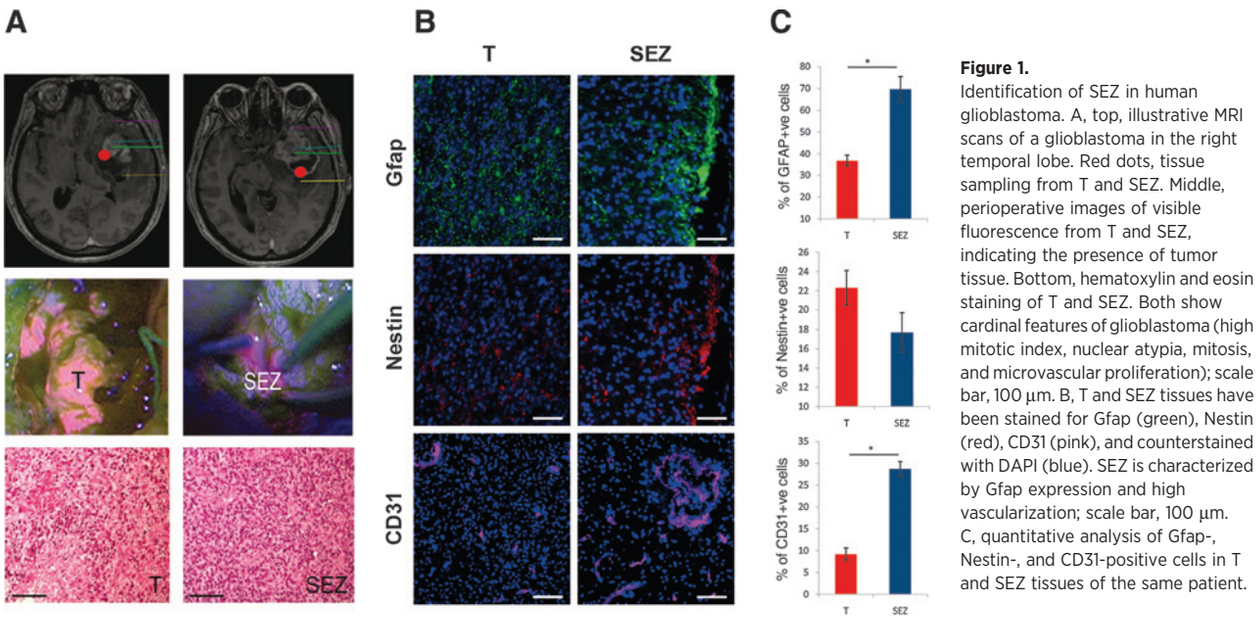

Figure 1.
Identification of SEZ in human glioblastoma. A, top, illustrative MRI scans of a glioblastoma in the right temporal lobe. Red dots, tissue sampling from T and SEZ. Middle, perioperative images of visible fluorescence from T and SEZ, indicating the presence of tumor tissue. Bottom, hematoxylin and eosin staining of T and SEZ. Both show cardinal features of glioblastoma (high mitotic index, nuclear atypia, mitosis, and microvascular proliferation); scale bar, 100 μm. B, T and SEZ tissues have been stained for Gfap (green), Nestin (red), CD31 (pink), and counterstained with DAPI (blue). SEZ is characterized by Gfap expression and high vascularization; scale bar, 100 μm. C, quantitative analysis of Gfap-, Nestin-, and CD31-positive cells in T and SEZ tissues of the same patient.

Nestin), stem cells (*Sox2*), proliferation (*MIB1*) on T and SEZ tissues of three glioblastomas in total (Supplementary Fig. S3). Our results show increased expression of *Gfap* in the SEZ compared with the corresponding T (Supplementary Fig. S3). The expression of *Nestin* and *Sox2* is similar between T and SEZ, except in sp10 for *Sox2* (Supplementary Fig. S3).

We applied high-throughput genomic profiling techniques to the SEZ and T to characterize each of these regions. DNA/RNA were extracted from the tissues of the 14 patients (Supplementary Table S2A). After quality assessment, we analyzed copy-number aberrations (CNA) of 8 patients and gene-expression profiles of 9 patients (6 of whom were common to both analyses; Supplementary Table S2B shows the patient clinical information). Our data reveal multiple aberrations (e.g., *EGFR* amplification and *CDKN2A* deletions) common to T and the corresponding SEZ in individual patients (Fig. 2A and Supplementary Fig. S4). In 6 of 8 patients, the SEZ had an equal or smaller number of putative driver aberrations with respect to the corresponding T (mean difference in the number of aberrations is 1.27 ± 0.38; P value $= 0.12$). CNA results were validated by FISH for three glioblastoma drivers, *EGFR*, *MET*, and *PTEN* (4), in 3 patients with available tissue (Fig. 2B and Supplementary Fig. S5A–S5H). Because we observed *in vitro* aberrations in the corresponding cell cultures (Supplementary Fig. S6), we restricted further genomic analysis to tissue samples.

Clustering of the gene-expression data (18) revealed that only three of nine paired samples (SEZ and T from the same patient) clustered tightly together, whereas five of nine SEZ were assigned to the same subcluster, suggesting a SEZ-specific expression profile across patients (Fig. 2C).

We used a previously published classifier to assign our samples into one of four glioblastoma subtypes (6). Seven of nine SEZ were classified as mesenchymal (sp41, sp42, sp52, sp54, sp56, sp57, and r4), and the remaining two were classical (sp49 and sp55). For 6 of 9 patients, the SEZ was assigned to a different subtype than the corresponding T. T samples were distributed amongst the four subtypes (classical, mesenchymal, neural, and proneural; Fig. 2D).

We next investigated whether gene-expression levels differed between SEZ and T. We rejected the hypotheses of no significant differences in the expression levels of all genes between SEZ and T (P value < 0.00001), which suggests that there are differentially expressed genes in SEZ and T. We next used the R package HDTD to identify gene ontology (GO) terms whose genes are differentially expressed (Supplementary Table S3).

TICs reside in the SEZ

We next extended the characterization of T and SEZ to TIC populations. In neuroepithelial malignancies, the purification of TICs remains challenging because no robust cell-surface marker has been identified to distinguish tumorigenic and nontumorigenic cells (19, 20). Initial data identifying CD133/Prominin1 as a marker in human glioblastoma (21) were subsequently challenged both in primary and cultured TICs (reviewed in ref. 19). More recently, the cell surface marker CD15/SSEA-1 has been identified as a possible TIC marker in glioblastoma and medulloblastoma (22, 23). CD15 is a carbohydrate moiety expressed by neural stem and progenitor cells (24), but its use as glioblastoma marker did not find additional confirmation (25).

We therefore used a marker-independent approach (9, 11, 12, 26) to isolate cells from T and SEZ under serum-free conditions *in vitro* (Fig. 3A). Growth curve analysis and limiting-dilution assays confirmed long-term self-renewal and expansion (Fig. 3B and Supplementary Fig. S7), clonogenicity, and multipotency similar to the corresponding T cells (Supplementary Fig. S8).

We evaluated the expression of the precursor marker Nestin and other putative TIC markers (A2B5, CD133, and CD15) from T and SEZ (reviewed in ref. 19) and found similar expression of Nestin in T and SEZ cells, in agreement with the data in Fig. 1B and C. In contrast, A2B5-, CD133-, and CD15-positive cells were rarely found (Supplementary Fig. S9A and S9B).

Published OnlineFirst November 18, 2014; DOI: 10.1158/0008-5472.CAN-13-3131

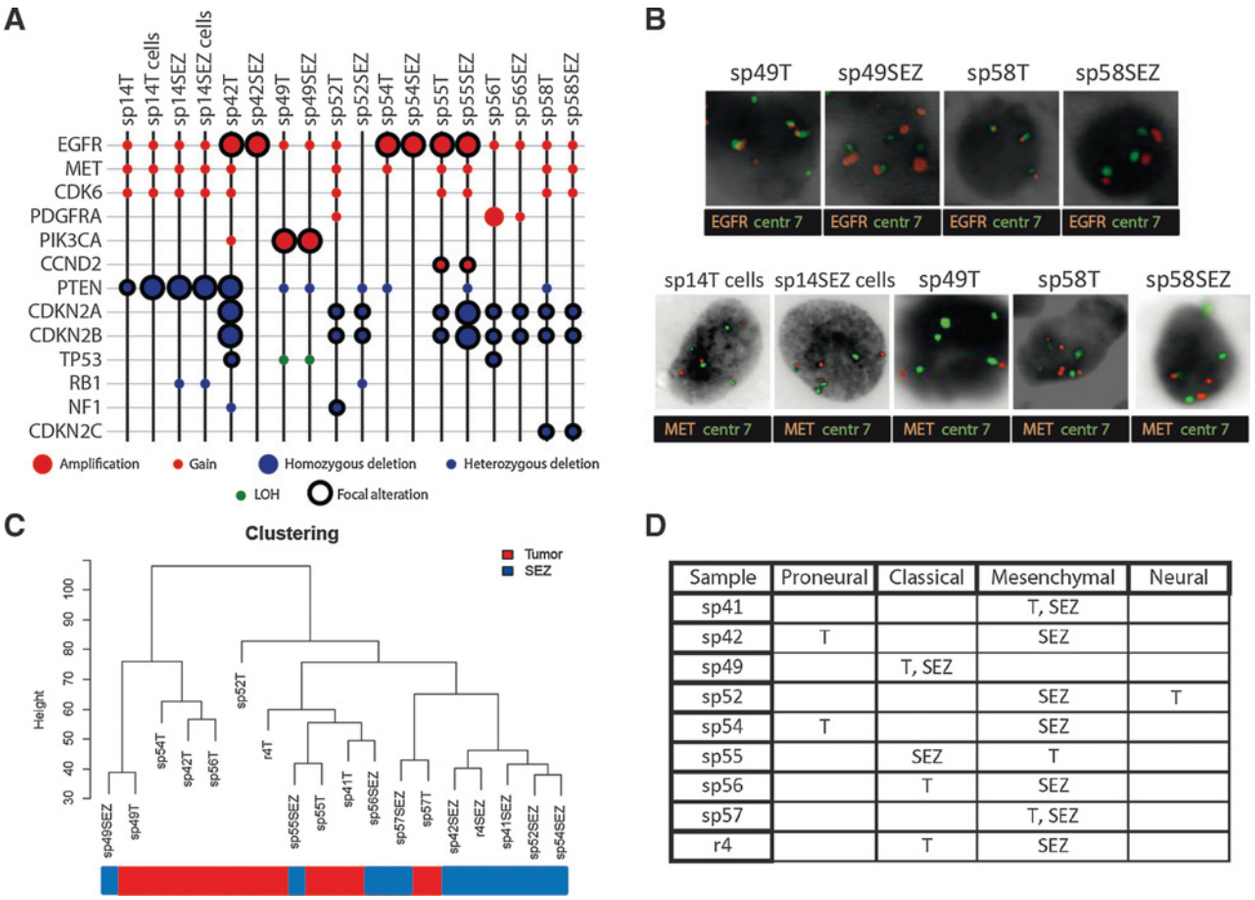

Sample	Proneural	Classical	Mesenchymal	Neural
sp41			T, SEZ	
sp42	T		SEZ	
sp49		T, SEZ		
sp52			SEZ	T
sp54	T		SEZ	
sp55		SEZ	T	
sp56		T	SEZ	
sp57			T, SEZ	
r4		T	SEZ	

Figure 2.
The SEZ harbors residual disease. A, summary of the most common putative drivers in glioblastoma. In 6 of 8 patients, the SEZ contains an equal or smaller number of aberrations with respect to its corresponding T. Cultured cells from T and SEZ of patient sp14 have been used for comparison with the corresponding tissues. B, FISH of 3 patients confirmed gain of the region of chromosome 7, including *EGFR* and the centromere (centr 7), in sp49 and sp58 (T and SEZ in both cases), and gain of the region, including *MET* and centr 7, in sp58 and cells from sp14 (T and SEZ in both cases); as expected, based on copy-number data, gain of *MET* was not observed in sp49T. Orange, *EGFR* or *MET*; and green, the centr 7. The single nuclei are representative of what was generally observed in each sample. C, clustering of gene-expression profiles from 9 patients revealed that five SEZ samples cluster tightly together instead of with their matched T. Samples are color-coded on the basis of their origin. D, each compartment of 9 glioblastomas has been assigned to a previously described classifier (6): T samples are either proneural, classical, mesenchymal, or neural, and 7/9 SEZ are mesenchymal.

Despite phenotypic differences *in vitro*, orthotopic inoculation of T and SEZ cells in NOD/SCID mice consistently generated tumors in all cases (Fig. 3C and D and Supplementary Fig. S10). Nonetheless, a statistically significant shorter survival was observed for animals injected with T cells compared with those injected with SEZ cells (Fig. 3C and Supplementary Fig. S10; P value < 0.05).

To our knowledge, this is the first time that SEZ cells from patients with glioblastoma have been tested for their tumorigenic potential. We analyzed the *in vivo* properties of enriched SEZ cells from three additional glioblastomas. In all cases, SEZ cells gave rise to tumors with similar patterns of growth and infiltration to those generated from TICs isolated from T, under the same experimental conditions (Supplementary Fig. S11A–S11C).

TICs from the SEZ contribute to drug resistance

The SEZ and T contained self-renewing TICs suitable for chemoresponse assays. These cells are grown in conditions that better preserve the genotype of the original disease (27) and have been proposed for use in high-throughput drug screening (28, 29). We tested the effects of the oral alkylating agent temozolomide, the current standard of care in patients with glioblastoma (30). To facilitate analysis, we assayed methylation in the promoter region of *MGMT*, a methyltransferase that inhibits the cytotoxic effect of temozolomide and is a predictive biomarker in glioblastoma (31).

We initially treated TICs isolated from T and SEZ of 7 patients with glioblastoma with temozolomide at maximum concentrations reported for the brain and plasma (50 μmol/L; refs. 32, 33), but no significant treatment response was observed relative to the corresponding controls (vehicle only). Only sp12 showed a significant response in both T and SEZ (Supplementary Fig. S12). We therefore analyzed a set of TICs isolated from T of 20 patients using a dose-escalation strategy ranging from 50 μmol/L to 2.5 mmol/L of temozolomide, and found that only 20% of the samples exhibited a significant response at ≥500 μmol/L (Supplementary Fig. S13A and S13B).

Published OnlineFirst November 18, 2014; DOI: 10.1158/0008-5472.CAN-13-3131

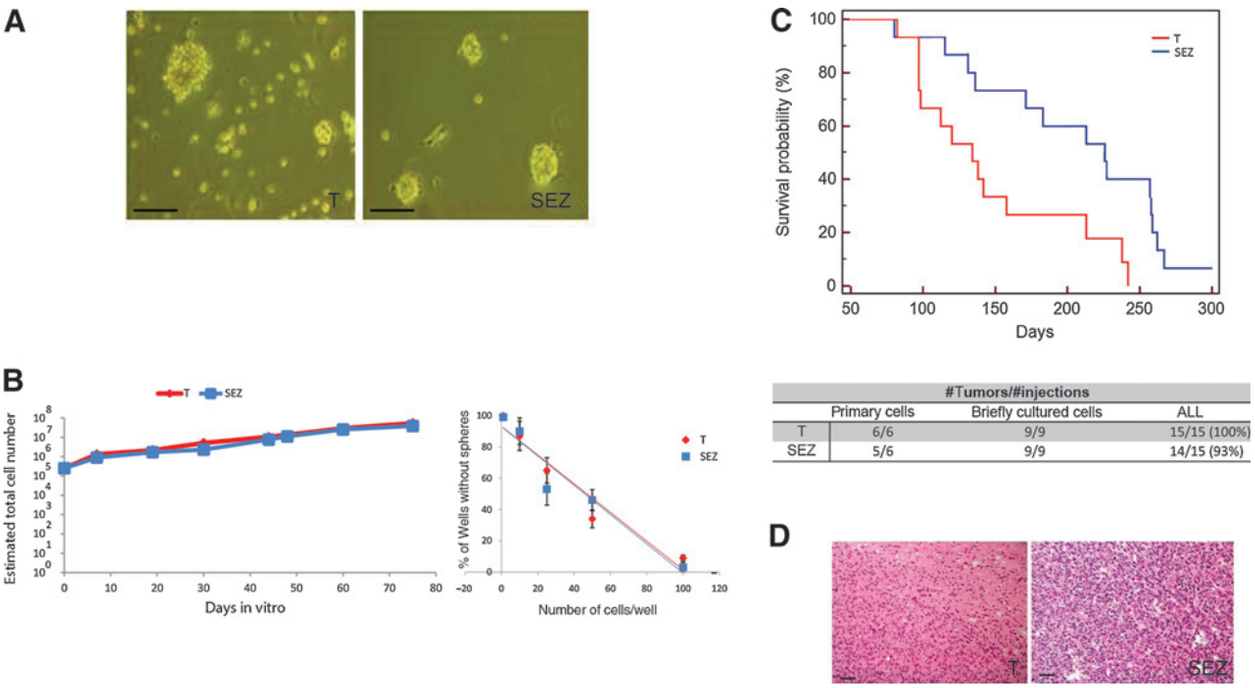

Figure 3.
TICs can be isolated from SEZ patients with of glioblastoma. A, cells from T and SEZ form spheres in serum-free medium; magnification, ×100; scale bar, 50 μm. B, left, growth curve analysis shows that cells from T and SEZ are capable of long-term expansion. Right, limiting-dilution assays revealed similar frequencies of sphere formation in T and SEZ. Each data point represents the average of triplicates; error bars, SD. C, top, cumulative Kaplan–Meier survival analysis of 30 animals revealed the tumorigenic potential of T and SEZ cells from five glioblastomas. There is a statistically significant difference ($P < 0.05$, log-rank test) between the survival of animals injected with T cells versus those injected with SEZ cells. Bottom, table summarizing the number of tumors/injections and the type of cells used (primary or briefly cultured). D, hematoxylin and eosin staining of T and SEZ cells derived xenografts; scale bar, 30 μm.

On the basis of these results, we performed cell proliferation assays for temozolomide concentrations between 50 μmol/L and 2.5 mmol/L on TICs isolated from T and SEZ of the same tumor for 8 patients. We noted that TICs continued to proliferate in the SEZ and T at supramaximal drug concentrations. We also observed that the response varied between T and SEZ of the same glioblastoma (Fig. 4A and Supplementary Fig. S14A). Three patterns emerged: differential response between T and SEZ (e.g., sp13, sp20, sp37, and sp42), both T and SEZ respond (e.g., sp17 and sp23), neither T nor SEZ respond (e.g., sp14, except at 2.5 mmol/L temozolomide for T, and sp52).

To test whether resistance to temozolomide was *MGMT*-dependent, we analyzed the DNA methylation status of the *MGMT* promoter by pyrosequencing (Supplementary Table S4) and methylation-specific PCR (Supplementary Fig. S15; ref. 13), and we found that the results were in agreement except for sp42.

Our PCR analysis revealed that four of seven paired TICs (sp14, sp23, sp37, and sp52) did not show methylation of the *MGMT* promoter in either the T or the SEZ consistent with the poor response to temozolomide, except for sp23 (T and SEZ) and sp37T. In contrast, sp17, sp20, and sp42 are methylated and showed a better response to temozolomide among all the tested TICs with the exception of sp20SEZ and sp42T (Fig. 4A and Supplementary Fig. S14A). All together, our results suggest that *MGMT* methylation status is homogeneous in T and SEZ of the same patients and generally predicts response to temozolomide (Supplementary Table S5).

We also evaluated the antimitotic agent cisplatin, previously used in glioblastoma therapy, and cediranib, an antiangiogenic inhibitor of VEGFRs with additional activity against PDGFRs, recently used in clinical trials (Fig. 4B and Supplementary Fig. S14B; refs. 34, 35). Although antiangiogenic therapies target the endothelial compartment, it has been reported that VEGFRs are enriched on the surface of TICs from glioblastoma (36). VEGF signals via its endothelial tyrosine kinase receptor 2 (VEGFR2; ref. 35), so we first confirmed that this receptor is expressed in TICs from T and SEZ (Supplementary Fig. S16). We next quantified the expression of VEGF and PDGF receptors. No significant difference was present between T and SEZ (no VEGFR1 nor VEGFR3 probe was available in the Illumina arrays; Supplementary Table S6).

Exposure to cisplatin and cediranib revealed resistant TICs in T and SEZ together with a heterogeneous response profile (Fig. 4B and Supplementary Fig. S14B). Whereas sp17 and sp23 showed sensitivity to these treatments in T and SEZ, a significant response was observed only in one of the two regions for sp13, sp20, and sp52 (Fig. 4B).

The drug response profile of TICs from T and SEZ of the same patients emphasizes their potential utility in drug development compared with standard glioma cell lines, for example, U87 and human fetal NSCs (HFNSC). U87 significantly responded to treatment with temozolomide, cisplatin, and cediranib, whereas two HFNSCs lines (HFNSC and HFNSC1) were resistant to temozolomide, as previously reported (37), and to cisplatin and cediranib (Supplementary Fig. S17).

Published OnlineFirst November 18, 2014; DOI: 10.1158/0008-5472.CAN-13-3131

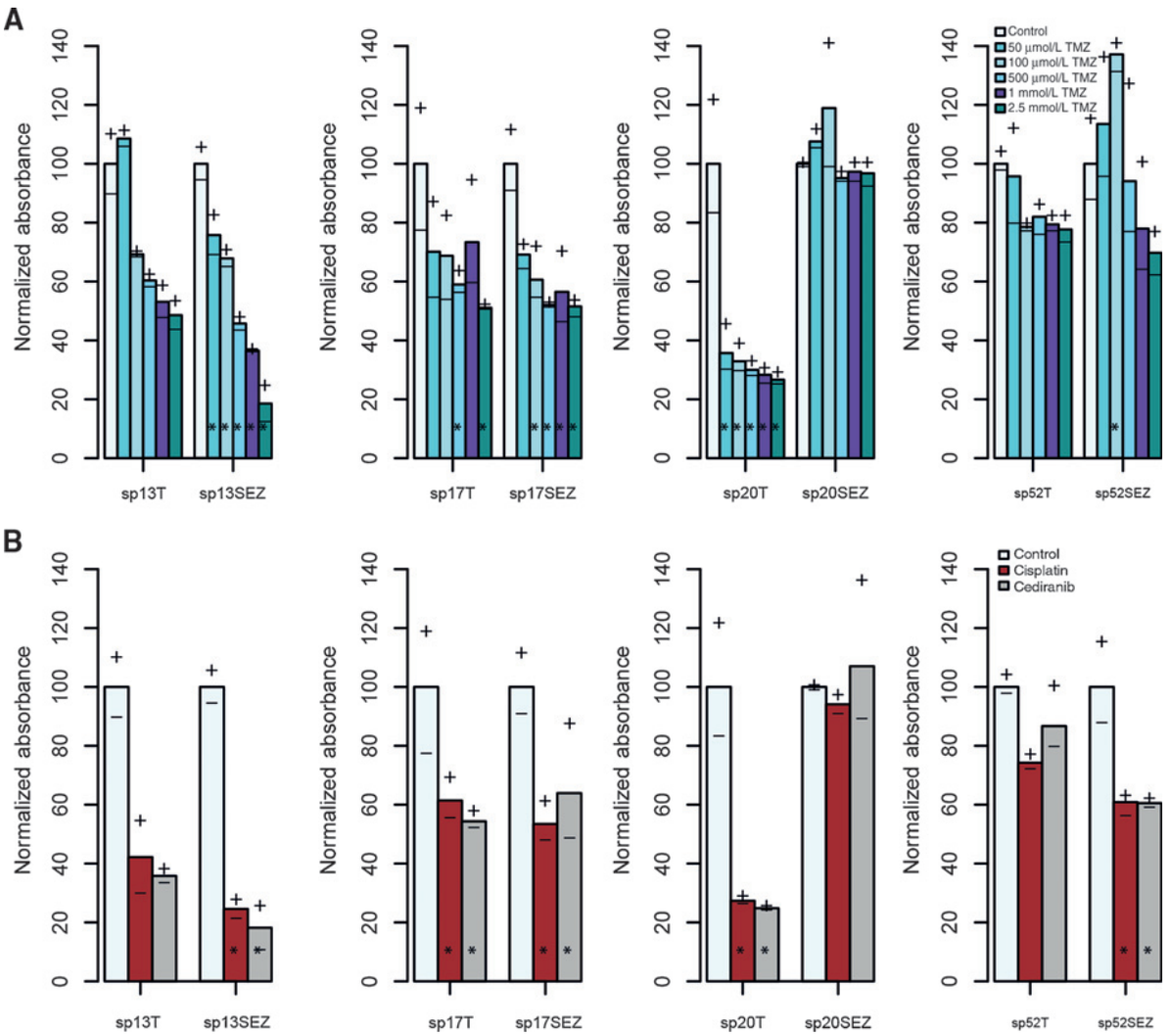

Figure 4.
TICs from SEZ contribute to drug resistance. Cells from T and SEZ of 4 patients were used to evaluate response to chemotherapeutics. A, differential response patterns to temozolomide (TMZ) were observed in T and SEZ cells of the same patients. Dose escalation has little impact on drug-resistant cells. B, distinct patterns of response were observed when the assay was performed with cisplatin and cediranib. Data are shown as normalized to control. The mean normalized absorbance as well as the minimum (−) and maximum (+) absorbance are plotted. Asterisks, statistical significance.

Phylogenetic reconstruction suggests different patterns of glioblastoma evolution involving SEZ malignant cells

Our genomic and chemoresponse assays data show that the SEZ harbors malignant cells that contribute to tumor growth and murine models of glioblastoma indicate that the SEZ is enriched for tumor ancestors (2, 38–40). However, this has not been confirmed in patients with glioblastoma. We analyzed SEZ and T samples to determine whether tumor cells grow out of the SEZ or into the SEZ. We reconstructed tumor ancestral trees in 8 patients, using several genomic measurements derived from multiple spatially separated samples taken from the glioblastoma mass (T1–T6) and SEZ. We have previously used this approach to describe intratumor heterogeneity in T and infer tumor evolution (7), and we now used FGMS to position the SEZ. In particular, we reconstructed phylogeny based on genome-wide DNA copy number (41). In an independent assay, we exploited the observation that cells record their ancestral history in the form of neutral DNA methylation patterns (42, 43). This analysis is not biased by the presence of non-neoplastic cells, as only highly proliferative tissues accumulate sufficient methylation events (tumors and colonic epithelium; Fig. 5A; ref. 44). We first validated the molecular clock loci chosen for this analysis (Fig. 5B and C, top) and then calculated the normal cell content in SEZ and T. The values of cellularity indicate no significant difference (Fig. 5B and C, bottom).

These orthogonal techniques yielded highly concordant phylogenies: in sp52, sp54, sp56, and sp57, the SEZ harbors tumor precursor cells that gave rise to the glioblastoma mass (Fig. 5D). In sp42 and sp49, we observed a similar trend, although the two methods are not in full agreement (Fig. 5D). Analysis of sp55 and sp58 suggests a different pattern of evolution and emphasizes the heterogeneous nature of

Published OnlineFirst November 18, 2014; DOI: 10.1158/0008-5472.CAN-13-3131

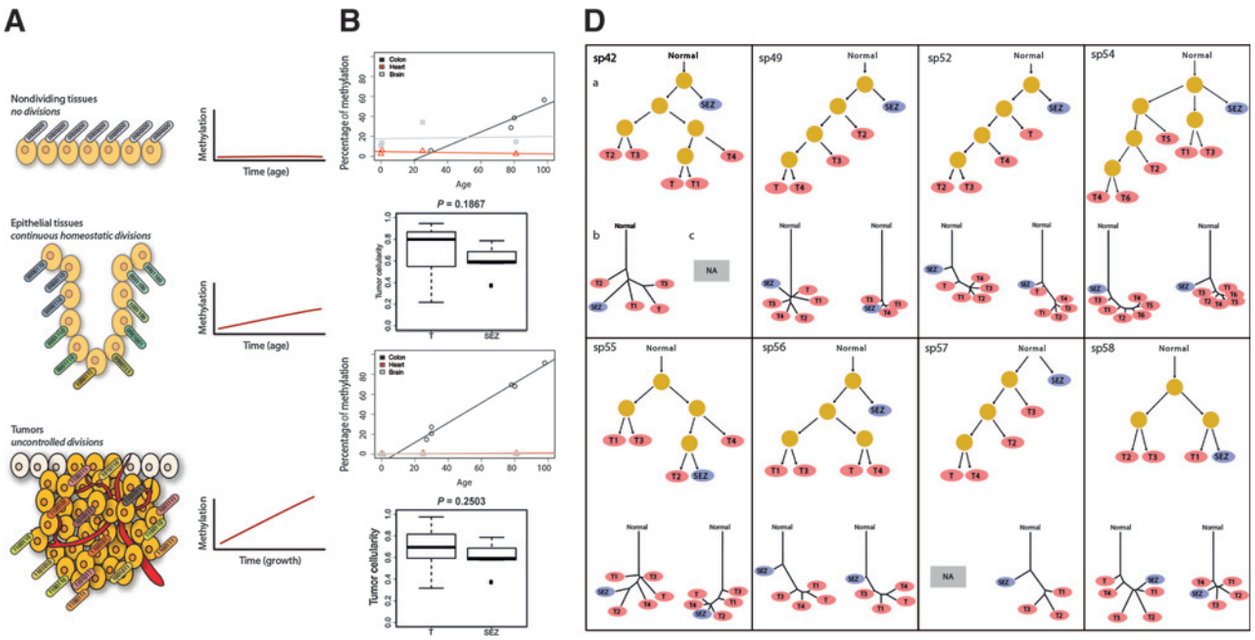

Figure 5.
Phylogenetic reconstruction reveals different patterns of tumor evolution involving SEZ malignant cells. A, cartoon illustrating the phylogeny based on molecular clock analysis. Non-dividing tissues, such as heart and brain, do not undergo mitotic events and do not accumulate methylation errors. Epithelial tissues, such as colon, show increased methylation with age due to the mitotic turnover of cells maintaining tissue homeostasis. Tumors undergo a large number of divisions and accumulate methylation changes in a manner proportional to the number of mitotic events. B and C, top, the *IRX2* locus on chromosome 5 in B and the *NETO1* locus on chromosome 18 in C have been validated as molecular clock loci by verifying that age-related methylation increases as a result of cell division in patient-derived tissues by comparing heart, brain, and colon. Bottom, the graphs show tumor cellularity using *IRX2* in B and *NETO1* in C molecular clock data. The values of cellularity indicate no significant difference between T and SEZ. D, tumor phylogenies based on SEZ and multiple tumor mass samples (T, T1–T6) were reconstructed independently with two methods: copy-number breakpoints (a) and two molecular clock loci [*IRX2* (b) and *NETO1* (c)]. As an example, in sp52, the SEZ (blue) harbors cells that arise earlier than tumor mass cells (red; sample T1 failed hybridization); NA, not available.

glioblastoma (Fig. 5D). Taken together, these data suggest that the SEZ contains a reservoir of malignant cells that are either tumor precursor clones or clones generated during glioblastoma evolution.

Discussion

Our comprehensive phenotypic, genomic, and functional analysis reveals residual disease in the SEZ of patients with glioblastoma (Fig. 1A and Supplementary Fig. S1A and S1B). TICs are present in T and SEZ of the same glioblastomas (Fig. 3C and Supplementary Fig. S10) and show differential patterns of therapeutic responsiveness and drug resistance (Fig. 4A and B and Supplementary Fig. S14A and S14B), suggesting that the SEZ should be considered as a novel potential therapeutic target in a subset of patients with glioblastoma. This is confirmed by phylogenetic reconstruction showing different patterns of tumor evolution with the SEZ harboring precursor clones or clones generated during the glioblastoma growth (Fig. 5D).

Gene-expression profiling of SEZ reveals that different glioblastoma subtypes (6) are present within the same patient. The SEZ is predominantly mesenchymal (7 patients) or classical (2 patients). T is more diverse, with representation from all four subtypes (Fig. 2D). Thus, it is possible to envisage a spectrum of expression patterns with mesenchymal/classical representing proliferative diversification at the tumor core.

Previous reports suggested that proximity to the SEZ predicts a multifocal tumor phenotype and recurrences that arise at locations distant from the initial lesion (45). More recently, it has also been reported that contact of the tumor mass with the SEZ correlates with shorter survival (46). To explore this, we isolated TICs from T and SEZ of the same patients. TICs have been described in human glioblastoma but no analysis based on FGMS has been performed. Our results show that *in vivo* both T- and SEZ-derived cells generated tumors; however, cells from T are more tumorigenic in comparison with the SEZ in agreement with the CNAs of the patient samples showing a trend toward a smaller number of aberrations in the SEZ. These data suggest that the tumorigenic potential is exacerbated when increased genetic alterations are acquired by the cancer genome in line with previous reports (47, 48).

Because genomic and phenotypic analyses suggest that the SEZ harbors tumor cells, it is crucial to investigate whether there are differences in response to therapy in cells isolated from this region. It has been previously shown that patient-derived TICs accurately represent parent disease (27) and have potential application in high-throughput drug screening (28, 29). Our data reveal that TICs from T and SEZ of the same glioblastomas show different patterns of response to therapies that represent the current standard of care (Fig. 4A and B, Supplementary Fig. S14A and S14B and Supplementary Table S5). This suggests that they should be targeted using different approaches. Our results also reveal that a clinically significant

fraction of cells is resistant to current treatments. This is consistent with murine data (3), indicating that multimodal stratified approaches will be essential to improve therapeutic responsiveness.

Glioblastoma evolves by following poorly understood spatial and temporal dynamics arising from cells of origin that are yet to be defined. The presence of malignant cells in the SEZ suggests two different scenarios of evolution with the glioblastoma growing into the SEZ or out of this region. Our phylogenetic data indicate that in 4 of 8 patients, a pool of malignant precursor clones evolved in the SEZ (Fig. 5D). Given the presence of NSCs in the adult human SEZ (49), it has been suggested that glioblastoma is derived from those cells (50). This concept has been investigated in mouse models (2, 38–40), but until now there has been no direct evidence of the contribution of SEZ cells in human gliomagenesis. We show that the SEZ is a reservoir of disease and could be targeted therapeutically. Consistent with this, preliminary evidence suggest that irradiation of the SEZ in patients with glioblastoma is associated with improved progression-free survival (51, 52).

In summary, we present a phenotypic, genomic, and functional analysis of residual disease in human glioblastoma (Supplementary Fig. S18A and S18B). Our approach together with FGMS provides a coherent strategy for interrogating the mechanistic basis of clinical heterogeneity in future studies. This is likely to further refine our understanding of the complex molecular landscape of glioblastoma, resulting in improved therapeutic strategies specifically aimed at targeting the SEZ.

Disclosure of Potential Conflicts of Interest

S. Tavaré has provided expert testimony for Springer Verlag. No potential conflicts of interest were disclosed by the other authors.

Authors' Contributions

Conception and design: S.G.M. Piccirillo, A.R. Venkitaraman, C. Watts
Development of methodology: S.G.M. Piccirillo, I. Spiteri, A. Sottoriva, S.J. Price, C. Watts
Acquisition of data (provided animals, acquired and managed patients, provided facilities, etc.): S.G.M. Piccirillo, I. Spiteri, S. Ber, S.J. Price, R. Heywood, K.D. Howarth, V.P. Collins, C. Watts
Analysis and interpretation of data (e.g., statistical analysis, biostatistics, computational analysis): S.G.M. Piccirillo, I. Spiteri, A. Sottoriva, A. Touloumis, K.D. Howarth, V.P. Collins, A.R. Venkitaraman, C. Curtis, J.C. Marioni, S. Tavaré, C. Watts
Writing, review, and/or revision of the manuscript: S.G.M. Piccirillo, I. Spiteri, A. Sottoriva, S.J. Price, V.P. Collins, A.R. Venkitaraman, C. Curtis, J.C. Marioni, S. Tavaré, C. Watts
Administrative, technical, or material support (i.e., reporting or organizing data, constructing databases): S.G.M. Piccirillo, V.P. Collins, C. Watts
Study supervision: A.R. Venkitaraman, C. Curtis, S. Tavaré, C. Watts
Other (technical advice related to methodology): N.-J. Francis

Acknowledgments

The authors thank Amy Frary for tissue collection, Andy Lynch for help with the design of the expression array layout, Danita Pearson and Suet-Feung Chin for assistance in FISH, Cancer Research UK Cambridge Institute Genomics core facility for processing the Illumina arrays and Paul Edwards for comments during article preparation. We acknowledge the Human Research Tissue Bank and Biomedical Research Centre for the tissue being accessed through the Human Research Tissue Bank. The Human Research Tissue Bank is supported by the NIHR Cambridge Biomedical Research Centre.

Grant Support

This study was supported by the Addenbrooke's Charitable Trust; the National Institute for Health Research Cambridge Biomedical Research Centre; the Higher Education Funding Council for England; the Royal College of Surgeons of Edinburgh; the European Commission-Seventh Framework Program (Marie Curie Intra-European Fellowship; S.G.M. Piccirillo); Cancer Research UK Program grant C14303/A10825 (S. Tavaré, I. Spiteri, and A. Sottoriva); UK Medical Research Council (N.-J. Francis and A.R. Venkitaraman) and C1023/A14545 (K.D. Howarth); EBI funding (A. Touloumis and J.C. Marioni); University of Southern California (C. Curtis).

The costs of publication of this article were defrayed in part by the payment of page charges. This article must therefore be hereby marked *advertisement* in accordance with 18 U.S.C. Section 1734 solely to indicate this fact.

Received October 30, 2013; revised September 29, 2014; accepted October 22, 2014; published OnlineFirst November 18, 2014.

References

1. Zhu Y, Guignard F, Zhao D, Liu L, Burns DK, Mason RP, et al. Early inactivation of p53 tumor suppressor gene cooperating with NF1 loss induces malignant astrocytoma. Cancer Cell 2005;8:119–30.
2. Alcantara Llaguno S, Chen J, Kwon CH, Jackson EL, Li Y, Burns DK, et al. Malignant astrocytomas originate from neural stem/progenitor cells in a somatic tumor suppressor mouse model. Cancer Cell 2009;15:45–56.
3. Chen J, Li Y, Yu TS, McKay RM, Burns DK, Kernie SG, et al. A restricted cell population propagates glioblastoma growth after chemotherapy. Nature 2012;488:522–6.
4. Cancer Genome Atlas Research Network. Comprehensive genomic characterization defines human glioblastoma genes and core pathways. Nature 2008;455:1061–8.
5. Phillips HS, Kharbanda S, Chen R, Forrest WF, Soriano RH, Wu TD, et al. Molecular subclasses of high-grade glioma predict prognosis, delineate a pattern of disease progression, and resemble stages in neurogenesis. Cancer Cell 2006;9:157–73.
6. Verhaak RG, Hoadley KA, Purdom E, Wang V, Qi Y, Wilkerson MD, et al. Integrated genomic analysis identifies clinically relevant subtypes of glioblastoma characterized by abnormalities in PDGFRA, IDH1, EGFR, and NF1. Cancer Cell 2010;17:98–110.
7. Sottoriva A, Spiteri I, Piccirillo SG, Touloumis A, Collins VP, Marioni JC, et al. Intratumor heterogeneity in human glioblastoma reflects cancer evolutionary dynamics. Proc Natl Acad Sci U S A 2013;110:4009–14.
8. Stummer W, Pichlmeier U, Meinel T, Wiestler OD, Zanella F, Reulen HJ. Fluorescence-guided surgery with 5-aminolevulinic acid for resection of malignant glioma: a randomised controlled multicentre phase III trial. Lancet Oncol 2006;7:392–401.
9. Piccirillo SG, Dietz S, Madhu B, Griffiths J, Price SJ, Collins VP, et al. Fluorescence-guided surgical sampling of glioblastoma identifies phenotypically distinct tumour-initiating cell populations in the tumour mass and margin. Br J Cancer 2012;107:462–8.
10. Guilfoyle MR, Weerakkody RA, Oswal A, Oberg I, Jeffery C, Haynes K, et al. Implementation of neuro-oncology service reconfiguration in accordance with NICE guidance provides enhanced clinical care for patients with glioblastoma multiforme. Br J Cancer 2011;104:1810–5.
11. Piccirillo SG, Combi R, Cajola L, Patrizi A, Redaelli S, Bentivegna A, et al. Distinct pools of cancer stem-like cells coexist within human glioblastomas and display different tumorigenicity and independent genomic evolution. Oncogene 2009;28:1807–11.
12. Fael Al-Mayhani TM, Ball SL, Zhao JW, Fawcett J, Ichimura K, Collins PV, et al. An efficient method for derivation and propagation of glioblastoma cell lines that conserves the molecular profile of their original tumours. J Neurosci Methods 2009;176:192–9.
13. Esteller M, Hamilton SR, Burger PC, Baylin SB, Herman JG. Inactivation of the DNA repair gene O6-methylguanine-DNA methyltransferase by promoter hypermethylation is a common event in primary human neoplasia. Cancer Res 1999;59:793–7.

14. Malley DS, Hamoudi RA, Kocialkowski S, Pearson DM, Collins VP, Ichimura K. A distinct region of the MGMT CpG island critical for transcriptional regulation is preferentially methylated in glioblastoma cells and xenografts. Acta Neuropathol 2011;121:651–61.
15. Louis DN, Ohgaki H, Wiestler OD, Cavenee WK, Burger PC, Jouvet A, et al. The 2007 WHO classification of tumours of the central nervous system. Acta Neuropathol 2007;114:97–109.
16. Reifenberger G, Collins VP. Pathology and molecular genetics of astrocytic gliomas. J Mol Med 2004;82:656–70.
17. Karamitopoulou E, Perentes E, Diamantis I, Maraziotis T. Ki-67 immunoreactivity in human central nervous system tumors: a study with MIB 1 monoclonal antibody on archival material. Acta Neuropathol 1994;87:47–54.
18. Saeed AI, Bhagabati NK, Braisted JC, Liang W, Sharov V, Howe EA, et al. TM4 microarray software suite. Methods Enzymol 2006;411:134–93.
19. Piccirillo SG, Binda E, Fiocco R, Vescovi AL, Shah K. Brain cancer stem cells. J Mol Med 2009;87:1087–95.
20. Shackleton M, Quintana E, Fearon ER, Morrison SJ. Heterogeneity in cancer: cancer stem cells versus clonal evolution. Cell 2009;138:822–9.
21. Singh SK, Hawkins C, Clarke ID, Squire JA, Bayani J, Hide T, et al. Identification of human brain tumour initiating cells. Nature 2004;432:396–401.
22. Son MJ, Woolard K, Nam DH, Lee J, Fine HA. SSEA-1 is an enrichment marker for tumor-initiating cells in human glioblastoma. Cell Stem Cell 2009;4:440–52.
23. Ward RJ, Lee L, Graham K, Satkunendran T, Yoshikawa K, Ling E, et al. Multipotent CD15+ cancer stem cells in patched-1-deficient mouse medulloblastoma. Cancer Res 2009;69:4682–90.
24. Capela A, Temple S. LeX/ssea-1 is expressed by adult mouse CNS stem cells, identifying them as nonependymal. Neuron 2002;35:865–75.
25. Patru C, Romao L, Varlet P, Coulombel L, Raponi E, Cadusseau J, et al. CD133, CD15/SSEA-1, CD34 or side populations do not resume tumor-initiating properties of long-term cultured cancer stem cells from human malignant glio-neuronal tumors. BMC Cancer 2010;10:66.
26. Piccirillo SG, Reynolds BA, Zanetti N, Lamorte G, Binda E, Broggi G, et al. Bone morphogenetic proteins inhibit the tumorigenic potential of human brain tumour-initiating cells. Nature 2006;444:761–5.
27. Lee J, Kotliarova S, Kotliarov Y, Li A, Su Q, Donin NM, et al. Tumor stem cells derived from glioblastomas cultured in bFGF and EGF more closely mirror the phenotype and genotype of primary tumors than do serum-cultured cell lines. Cancer Cell 2006;9:391–403.
28. Pollard SM, Yoshikawa K, Clarke ID, Danovi D, Stricker S, Russell R, et al. Glioma stem cell lines expanded in adherent culture have tumor-specific phenotypes and are suitable for chemical and genetic screens. Cell Stem Cell 2009;4:568–80.
29. Danovi D, Folarin AA, Baranowski B, Pollard SM. High content screening of defined chemical libraries using normal and glioma-derived neural stem cell lines. Methods Enzymol 2012;506:311–29.
30. Stupp R, Mason WP, van den Bent MJ, Weller M, Fisher B, Taphoorn MJ, et al. Radiotherapy plus concomitant and adjuvant temozolomide for glioblastoma. N Engl J Med 2005;352:987–96.
31. Jansen M, Yip S, Louis DN. Molecular pathology in adult gliomas: diagnostic, prognostic, and predictive markers. Lancet Neurol 2010;9:717–26.
32. Ostermann S, Csajka C, Buclin T, Leyvraz S, Lejeune F, Decosterd LA, et al. Plasma and cerebrospinal fluid population pharmacokinetics of temozolomide in malignant glioma patients. Clin Cancer Res 2004;10:3728–36.
33. Portnow J, Badie B, Chen M, Liu A, Blanchard S, Synold TW. The neuropharmacokinetics of temozolomide in patients with resectable brain tumors: potential implications for the current approach to chemoradiation. Clin Cancer Res 2009;15:7092–8.
34. Dietrich J, Wang D, Batchelor TT. Cediranib: profile of a novel anti-angiogenic agent in patients with glioblastoma. Expert Opin Investig Drugs 2009;18:1549–57.
35. Batchelor TT, Duda DG, di Tomaso E, Ancukiewicz M, Plotkin SR, Gerstner E, et al. Phase II study of cediranib, an oral pan-vascular endothelial growth factor receptor tyrosine kinase inhibitor, in patients with recurrent glioblastoma. J Clin Oncol 2010;28:2817–23.
36. Hamerlik P, Lathia JD, Rasmussen R, Wu Q, Bartkova J, Lee M, et al. Autocrine VEGF-VEGFR2-Neuropilin-1 signaling promotes glioma stem-like cell viability and tumor growth. J Exp Med 2012;209:507–20.
37. Pistollato F, Abbadi S, Rampazzo E, Persano L, Della Puppa A, Frasson C, et al. Intratumoral hypoxic gradient drives stem cells distribution and MGMT expression in glioblastoma. Stem Cells 2010;28:851–62.
38. Holland EC, Celestino J, Dai C, Schaefer L, Sawaya RE, Fuller GN. Combined activation of Ras and Akt in neural progenitors induces glioblastoma formation in mice. Nat Genet 2000;25:55–7.
39. Zheng H, Ying H, Yan H, Kimmelman AC, Hiller DJ, Chen AJ, et al. p53 and Pten control neural and glioma stem/progenitor cell renewal and differentiation. Nature 2008;455:1129–33.
40. Wang Y, Yang J, Zheng H, Tomasek GJ, Zhang P, McKeever PE, et al. Expression of mutant p53 proteins implicates a lineage relationship between neural stem cells and malignant astrocytic glioma in a murine model. Cancer Cell 2009;15:514–26.
41. Letouze E, Allory Y, Bollet MA, Radvanyi F, Guyon F. Analysis of the copy number profiles of several tumor samples from the same patient reveals the successive steps in tumorigenesis. Genome Biol 2010;11:R76.
42. Yatabe Y, Tavaré S, Shibata D. Investigating stem cells in human colon by using methylation patterns. Proc Natl Acad Sci U S A 2001;98:10839–44.
43. Shibata D, Tavaré S. Counting divisions in a human somatic cell tree: how, what and why? Cell Cycle 2006;5:610–4.
44. Sottoriva A, Spiteri I, Shibata D, Curtis C, Tavaré S. Single-molecule genomic data delineate patient-specific tumor profiles and cancer stem cell organization. Cancer Res 2013;73:41–9.
45. Lim DA, Cha S, Mayo MC, Chen MH, Keles E, VandenBerg S, et al. Relationship of glioblastoma multiforme to neural stem cell regions predicts invasive and multifocal tumor phenotype. Neuro Oncol 2007;9:424–9.
46. Kappadakunnel M, Eskin A, Dong J, Nelson SF, Mischel PS, Liau LM, et al. Stem cell associated gene expression in glioblastoma multiforme: relationship to survival and the subventricular zone. J Neurooncol 2010;96:359–67.
47. Ye CJ, Stevens JB, Liu G, Bremer SW, Jaiswal AS, Ye KJ, et al. Genome based cell population heterogeneity promotes tumorigenicity: the evolutionary mechanism of cancer. J Cell Physiol 2009;219:288–300.
48. Stieber D, Golebiewska A, Evers L, Lenkiewicz E, Brons NH, Nicot N, et al. Glioblastomas are composed of genetically divergent clones with distinct tumourigenic potential and variable stem cell-associated phenotypes. Acta Neuropathol 2014;127:203–19.
49. Sanai N, Tramontin AD, Quinones-Hinojosa A, Barbaro NM, Gupta N, Kunwar S, et al. Unique astrocyte ribbon in adult human brain contains neural stem cells but lacks chain migration. Nature 2004;427:740–4.
50. Sanai N, Alvarez-Buylla A, Berger MS. Neural stem cells and the origin of gliomas. N Engl J Med 2005;353:811–22.
51. Evers P, Lee PP, DeMarco J, Agazaryan N, Sayre JW, Selch M, et al. Irradiation of the potential cancer stem cell niches in the adult brain improves progression-free survival of patients with malignant glioma. BMC Cancer 2010;10:384.
52. Chen L, Guerrero-Cazares H, Ye X, Ford E, McNutt T, Kleinberg L, et al. Increased subventricular zone radiation dose correlates with survival in glioblastoma patients after gross total resection. Int J Radiat Oncol Biol Phys 2013;86:616–22.

Published OnlineFirst November 18, 2014; DOI: 10.1158/0008-5472.CAN-13-3131

Cancer Research
The Journal of Cancer Research (1916–1930) | The American Journal of Cancer (1931–1940)

AACR American Association for Cancer Research

Contributions to Drug Resistance in Glioblastoma Derived from Malignant Cells in the Sub-Ependymal Zone

Sara G.M. Piccirillo, Inmaculada Spiteri, Andrea Sottoriva, et al.

Cancer Res 2015;75:194-202. Published OnlineFirst November 18, 2014.

Supplementary experimental procedure

5-ALA administration and GB sample collection

Patients were administered with 5-ALA (Medac UK) 5 hours before surgery as an oral dose of 20 mg/kg as described previously(1, 2). The fluorescence microscope used in the surgical theatre was a Zeiss Pentero Microscope (Zeiss UK). PpIX was excited with blue-violet light (wavelength 375-400 nm) and fluorescence emission was read at 600-700 nm (1). In 42 out of 65 patients we collected T and SEZ tissues. T was collected using fluorescence-guided resection as previously described (2). When fluorescence was detected in the SEZ, we collected this tissue based on anatomical location and confirmed the presence of the ependymal layer staining for S100β (Abgent) 1:100 (3).

After GB surgical resection, detection of sample fluorescence was confirmed after arrival at the laboratory. Briefly, a small part of each sample was put on a glass slide and each slide was mounted with a few drops of Vectashield (Vectorlabs) and analyzed at the confocal fluorescence microscope (Leica). PpIX was excited under the same conditions used in the surgical theatre. Of the 42 patients from whom we collected SEZ samples, 39 had contrast enhancing disease extending to the ventricle and visible fluorescent disease extending to the SEZ at surgery. The remaining 3 patients had contrast enhancing disease not extending to the ventricle but fluorescence in the SEZ.

Tissue was collected using separate rongeurs to avoid sample contamination. Haematoxylin and Eosin staining and immunohistochemistry were performed on 4μm thick sections of T and SEZ and processed as previously described (4).

The extent of necrosis was scored based upon review of Haematoxylin and Eosin sections by a neuropathologist as 0 = no necrosis and 1 = focal necrosis involving <20% of the tissue area. The presence of tumor cells in each samples was scored as 0 = cellular tumor and 1 = highly cellular tumor involving ≥70% of the tissue. Tumor cells were identified based upon morphologic features, including cytologic atypia, enlarged nuclear to cytoplasmic and volume ratio.

Cell lines propagation, immunofluorescence and *in vivo* tumorigenicity

Immunofluorescence was performed on cells derived from 11 patients. The following antibodies have been used: Gfap (DAKO) 1:400, O4 (gift from Dr. Chandran) 1:5, Tuj1 (Covance) 1:400, Nestin (Millipore) 1:200, Cd133 (Abcam) 1:100, Cd15 (BD Biosciences) 1:50, A2B5 (Millipore) 1:100, VEGFR2 (Cell Signaling) 1:100. To avoid the possibility that cells from the SEZ originated from non-neoplastic tissues, we collected two non-fluorescent SEZ (from samples sp2 and sp19) and we evaluated their proliferative ability *in vitro*. In contrast to the 42 fluorescent SEZ samples, these two samples did not give rise to long-term expanding cell cultures, further emphasizing that presence of tumor cells in the SEZ is necessary to derive TICs from this sample (Supplementary Fig. S19).

To derive TICs, primary cells were plated in 25 cm^2 tissue culture flasks plated at clonal density (2500–5000 cells/cm^2) in Neurobasal medium with B27 and N2 Supplement (GIBCO) containing 20 ng/mL of both epidermal growth factor (EGF) and fibroblast growth factor-2 (FGF-2). To assess multipotency, cells were plated at a density of 2.5×10^4 cells/cm^2 onto Matrigel-coated glass coverslips (12 mm diameter) in the presence of leukemia inhibitory factor (R&D Systems) (10 ng/mL) for 10 days. Limiting dilution assays were performed as described by (5). Spheres were dissociated into single cells and plated in 96-well plates in 0.2 ml of medium. Cultures were left undisturbed for approximately 10 days after which time the percentage of wells not containing spheres for each cell plating density was calculated and plotted against the number of cells plated per well. Linear regression lines were plotted, and the number of cells required to generate at least one sphere in every well was determined. The experiment was repeated three times.

Intracerebral transplantation in 60 animals with $3x10^5$ cells from T or SEZ of 10 GBs into the right striatum of Nod/Scid mice (Charles River) was performed as previously described (4, 6). Primary cells or briefly cultured cells were used for injections. 30 animals were injected with T cells and another 30 with SEZ cells. Mice were sacrificed when symptomatic according to the Home Office guidelines.

Copy number and gene expression analysis

To identify copy number aberrations in the samples Affymetrix SNP6 arrays were used. The raw data were processed with CRMAv2 (7) within the AROMA framework. Parent-specific circular binary segmentation (PSCBS) (8) was used to identify regions with aberrant DNA copy number. The copy number data for each patient were normalized to their respective germline status (blood DNA). Defining σ to be the standard deviation of the central 50% of probes in the array (sorted by intensity), amplifications were called when the log ratio (LRR) was $>6\sigma$, gains when $6\sigma>LRR>1.7\sigma$, losses for $-1.7\sigma>LRR>-7\sigma$ and homozygous deletions for $LRR<-7\sigma$, adapted from (9).

Illumina HT12v4 arrays were used to obtain gene expression data, which were analyzed using R and the beadarray package (10). All samples were labeled together and hybridized simultaneously onto expression arrays to avoid batch effects. When multiple high-quality probes were available per gene, we selected one at random. Median normalization was applied to the dataset. To classify our samples we mean-centered the dataset (11) and used the ClaNC package (12) to predict the sample subtype according to the Verhaak classifier using 836 genes with high quality probes out of the 841 total proposed by Verhaak and co-authors (13). Hierarchical clustering was performed with R using an average linkage method and an Euclidean distance. To assess whether SEZ and T were differentially expressed, we performed an analysis of variance (ANOVA)-type hypothesis testing based on matrix-variate distributions. As a negative control we used a list of genes validated by qRT-PCR that yielded no significant difference between SEZ and T (p-value=0.804). The R package HDTD was used to identify GO terms bearing at least one gene which is differentially expressed between SEZ and T.

Fluorescence in situ hybridization

Fluorescence in situ hybridization (FISH) was performed on SEZ- and T-derived cells from one

patient (sp14) as well as on 4 μm sections from four paraffin-embedded tissue specimens (sp49T, sp49SEZ, sp58T and sp58SEZ). Two control tissues (A1219, A887) and one normal lymphoblastoid cell line were included in the panel. Three commercial DNA probes (EGFR (7p11), MET (7q31) and PTEN (10q23), Kreatech Diagnostics) and DNA isolated from two BAC clones (RP11-339F13 (EGFR) and RP11-380G5 (PTEN)) were checked by hybridization to normal metaphase chromosomes. Metaphase chromosome preparation and hybridizations were performed as previously described (14, 15) and the SmartCapture software (Digital Scientific, Cambridge, UK) was used for image analysis.

Molecular clock analysis

We obtained between 4 and 6 multiple samples (T1-T6), spatially separated by approximately 10mm, from different areas of each tumor mass and we have presented the results of this analysis in a previous report (16). Due to the small size of the SEZ it was impossible to obtain several subsamples from this area. We have previously demonstrated the utility of molecular clock analysis based on the patterns of neutral methylation tags to reconstruct the phylogenies of cell populations. Neutral methylation tags report on the number of cell divisions as a result of the accumulation of random methylation errors. Related cell populations will have similar methylation errors, allowing for the reconstruction of the phylogeny based on the mitotic distance of samples (17, 18). The normal brain tissue can be filtered out from the molecular clock profile as having virtually no methylated CpGs. Tumor cells instead have undergone a large number of divisions and therefore show higher methylation. This can be used to calculate the normal contamination of samples.

DNA was extracted from tissue samples, as described above and was bisulfite converted using the EZ DNA Methylation Direct kit (Zymo). The IRX2 (chr5) molecular clock locus was PCR amplified as we previously described (18), using custom bisulfite-specific primers (5' GTATATTTTGTTAGGATTGGAGTTG 3' and 5' CATAAAACCCACATCTCTTTCAAAC 3' as forward and reverse primers respectively) bearing LibA 454 adapters and specific barcodes for each sample on their 5' end. Successfully amplified loci from each sample were pooled in an equimolar

ratio, and sequenced using a Roche 454 GS Junior system to >400X average coverage per sample. The same procedure has been performed using a distinct molecular clock locus, NETO1 (chr18, 5' GTTTTTGTAGGAGTAATTTGGTGG 3' and 5' CTCTCCCTCCCTCCCTAAAAC 3'). Both have been validated by showing that they report low methylation in non-dividing tissues (i.e. brain and heart), but age-related methylation due to cell divisions in mitotic tissues (i.e. colon) from autopsy samples of different patient ages (Fig. 5, B and C). The resulting single-molecule data were processed and analyzed as previously reported (18). A neighbor joining algorithm was used to reconstruct the phylogeny of the molecular clock patterns for each patient. We did not find samples displaying concerted hypo- or hyper-methylation at the analyzed loci. At the same time, tumor phylogenies were also inferred based on the underlying copy number profiles using the Tumult algorithm (19) and we note that these orthogonal methods yield highly similar results.

Drug concentration in the BrdU cell proliferation assay

Concentration for Cisplatin was 5 μg/ml and for Cediranib 5 μM. This concentration of Cisplatin is pharmacologically relevant since the peak serum level of the drug is about 5 μg/ml (20) and it has been used *in vitro* to test sensitivity of glioma cells to Cisplatin (21). As *in vitro* data on Cediranib and glioma cell cultures are limited, concentration of Cediranib was determined by testing two TICs (sp15 and sp19) with 4 nM to 80 μM as in a previous report on human gastric cancer cell lines (22). We found that Cediranib directly inhibited the growth of the two TICs with an IC_{50} of 5 μM.

MGMT promoter methylation

Analysis of MGMT promoter methylation was performed as previously described (23).

The methylation status of the MGMT promoter was also assessed by pyrosequencing as previously described (24). Templates for pyrosequencing were prepared using bisulfite converted DNA samples and run on the PyroMark ID pyrosequencer (Qiagen). The results are based on the average % methylation of the first 5 CpGs in accordance with the paper published by Quillien and colleagues (25).

References

1. Stummer W, Pichlmeier U, Meinel T, Wiestler OD, Zanella F, Reulen HJ. Fluorescence-guided surgery with 5-aminolevulinic acid for resection of malignant glioma: a randomised controlled multicentre phase III trial. The lancet oncology. 2006;7:392-401.

2. Piccirillo SG, Dietz S, Madhu B, Griffiths J, Price SJ, Collins VP, et al. Fluorescence-guided surgical sampling of glioblastoma identifies phenotypically distinct tumour-initiating cell populations in the tumour mass and margin. Br J Cancer. 2012;107:462-8.

3. Steiner J, Bernstein HG, Bielau H, Berndt A, Brisch R, Mawrin C, et al. Evidence for a wide extra-astrocytic distribution of S100B in human brain. BMC Neurosci. 2007;8:2.

4. Piccirillo SG, Combi R, Cajola L, Patrizi A, Redaelli S, Bentivegna A, et al. Distinct pools of cancer stem-like cells coexist within human glioblastomas and display different tumorigenicity and independent genomic evolution. Oncogene. 2009;28:1807-11.

5. Tropepe V, Sibilia M, Ciruna BG, Rossant J, Wagner EF, van der Kooy D. Distinct neural stem cells proliferate in response to EGF and FGF in the developing mouse telencephalon. Dev Biol. 1999;208:166-88.

6. Piccirillo SG, Reynolds BA, Zanetti N, Lamorte G, Binda E, Broggi G, et al. Bone morphogenetic proteins inhibit the tumorigenic potential of human brain tumour-initiating cells. Nature. 2006;444:761-5.

7. Bengtsson H, Wirapati P, Speed TP. A single-array preprocessing method for estimating full-resolution raw copy numbers from all Affymetrix genotyping arrays including GenomeWideSNP 5 & 6. Bioinformatics. 2009;25:2149-56.

8. Olshen AB, Bengtsson H, Neuvial P, Spellman PT, Olshen RA, Seshan VE. Parent-specific copy number in paired tumor-normal studies using circular binary segmentation. Bioinformatics. 2011;27:2038-46.

9. Curtis C, Shah SP, Chin SF, Turashvili G, Rueda OM, Dunning MJ, et al. The genomic and transcriptomic architecture of 2,000 breast tumours reveals novel subgroups. Nature. 2012;486:346-52.

10. Dunning MJ, Smith ML, Ritchie ME, Tavaré S. beadarray: R classes and methods for Illumina bead-based data. Bioinformatics. 2007;23:2183-4.

11. Sorlie T, Borgan E, Myhre S, Vollan HK, Russnes H, Zhao X, et al. The importance of gene-centring microarray data. Lancet Oncol. 2010;11:719-20; author reply 20-1.

12. Smih F, Desmoulin F, Berry M, Turkieh A, Harmancey R, Iacovoni J, et al. Blood signature of pre-heart failure: a microarrays study. PLoS One. 2011;6:e20414.

13. Verhaak RG, Hoadley KA, Purdom E, Wang V, Qi Y, Wilkerson MD, et al. Integrated genomic analysis identifies clinically relevant subtypes of glioblastoma characterized by abnormalities in PDGFRA, IDH1, EGFR, and NF1. Cancer Cell. 2010;17:98-110.

14. Chin SF, Daigo Y, Huang HE, Iyer NG, Callagy G, Kranjac T, et al. A simple and reliable pretreatment protocol facilitates fluorescent in situ hybridisation on tissue microarrays of paraffin wax embedded tumour samples. Mol Pathol. 2003;56:275-9.

15. Pole JC, Courtay-Cahen C, Garcia MJ, Blood KA, Cooke SL, Alsop AE, et al. High-resolution analysis of chromosome rearrangements on 8p in breast, colon and pancreatic cancer reveals a complex pattern of loss, gain and translocation. Oncogene. 2006;25:5693-706.

16. Sottoriva A, Spiteri I, Piccirillo SG, Touloumis A, Collins VP, Marioni JC, et al. Intratumor heterogeneity in human glioblastoma reflects cancer evolutionary dynamics. Proc Natl Acad Sci U S A. 2013;110:4009-14.

17. Yatabe Y, Tavaré S, Shibata D. Investigating stem cells in human colon by using methylation patterns. Proc Natl Acad Sci U S A. 2001;98:10839-44.

18. Sottoriva A, Spiteri I, Shibata D, Curtis C, Tavaré S. Single-molecule genomic data delineate patient-specific tumor profiles and cancer stem cell organization. Cancer Res. 2013;73:41-9.

19. Letouze E, Allory Y, Bollet MA, Radvanyi F, Guyon F. Analysis of the copy number profiles of several tumor samples from the same patient reveals the successive steps in tumorigenesis. Genome Biol. 2010;11:R76.

20. Iwadate Y, Tagawa M, Fujimoto S, Hirose M, Namba H, Sueyoshi K, et al. Mutation of the p53 gene in human astrocytic tumours correlates with increased resistance to DNA-damaging agents but not to anti-microtubule anti-cancer agents. Br J Cancer. 1998;77:547-51.

21. Datta K, Shah P, Srivastava T, Mathur SG, Chattopadhyay P, Sinha S. Sensitizing glioma cells to cisplatin by abrogating the p53 response with antisense oligonucleotides. Cancer Gene Ther. 2004;11:525-31.

22. Takeda M, Arao T, Yokote H, Komatsu T, Yanagihara K, Sasaki H, et al. AZD2171 shows potent antitumor activity against gastric cancer over-expressing fibroblast growth factor receptor 2/keratinocyte growth factor receptor. Clin Cancer Res. 2007;13:3051-7.

23. Esteller M, Hamilton SR, Burger PC, Baylin SB, Herman JG. Inactivation of the DNA repair gene O6-methylguanine-DNA methyltransferase by promoter hypermethylation is a common event in primary human neoplasia. Cancer Res. 1999;59:793-7.

24. Malley DS, Hamoudi RA, Kocialkowski S, Pearson DM, Collins VP, Ichimura K. A distinct region of the MGMT CpG island critical for transcriptional regulation is preferentially methylated in glioblastoma cells and xenografts. Acta Neuropathol. 2011;121:651-61.

25. Quillien V, Lavenu A, Karayan-Tapon L, Carpentier C, Labussiere M, Lesimple T, et al. Comparative assessment of 5 methods (methylation-specific polymerase chain reaction, MethyLight, pyrosequencing, methylation-sensitive high-resolution melting, and immunohistochemistry) to analyze O6-methylguanine-DNA-methyltranferase in a series of 100 glioblastoma patients. Cancer. 2012;118:4201-11.

Supplementary Figure Legends

Supplementary Figure S1. Identification of the SEZ in human GB. (A, **B**) **Top panel.** Illustrative MRI scans of two additional GBs (coronal view in **A** and axial view in **B**). Samples were collected from the tumor mass (T) and the sub-ependymal zone (SEZ) (red dots indicate tissue sampling). **Middle panel.** Peri-operative images of visible fluorescence from T and SEZ indicating tumor tissue in these areas. **Bottom panel.** Haematoxylin and Eosin staining of T and SEZ. Cardinal GB features (high mitotic index, nuclear atypia, mitosis and microvascular proliferation) are present in T (left) and SEZ (centre). Scale bar, 100 μm. **(C) Top panel.** Double-labelling with markers of glial and precursors cells (Gfap in green and Nestin in pink) confirms the results shown in Fig. 1. **Bottom panel.** Weak expression of the neuronal marker Tuj1 is observed in T and SEZ (in pink in a double staining with Gfap in green). **Right.** The MIB1 staining shows similar numbers of mitotic cells in T and SEZ (green). Tissues have been counterstained with DAPI (blue). Scale bar, 100 μm. The table shows a quantitative analysis of the % of +ve cells for Gfap, Nestin, Tuj1 and the MIB1 index.

Supplementary Figure S2. Sampling of the SEZ. Left. Haematoxylin and Eosin staining reveals the typical morphology of the SEZ. The dashed line indicates the ependymal layer. **Right.** Staining for the ependymal marker S100β confirms the presence of ependymal cells. Cells have been counterstained with DAPI (blue). The arrow indicates the ependymal layer. Scale bar, 50 μm.

Supplementary Figure S3. Real-time analysis on tissues: markers of glial, precursor, stem cells and proliferation. Analysis of expression of a panel of markers for precursor and glial cells (*Nestin* and *Gfap*), stem cells (*Sox2*) and proliferation (*MIB1*) has been performed on T and SEZ tissues. This analysis shows increased expression of Gfap in SEZ in agreement with the data shown in Figure 1, B and C. Asterisks indicates statistical significance (p-value <0.05) in comparison to

the T of each patient. All error bars represent s.e.m.

Supplementary Figure S4. Common CNA breakpoints between the SEZ and the corresponding tumor mass. For each patient we report an example of chromosome where it is evident that the SEZ and T samples from the same tumor share common breakpoints. This is evidence of a common origin of the two from the same patient.

Supplementary Figure S5. FISH results for EGFR, MET and PTEN between T and SEZ in 3 GBs. FISH confirms the copy number results for EGFR in patients sp49 (in **A**) and sp58 (in **B**) and the results for MET in sp49T and sp58 (in **C**). SNP plots show the status of EGFR and MET in each sample. The position of the gene is shown by a black box. Orange denotes EGFR or MET and green the centromeric probe of chromosome 7 (centr 7), magnification 63X. In **A**, normal tissue of sample sp49 has been used as internal control. This tissue shows 2 copies of EGFR and centr 7 as expected by normal cells. **(D)** A1219 and A887 have been used as controls. Both have trisomy of chromosome 7 (green) but only A1219 contains 68 copies of EGFR (orange), whereas A887 shows no amplification of the gene (magnification 63X). **(E)** Sp14SEZ cells and sp14T cells show gain of the region of chromosome 7 including EGFR and centr 7, in agreement with the copy number results. Sp14SEZ cells have generally 4 copies of EGFR (red) and centr 7 (green). **(F)** Both sp14SEZ and T cells have more than two copies of MET (red) and centr 7 (green). Generally, sp14SEZ cells have 4 copies of MET and centr 7 in agreement with the results shown in Fig. 2A. **(G)** A focal deletion of PTEN (orange) is found in sp14SEZ and T cells. The centromeric probe of chromosome 10 (centr 10) is shown in green. The normal control metaphases show 2 copies of chromosome 7 and EGFR, MET (in **E** and **F**) and 2 copies of chromosome 10 and PTEN (in **G**) (magnification 63X). **(H)** SNP plots of sp14 SEZ and T cells show the status of EGFR, MET and PTEN. The position of the gene is shown by a black box.

Supplementary Figure S6. CNA breakpoints between T and SEZ and the corresponding cells. The copy number profiles of T and SEZ in patient sp14 are highly similar, in particular they show common gains/amplifications in chromosomes 1, 7 (EGFR, CDK6, MET), 20 and 21, and a loss/deletion in chromosome 10 (PTEN). We found a largely overlapping profile between cells and tissues. The corresponding cell lines share all these aberrations with the tissues, but both also display an evident loss of chromosome 13, suggesting an *in vitro* aberration that, due to its magnitude, may pose concerns in using cell lines as surrogate of the original tumor tissue.

Supplementary Figure S7. Growth curve analysis of TICs from 5 additional GBs. Growth curve analysis reveals that cells derived from T and SEZ are capable of long-term *in vitro* propagation. Sp14, 17, 20, 37 and 52 are five additional patients of the dataset.

Supplementary Figure S8. Clonogenic index and multipotency of SEZ cells. Left. Clonogenic index of T and SEZ cells provides an estimation of the number of stem cells/precursors in the culture. Three paired T and SEZ cells are shown. **Right.** Immunofluorescence staining of SEZ cells: left, all the cells express the neural precursor marker Nestin (red); middle, Gfap (green) and Tuj1 (red) are used as markers for astroglial and neuronal cells, upon differentiation. Note a double positive Gfap/Tuj1 cell (yellow); right, an SEZ cell expressing the oligodendroglial marker O4 (red). Scale bars, 20 μm.

Supplementary Figure S9. Immunofluorescence analysis for "stem cell markers" on T and SEZ cells. Immunofluorescence analysis for stem cell markers (Nestin, A2B5, CD133 and CD15) on T and SEZ cells isolated from sp17 (in **A**) and from sp20 (in **B**). Whereas Nestin is widely expressed in T and SEZ, A2B5-, CD133- and CD15-positive cells are rarely expressed with the exception of some CD15+ve cells found in T cells from the case shown in **A**. Cells have been counterstained with DAPI (blue). Scale bars, 50 μm. The table shows a quantitative analysis of the

expression of these markers for T and SEZ cells.

Supplementary Figure S10. Survival analysis of 5 additional GBs. Cumulative Kaplan-Meier survival analysis from 5 additional GBs reveals that T and SEZ are tumorigenic. T cells are highly tumorigenic and there is a statistically significant difference (*p*-value <0.05) between the survival of animals injected with these cells *versus* those injected with SEZ cells. The table summarizes the number of tumors/injections and the type of cells used (primary cells or briefly cultured cells).

Supplementary Figure S11. Analysis of *in vivo* properties of TICs from SEZ. (A) The table summarizes the data based on Haematoxylin and Eosin staining confirming absence of migration of SEZ cells towards the two neurogenic niches in the adult mouse brain, i.e. the SEZ and hippocampus. No migration towards anatomical regions such as olfactory bulbs and cerebellum was observed. In presence of a large tumor formation (derived from SEZ3) we found that the tumor cells infiltrate the SEZ and corpus callosum (CC). This behaviour mimics that of TICs isolated from T under the same experimental setting. **(B)** We present here a reconstruction for a tumor derived from SEZ1. The tumor develops from the injection site, the striatum (ST) and shows dorso-ventral and rostro-caudal extension. Using this approach, we show that there is no migration towards the ventricle (V), the cerebellum (C) and the olfactory bulbs (OB). This has been obtained using serial tissue sections stained for Haematoxylin and Eosin. Two representative sections are presented here. **(C)** On the left, Haematoxylin and Eosin staining of a brain injected with SEZ3 cells shows tumor cells in proximity of the lateral ventricle (V) and along the corpus callosum (CC) and SEZ. On the right, we show a statistically significant increase in numbers of cells in the SEZ and corpus callosum (CC) (*p*-value <0.05 for each of these regions in comparison to control brains).

Supplementary Figure S12. BrdU cell proliferation assay of 7 paired TICs using 50µM TMZ. Cell proliferation assay was initially performed using the physiological TMZ concentration of 50

μM as reported in brain and plasma. Response to this concentration was very poor, with only sp12 (T and SEZ) responding. Red indicates T compartment, blue SEZ. Asterisks indicate statistical significance.

Supplementary Figure S13. BrdU cell proliferation assay of additional 20 TICs for dose escalation analysis with TMZ. (A) Four of the twenty samples are shown. These TICs are all derived from the T compartment. Sp15 and sp19 do not respond to TMZ. In contrast, sp21 and sp36 respond to ≥ 500μM concentration. **(B)** Table summarizing the 20 TICs tested. Only 20% of them respond to ≥ 500μM concentration of TMZ (sp21, sp28, sp34, sp36, highlighted in green boxes). Asterisks indicate statistical significance.

Supplementary Figure S14. BrdU cell proliferation assay of additional 4 paired TICs. The cell proliferation assay shown in Fig. 4 was performed on additional 4 patients. We tested response to TMZ (in **A**), Cisplatin and Cediranib (in **B**). Sp14 does not respond to TMZ in either the T or the SEZ, except at 2.5 mM TMZ for T; only sp14T shows a significant response to Cisplatin and Cediranib. Conversely, sp23 shows a similar response between T and SEZ with the latter responding slightly better to treatment with TMZ, Cisplatin and Cediranib. In sp37 the differential pattern of response is more pronounced with respect to TMZ, Cisplatin and Cediranib with T being more sensitive to these treatments in comparison to SEZ. Sp42T is resistant to TMZ and Cediranib but not to Cisplatin. In contrast, the SEZ does respond significantly to ≥ 100 μM concentration of TMZ and to Cisplatin and Cediranib. Asterisks indicate statistical significance.

Supplementary Figure S15. MGMT promoter status for T and SEZ of the analyzed 7 paired TICs by PCR. 7 out of the 8 paired TICs used for the BrdU cell proliferation assay were analyzed for MGMT promoter methylation status by PCR using specific primer pairs for the methylated or the modified unmethylated DNA (13). A visible 81-bp PCR product in T and SEZ of sp17, 20 and

42 indicates the presence of methylation, whereas a 109-bp PCR product in T and SEZ of sp14, 23, 37 and 52 indicates unmethylation. MSP=methylation-specific PCR, USP=unmethylation-specific PCR.

Supplementary Figure S16. Immunofluorescence analysis for Vegfr2 on T and SEZ cells. Top. Immunofluorescence has been performed on T and SEZ cells isolated from three GBs (sp13, sp20 and sp37). We could detect expression of Vegfr2 in all the cell populations. **Bottom.** A quantitative analysis of Vegfr2+ve cells suggests similar expression in T and SEZ cells from the same GB. Cells have been counterstained with DAPI (blue). Scale bars, 50 μm.

Supplementary Figure S17. BrdU cell proliferation assay of control lines. Pattern of response to TMZ, Cisplatin and Cediranib of U87 and two different cell lines of human fetal neural stem cells (HFNSC and HFNSC1). U87, HFNSC and HFNSC1 have been subjected as controls to the same BrdU cell proliferation assays. As expected, U87 significantly respond to TMZ, Cediranib and Cisplatin. In contrast, HFNSC and HFNSC1 are resistant to all treatments. Asterisks indicate statistical significance.

Supplementary Figure S18. A model of residual disease in human GB. (A) Residual disease in human GB can be found in the SEZ (blue cells), the tumor mass is indicated by red cells. Identification of residual disease in SEZ is based on visible fluorescence during surgery. SEZ and T cells are endowed with self-renewal ability and sphere-forming capacity *in vitro. In vivo*, all these cells generate tumors. When treated with drugs, SEZ and T cells from the same GB respond differently. **(B)** Table summarizing the major characteristics of T and SEZ.

Supplementary Figure S19. Growth curve of cells from two SEZ in absence of fluorescence. Growth curve analysis of cells derived from non-fluorescent SEZ (sp2 and sp19) show that in

absence of fluorescence in the SEZ it is not possible to generate self-renewing, long-term expanding TICs. This material derives from two patients with no extension of fluorescence to the SEZ.

Supplementary Table Legends

Supplementary Table S1. Histological features of T and SEZ tissues. The table shows a summary of the histological values obtained from T and SEZ of the 14 patients included in this study. Necrosis: 0 = no necrosis and 1 = focal necrosis involving <20% of the tissue area. Tumor score: 0 = cellular tumor, and 1 = highly cellular tumor involving ≥70% of the tissue.

Supplementary Table S2. Summary of the patients and samples used for the genomic analysis. **(A)** The table summarizes the samples collected for the genomic study and those available for gene expression and SNP array analysis. The "YES" and "NO" indicate samples with RNA/DNA available or unavailable (due to quality control failure) for the downstream genomic analysis. In total, we collected 14 patients out of the 42 and of these we included 9 patients for gene expression studies and 8 patients for copy number profiles (6 of whom were common to both analyses). **(B)** The clinical information of the 11 GB patients included in the genomic analysis are shown here. The corresponding samples have been used for genomic analysis and *in vitro*/*in vivo* assays. These patients were prospectively recruited through the neurosurgical research clinic. All patients had suspected high-grade glioma (HGG) on imaging review by a consultant neuroradiologist at the MDT. This study included 8 men and 3 women. Mean age was 63.8 years at diagnosis (range 55-79). WHO performance status before surgery was 0-2. All the patients received 5-ALA preoperatively, three of them also received chemotherapy with Gliadel at the end of the surgery. Treatment post-surgery was chemo-and radio-therapy followed by chemotherapy (ChemoRT), whole brain radio-therapy (WBRT) or short course of radiotherapy (SCRT). Four patients did not receive any treatment.

Supplementary Table S3. Gene ontology terms bearing at least one differentially expressed gene between SEZ and T. Differentially expressed genes between SEZ and T were identified using the R package HDTD. The table shows gene ontology (GO) terms whose genes are differentially expressed. C= cellular component, F= molecular function, P= biological process.

Supplementary Table S4. MGMT methylation level using pyrosequencing. A total of 16 samples were subjected to pyrosequencing to assess the MGMT methylation status. The results shown in the table are based on the average % methylation of the first 5 CpGs sequenced. This is in accordance with the paper published by Quillien and colleagues ((25) of the Supplementary Experimental Procedure reference list).

Supplementary Table S5. Summary of the survival of 8 GB patients and response to drugs by TICs from T and SEZ. The table summarizes the overall survival of the 8 patients whose TICs were used for the BrdU cell proliferation assay. The MGMT methylation status is taken from the pyrosequencing results. Of note, TICs from T of sp42 and sp52 were not sensitive to TMZ *in vitro* and in both cases survival was poor. M=methylated, u=unmethylated, y=yes, n=no, PE=pulmonary embolus, Rx=radiotherapy.

Supplementary Table S6. Expression of PDGF and VEGF receptors in T and SEZ. There is no significant difference in PDGFRA, PDGFRB and VEGFR2 expression in T compared to SEZ (our expression data lacks the information about VEGFR1 and VEGFR3).

Supplementary Figure S1. Identification of the SEZ in human GB.

A

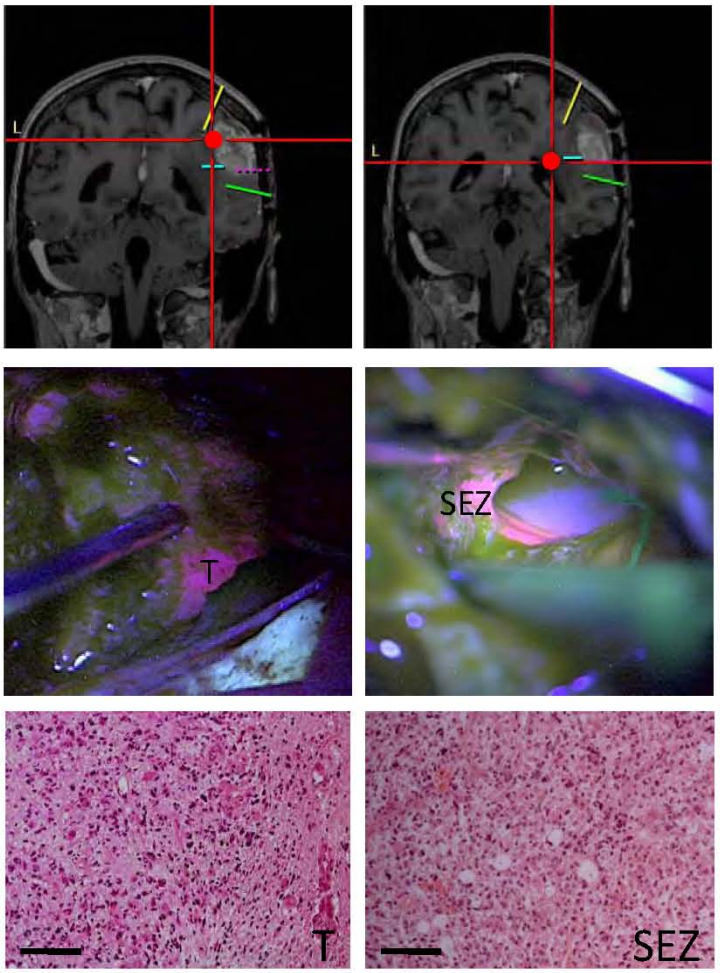

B

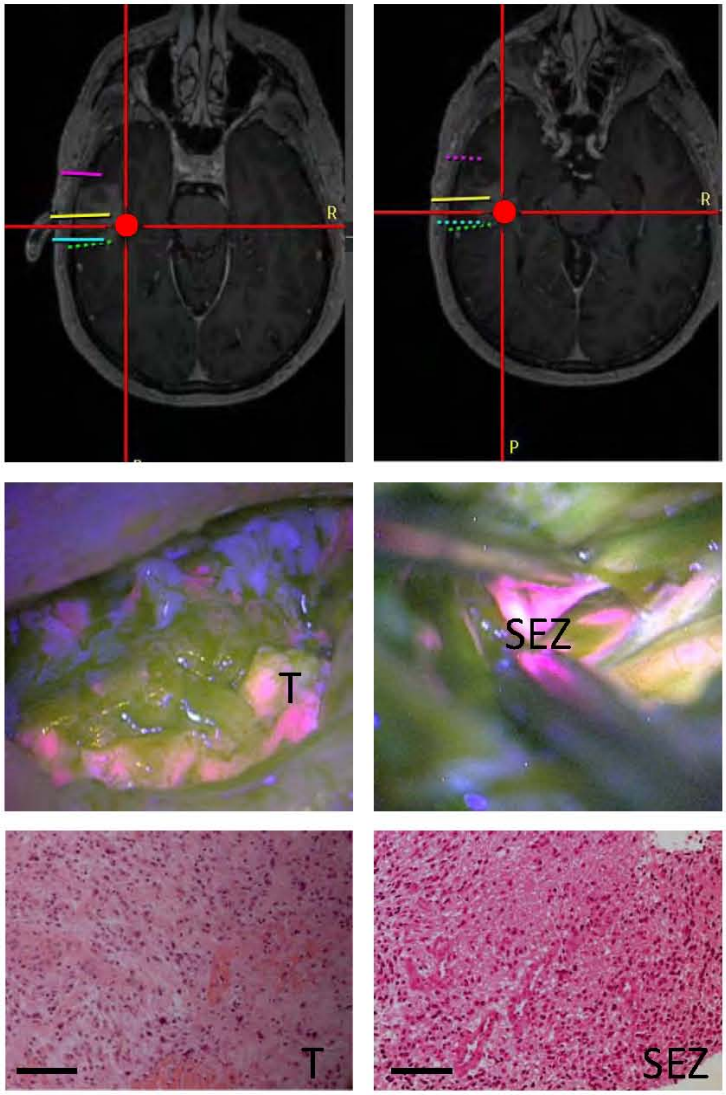

C

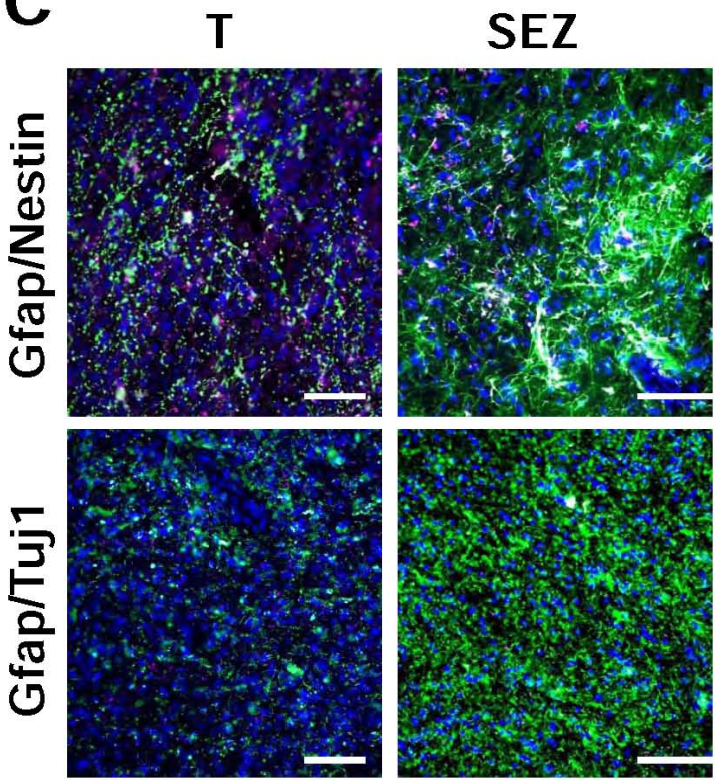

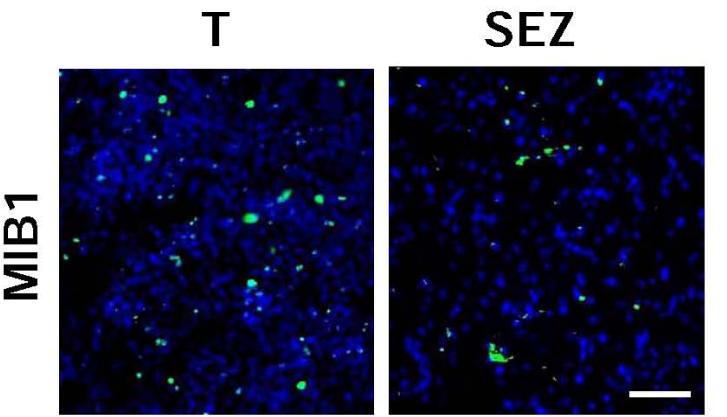

	T	SEZ
Gfap-IR cells (%)	42,3±0,6	73,9±3,3
Nestin-IR cells (%)	24,0±6,4	26,7±4,9
Gfap-IR cells (%)	33,8±4,6	81,5±8,2
Tuj1-IR cells (%)	6,7±2,8	7,1±3,5

	T	SEZ
MIB1 index	20.5±2	18.1±1

Supplementary Figure S2. Sampling of the SEZ.

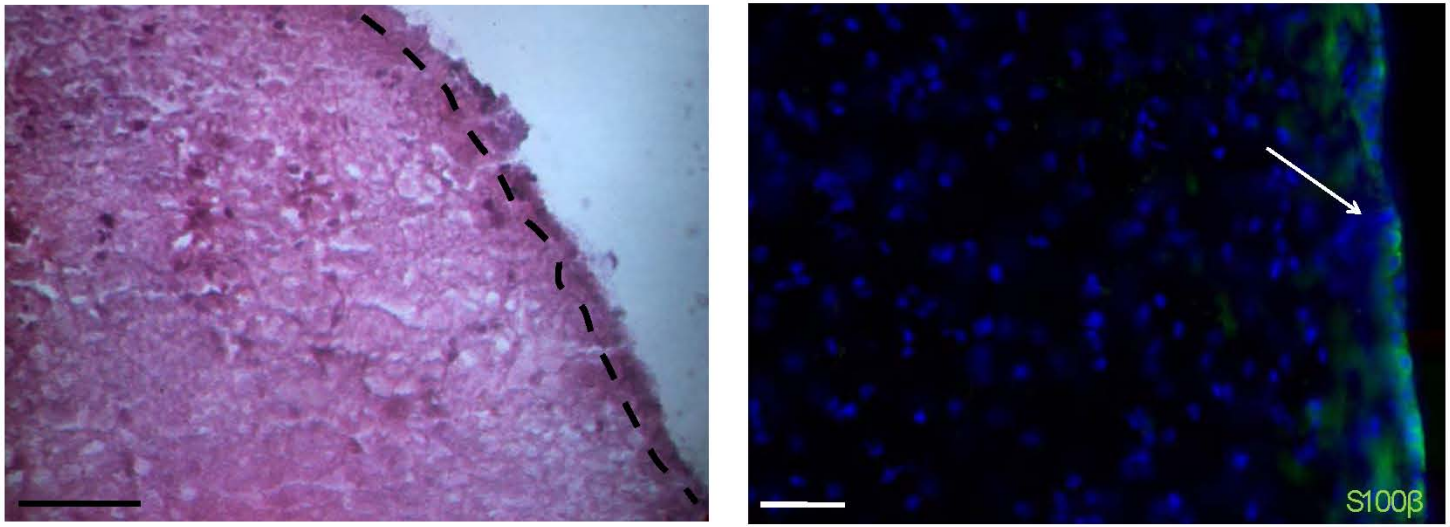

Supplementary Figure S3. Real time analysis on tissues: markers of glial, precursor, stem cells and proliferation.

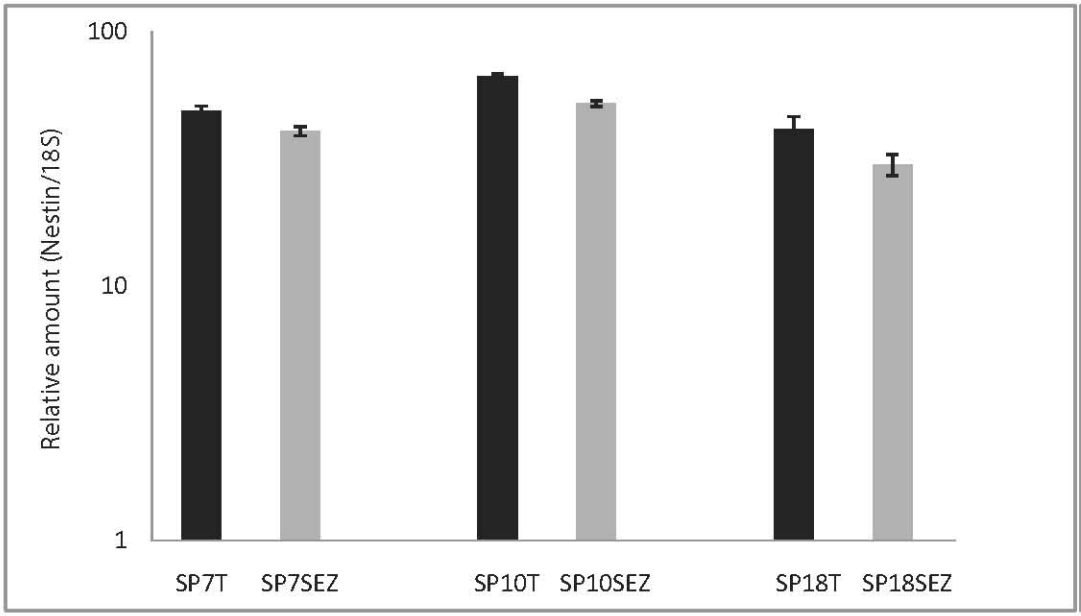

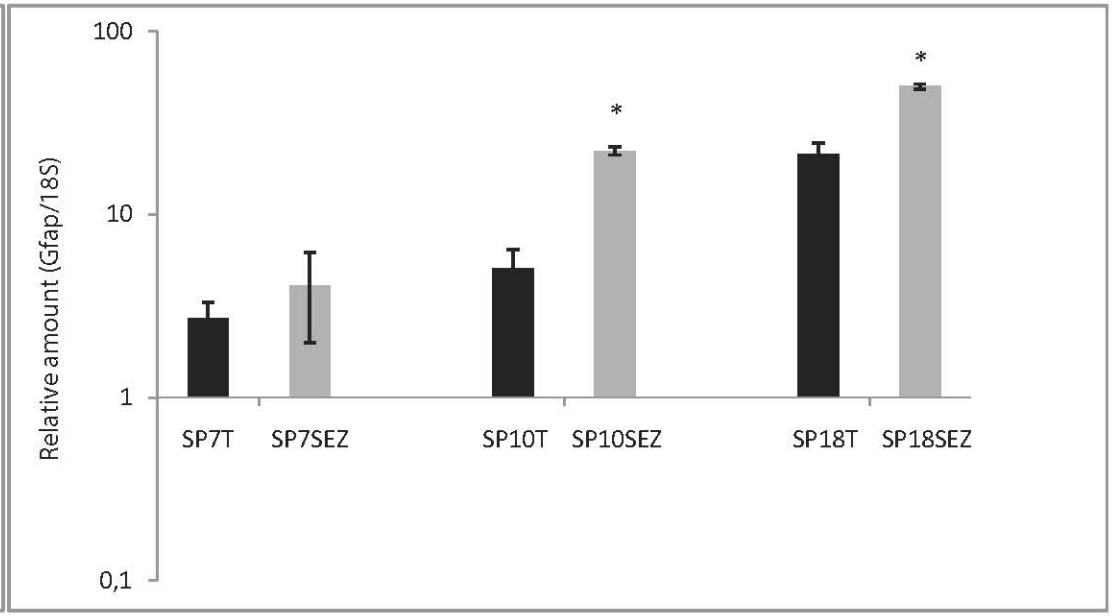

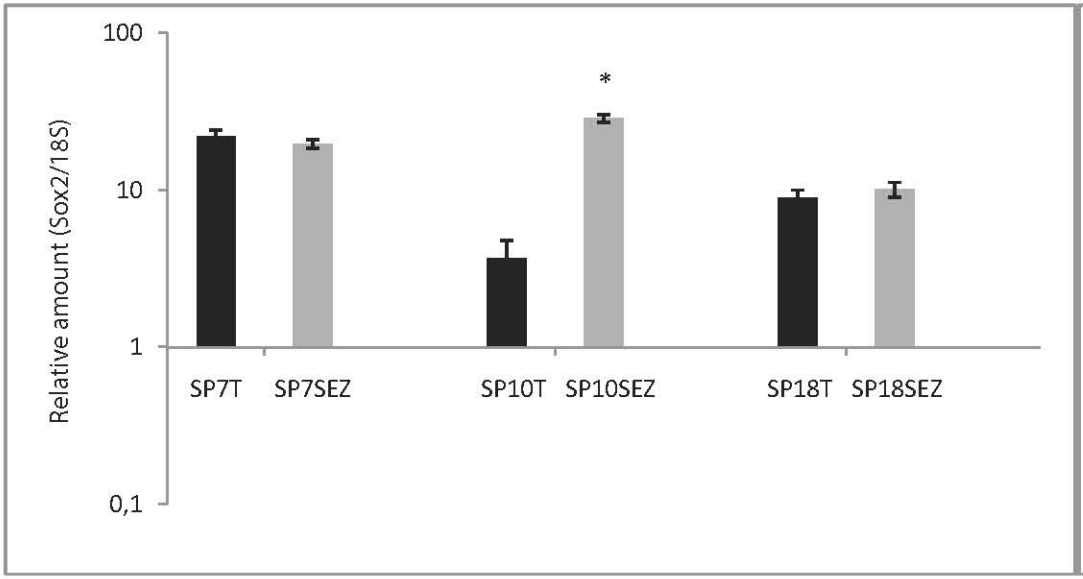

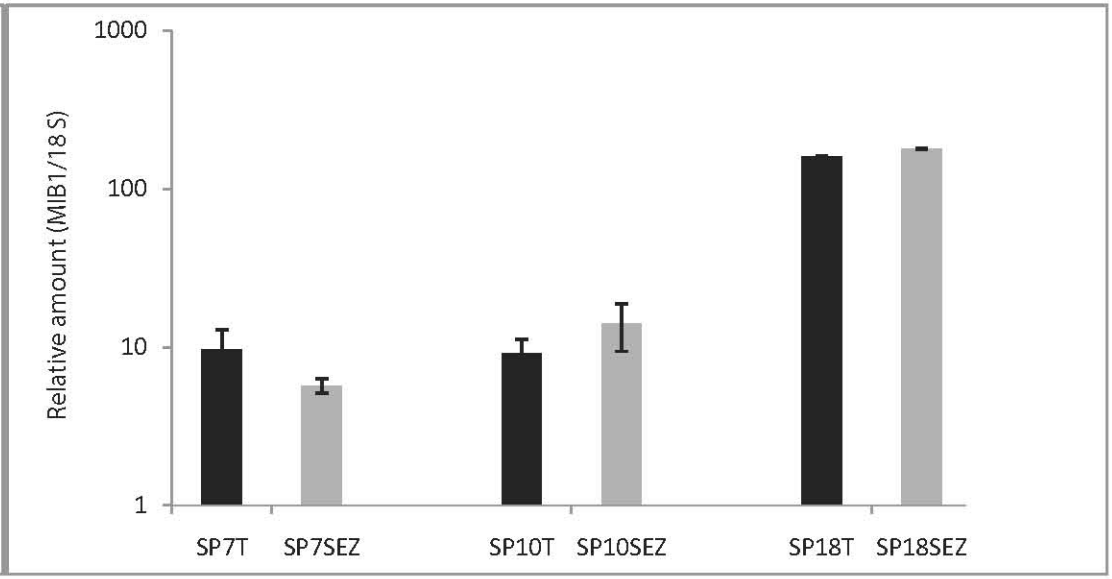

Supplementary Figure S4. Common CNA breakpoints between the SEZ and the corresponding tumor mass.

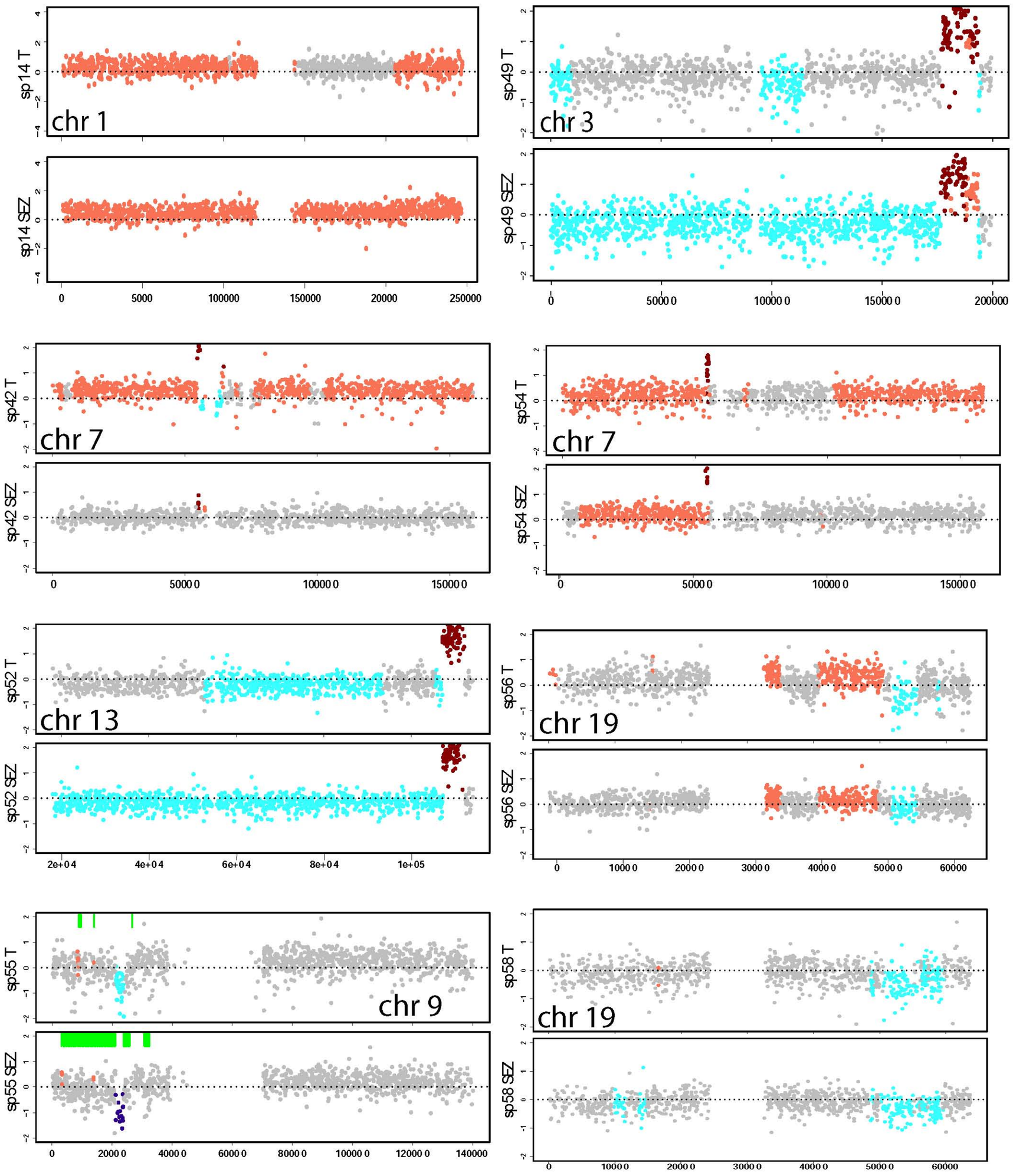

Supplementary Figure S5. FISH results for EGFR, MET and PTEN between T and SEZ in 3 GBs.

A

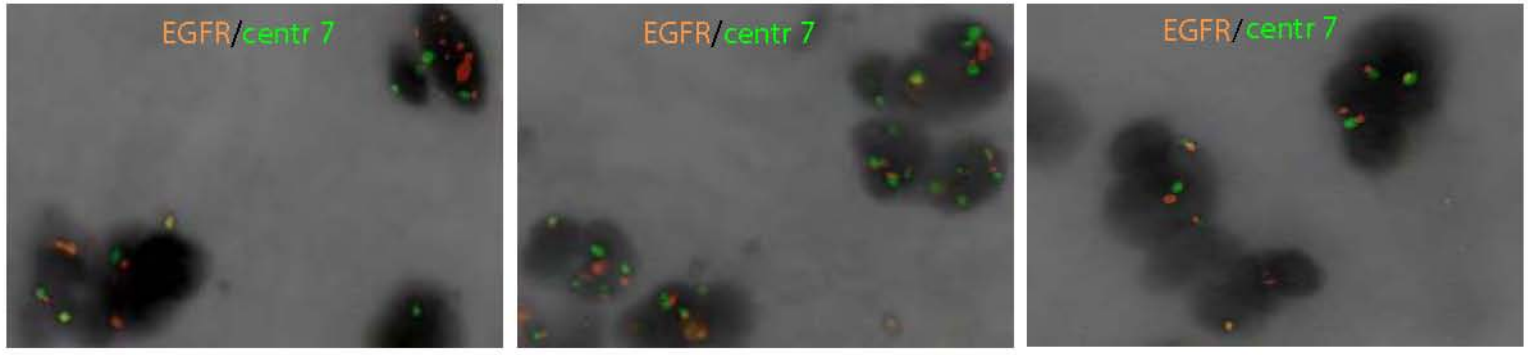

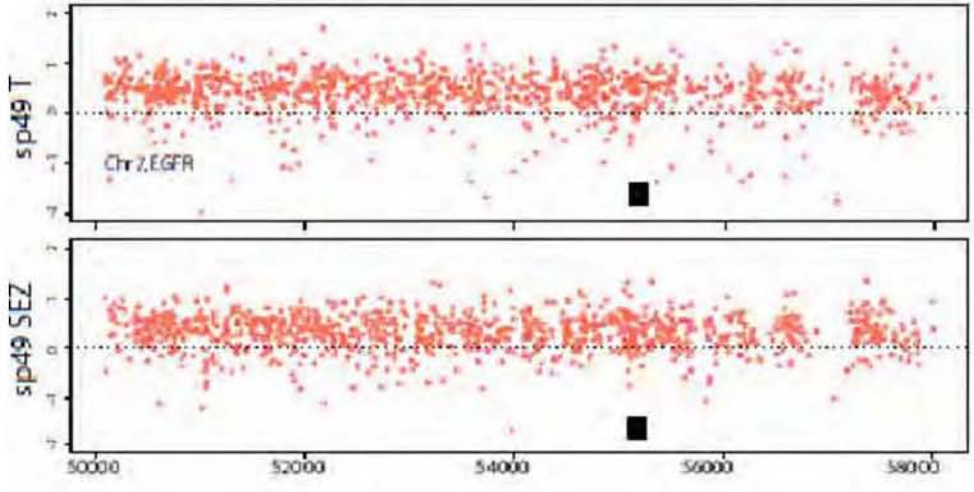

B

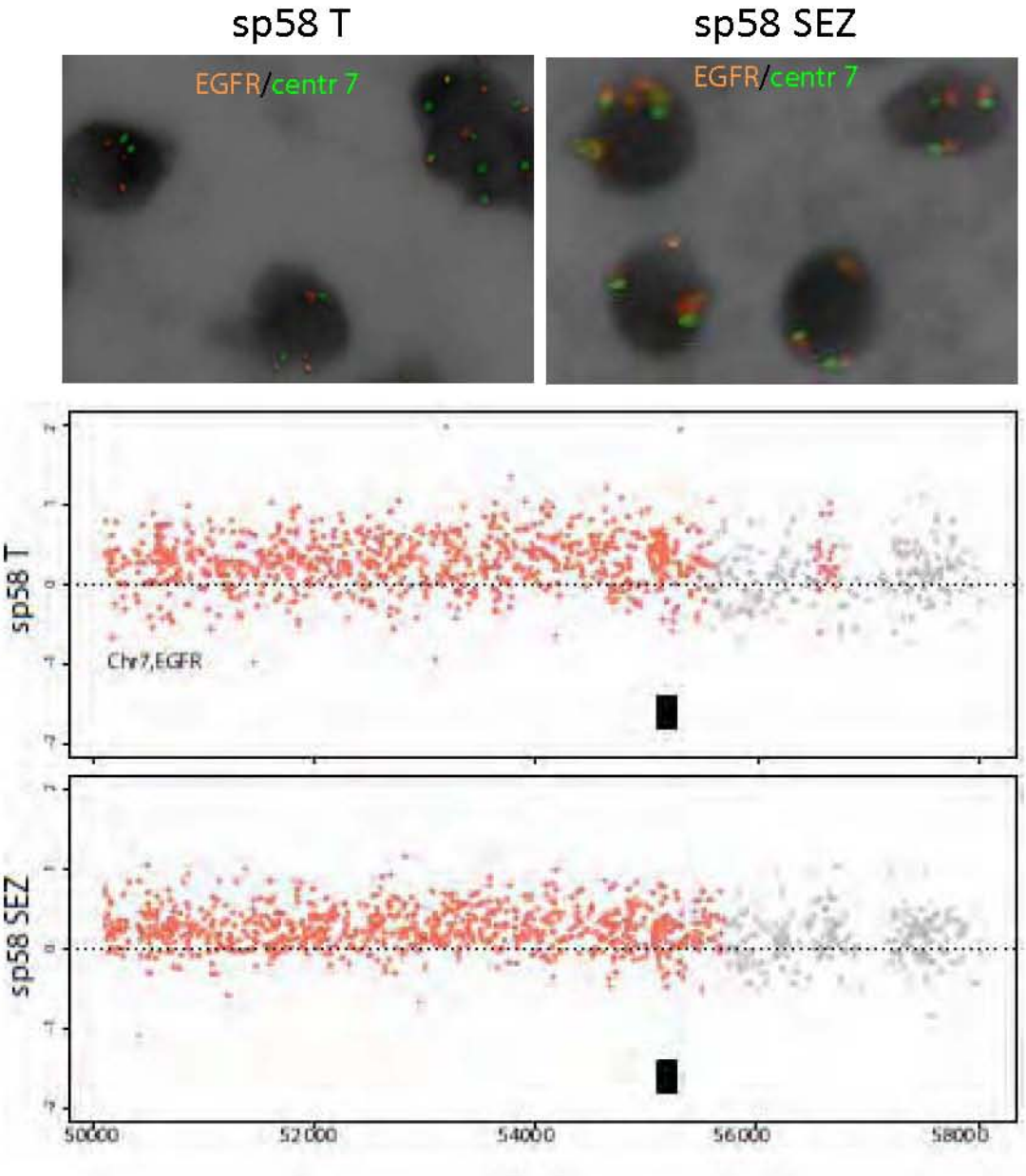
sp58 T
sp58 SEZ
EGFR/centr 7
EGFR/centr 7
sp58 T
Chr7,EGFR
sp58 SEZ
50000
52000
54000
56000
58000

C

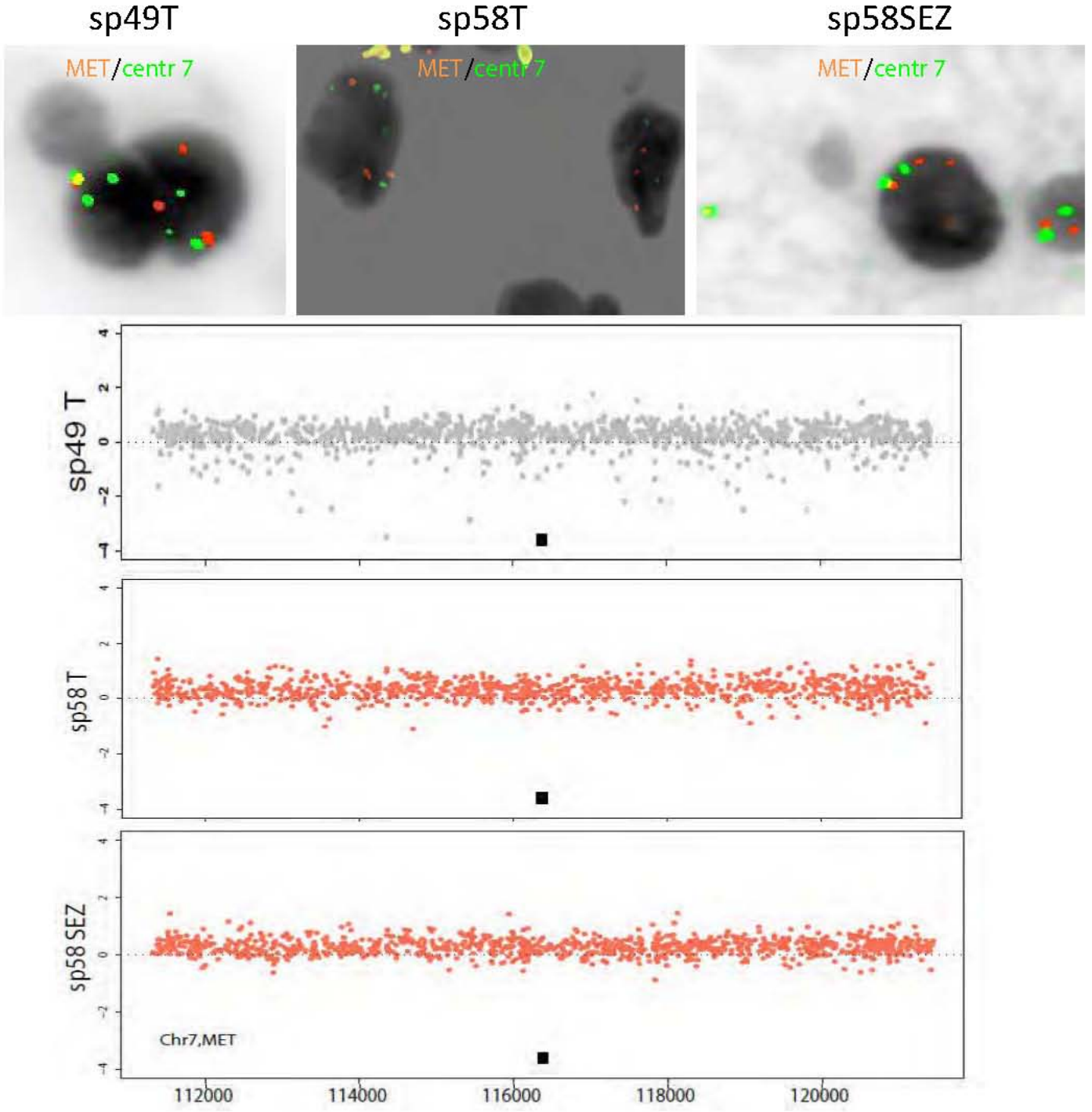
sp49T
sp58T
sp58SEZ
MET/centr 7
MET/centr 7
MET/centr 7
sp49 T
sp58 T
sp58 SEZ
Chr7,MET
112000
114000
116000
118000
120000

D

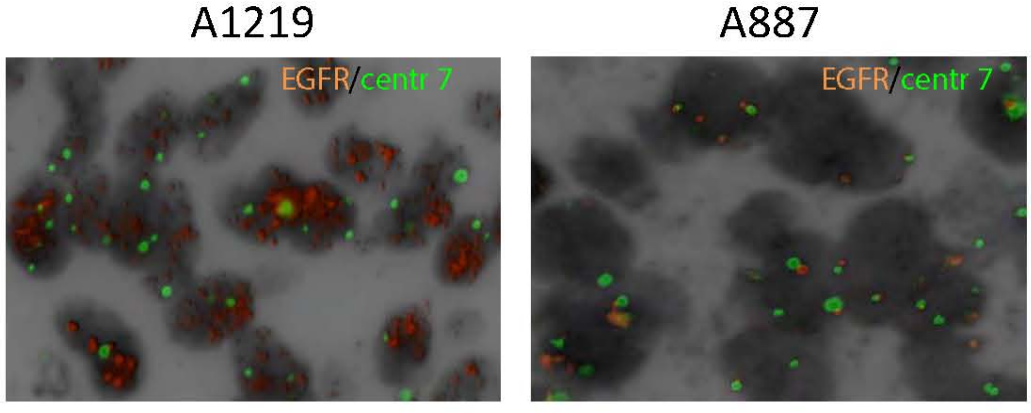

E

Normal control metaphases

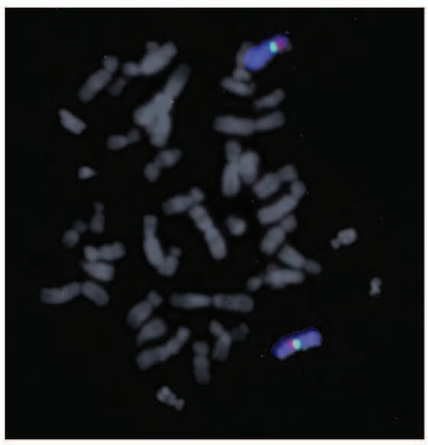

Chr7paint-BIO-Cy5 (Blue)
Chr7-CEN (Green)
EGFR (Red)

SP14SEZ cells

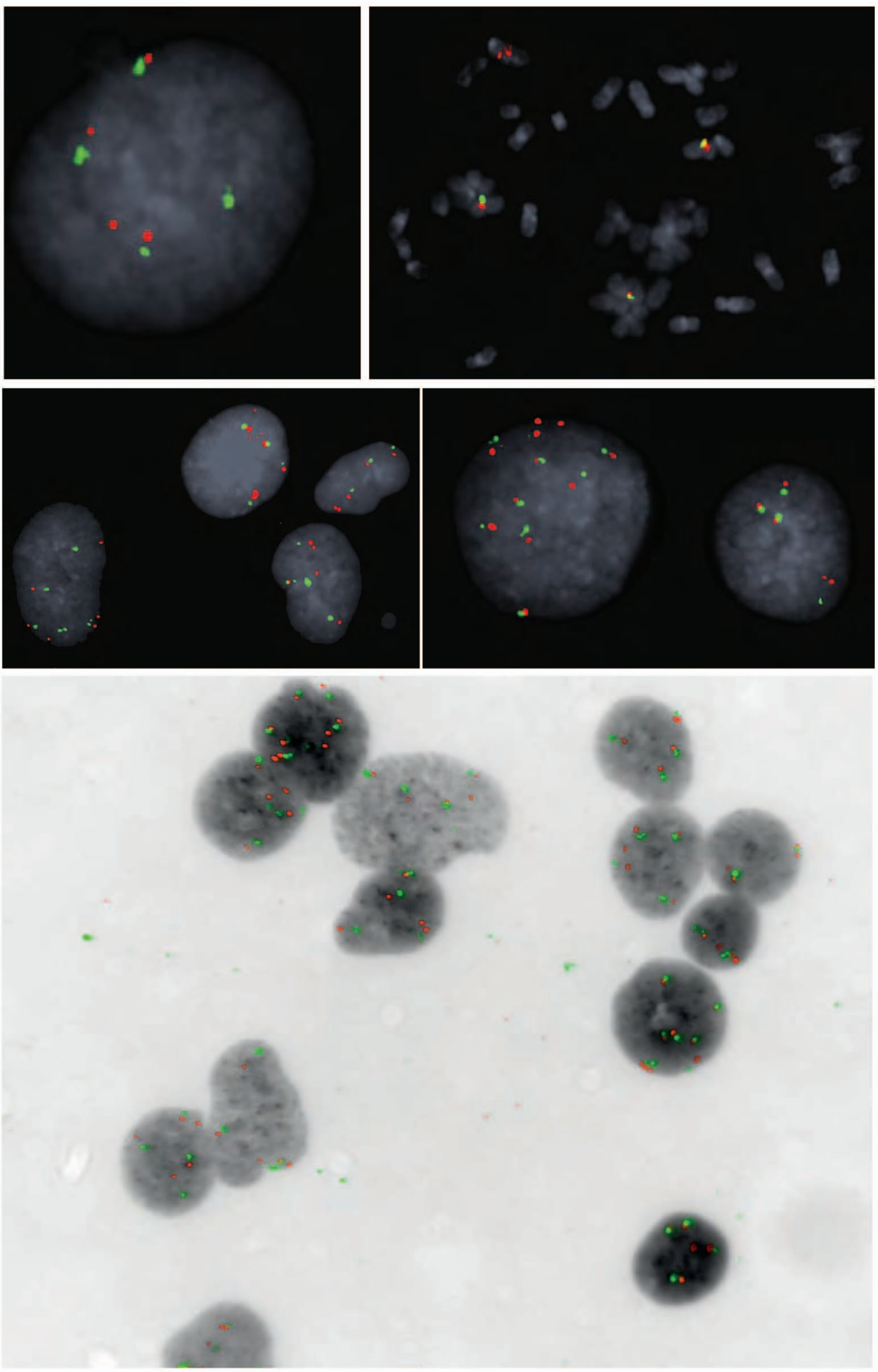

SP14T cells

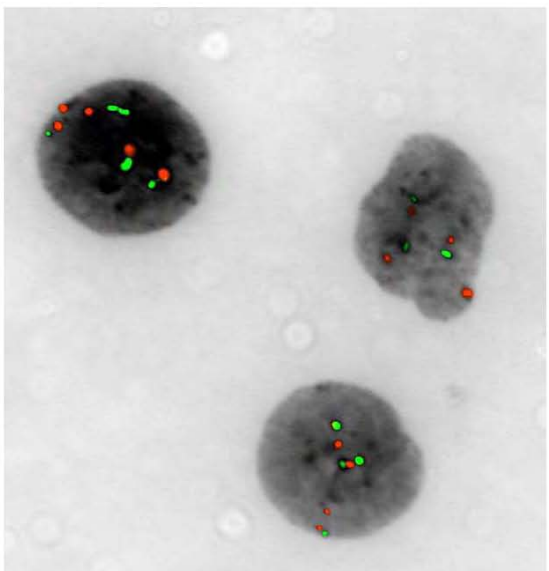

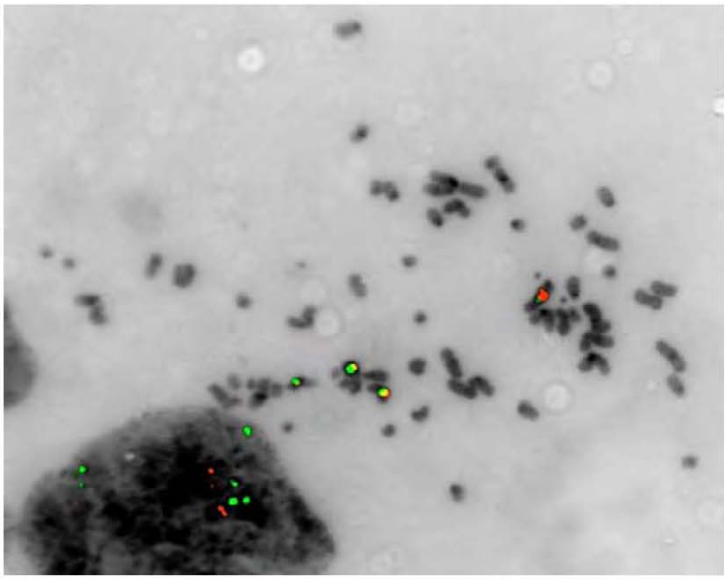

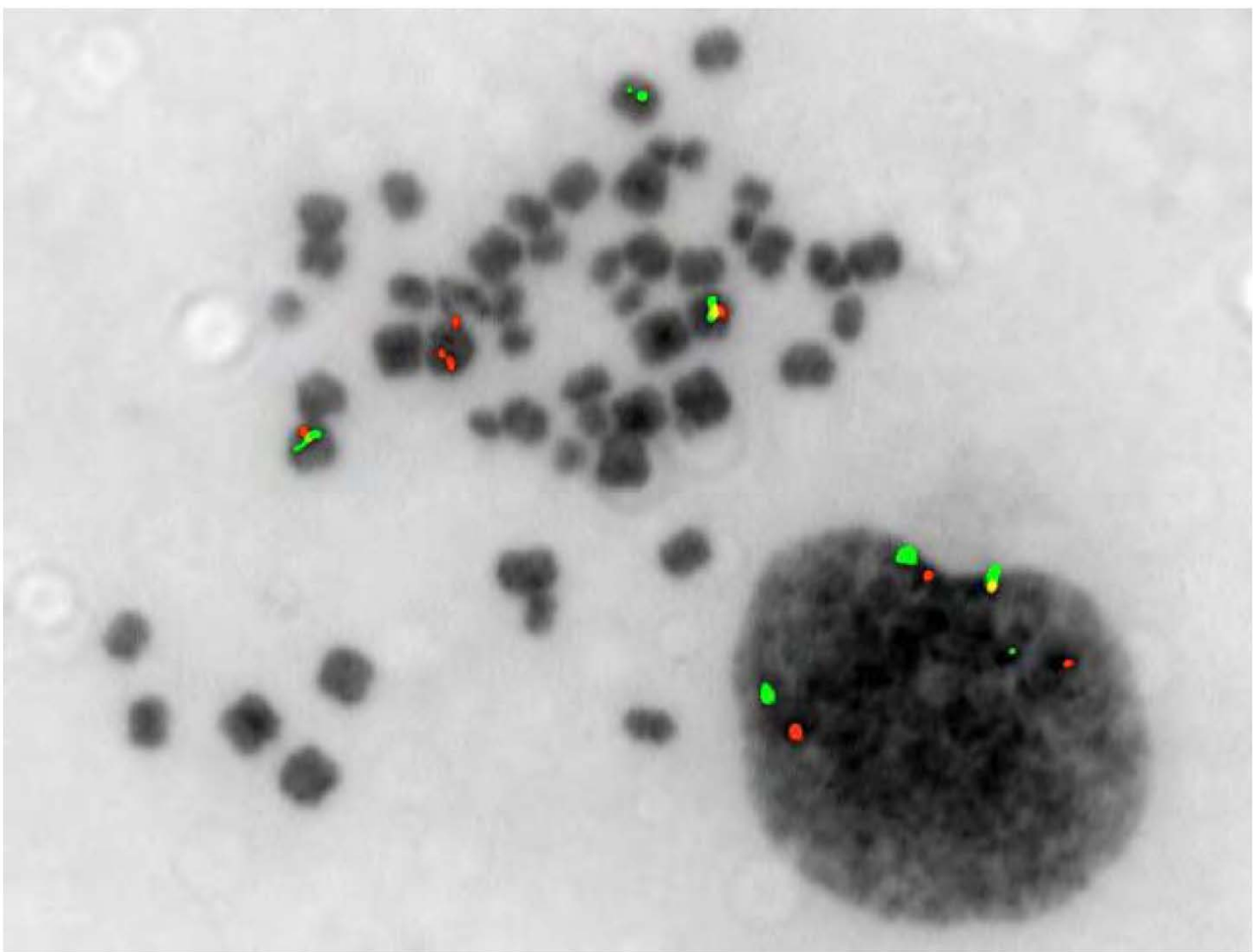

F

Normal control metaphases

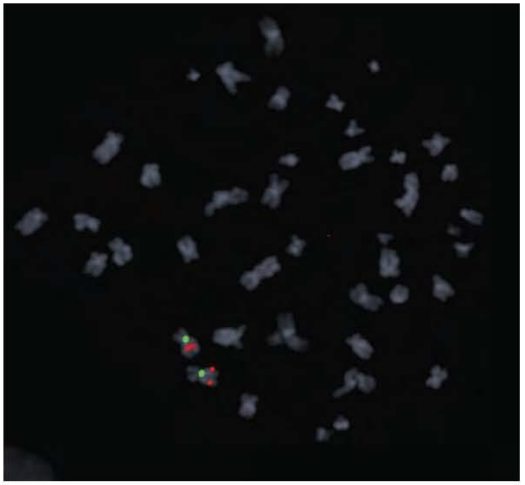

Chr7paint-BIO-Cy5 (Blue)
Chr7-CEN (Green)
MET (Red)

SP14SEZ cells

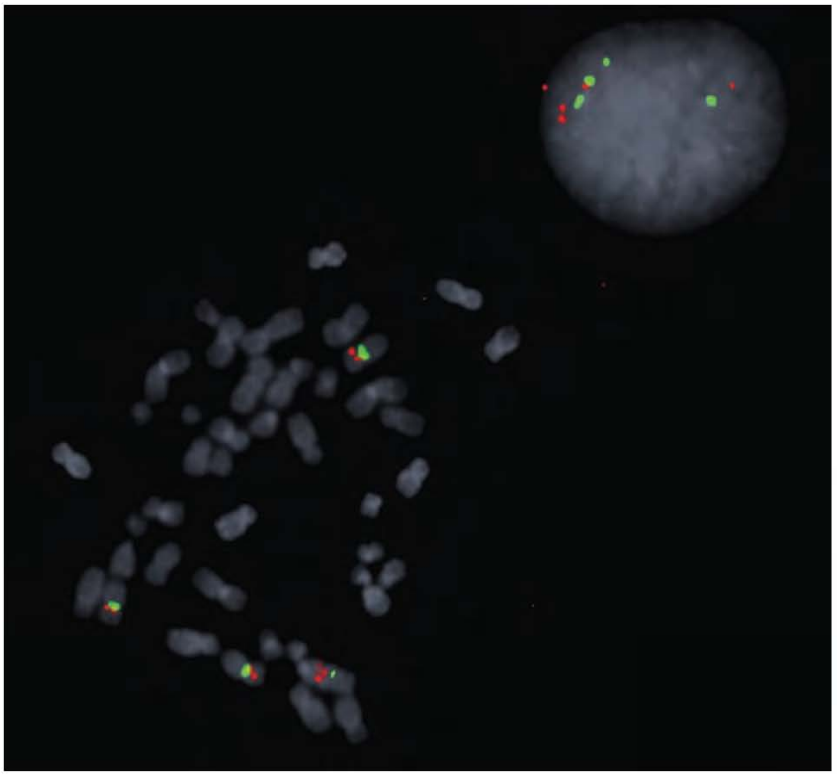

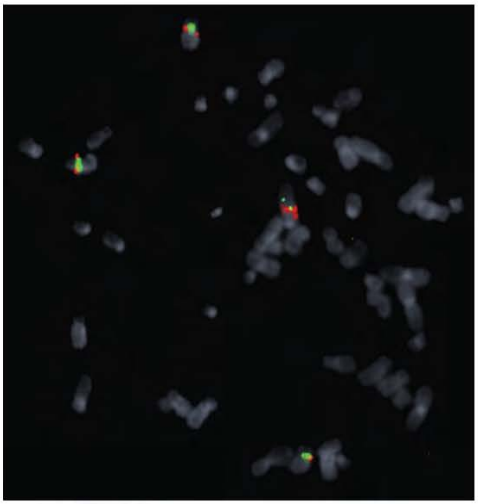

SP14T cells

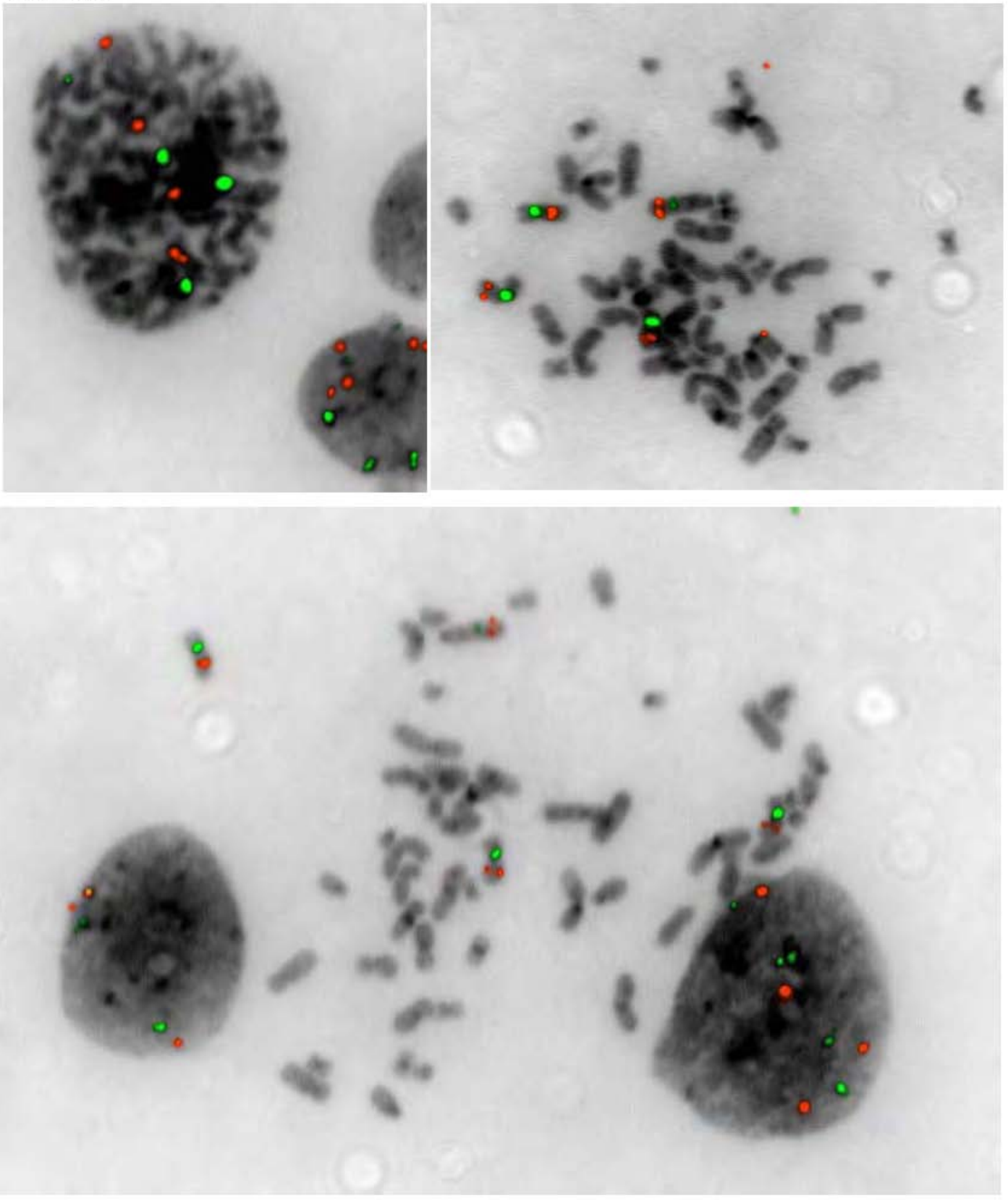

G

Normal control metaphases

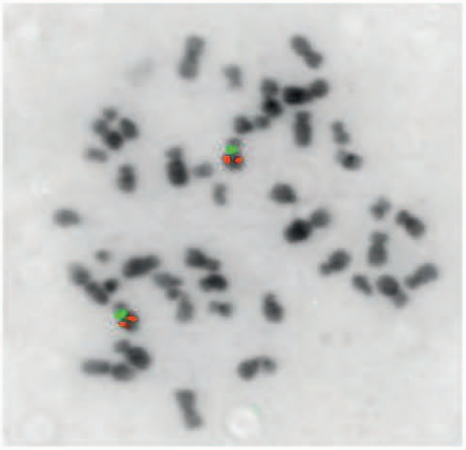

Chr10-CEN(Green)
PTEN (Orange)

SP14SEZ cells

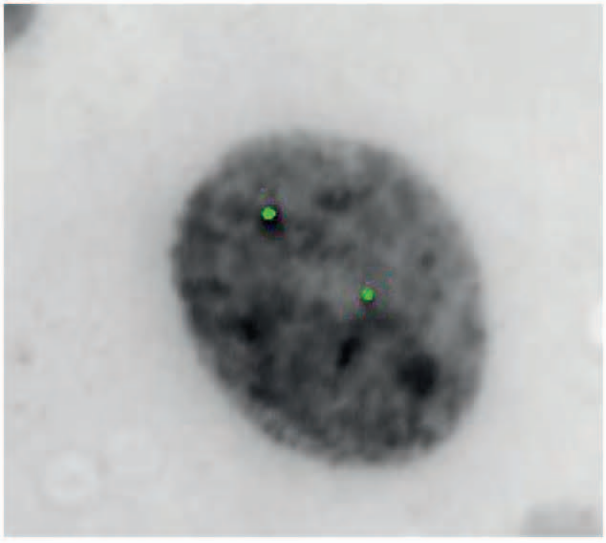

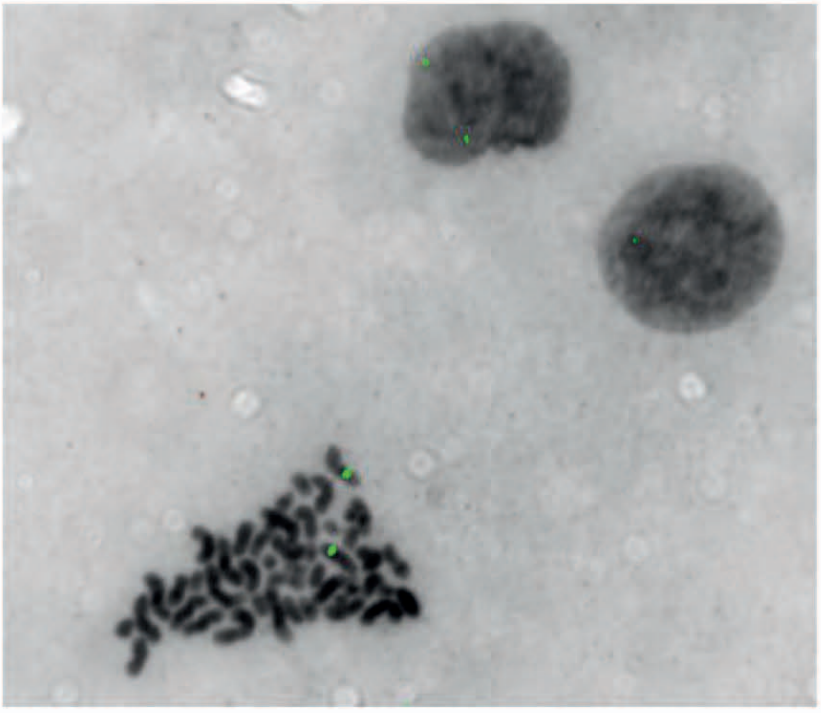

SP14T cells

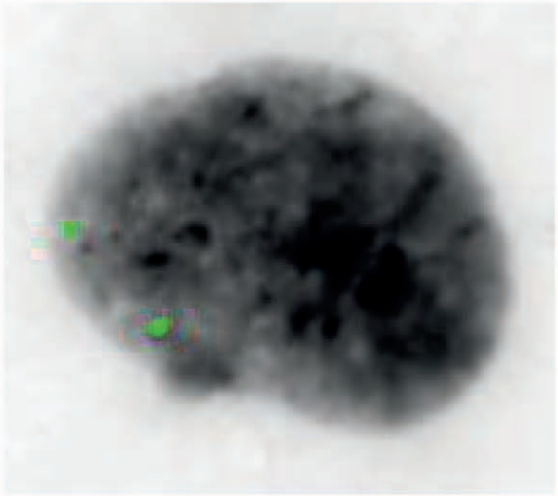

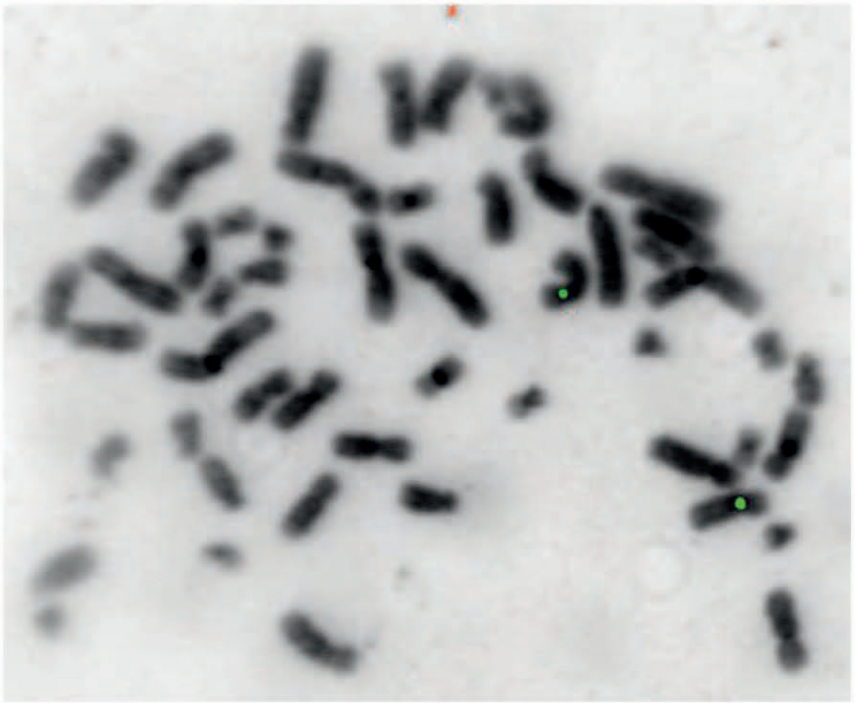

H

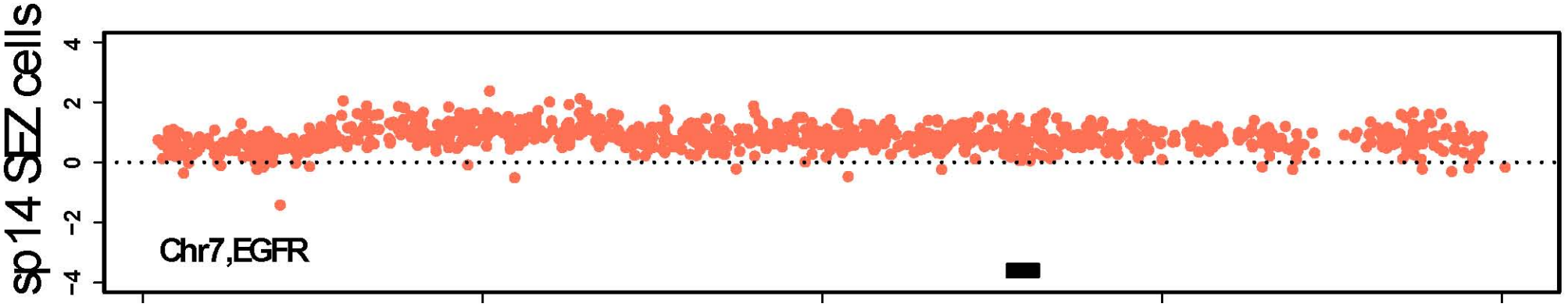
sp14 SEZ cells
4
2
0
−2
−4
Chr7,EGFR

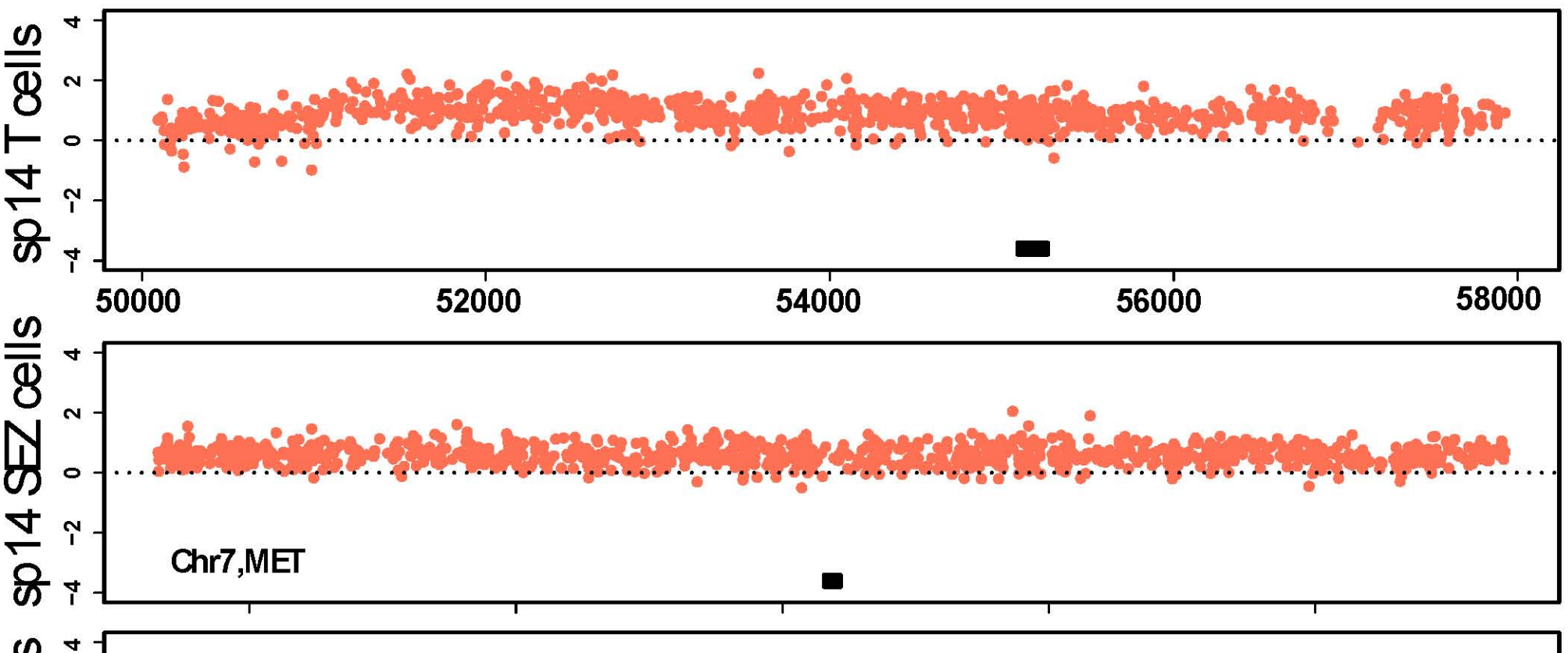
sp14 T cells
4
2
0
−2
−4
50000
52000
54000
56000
58000

sp14 SEZ cells
4
2
0
−2
−4
Chr7,MET
sp14 T cells
112000
114000
116000
118000
120000

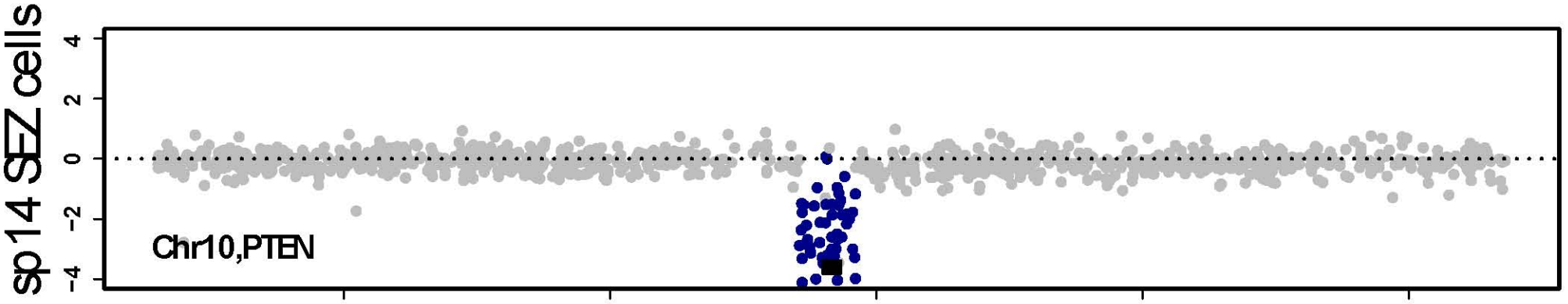
sp14 SEZ cells
4
2
0
−2
−4
Chr10,PTEN

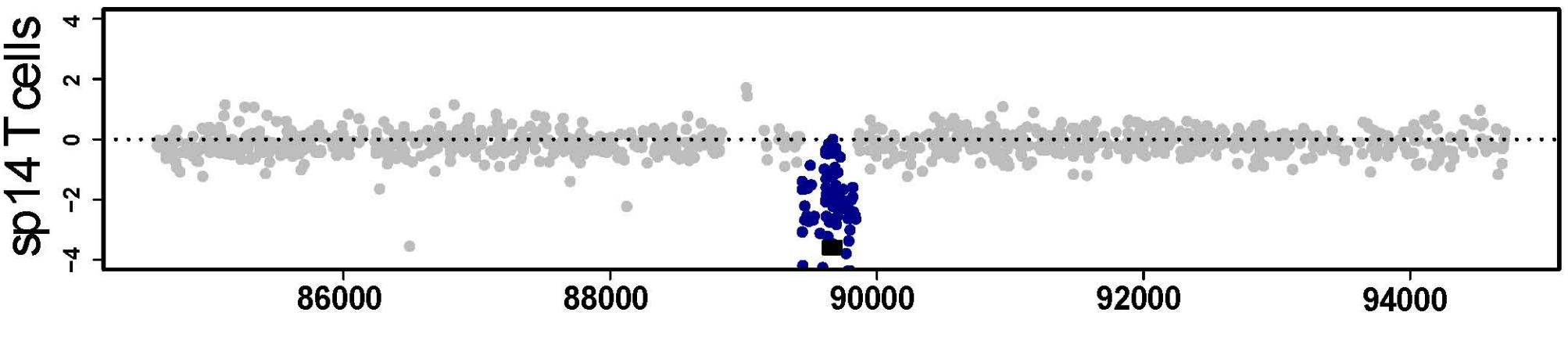
sp14 T cells
4
2
0
−2
−4
86000
88000
90000
92000
94000

Supplementary Figure S6. CNA breakpoints between T and SEZ and the corresponding cells.

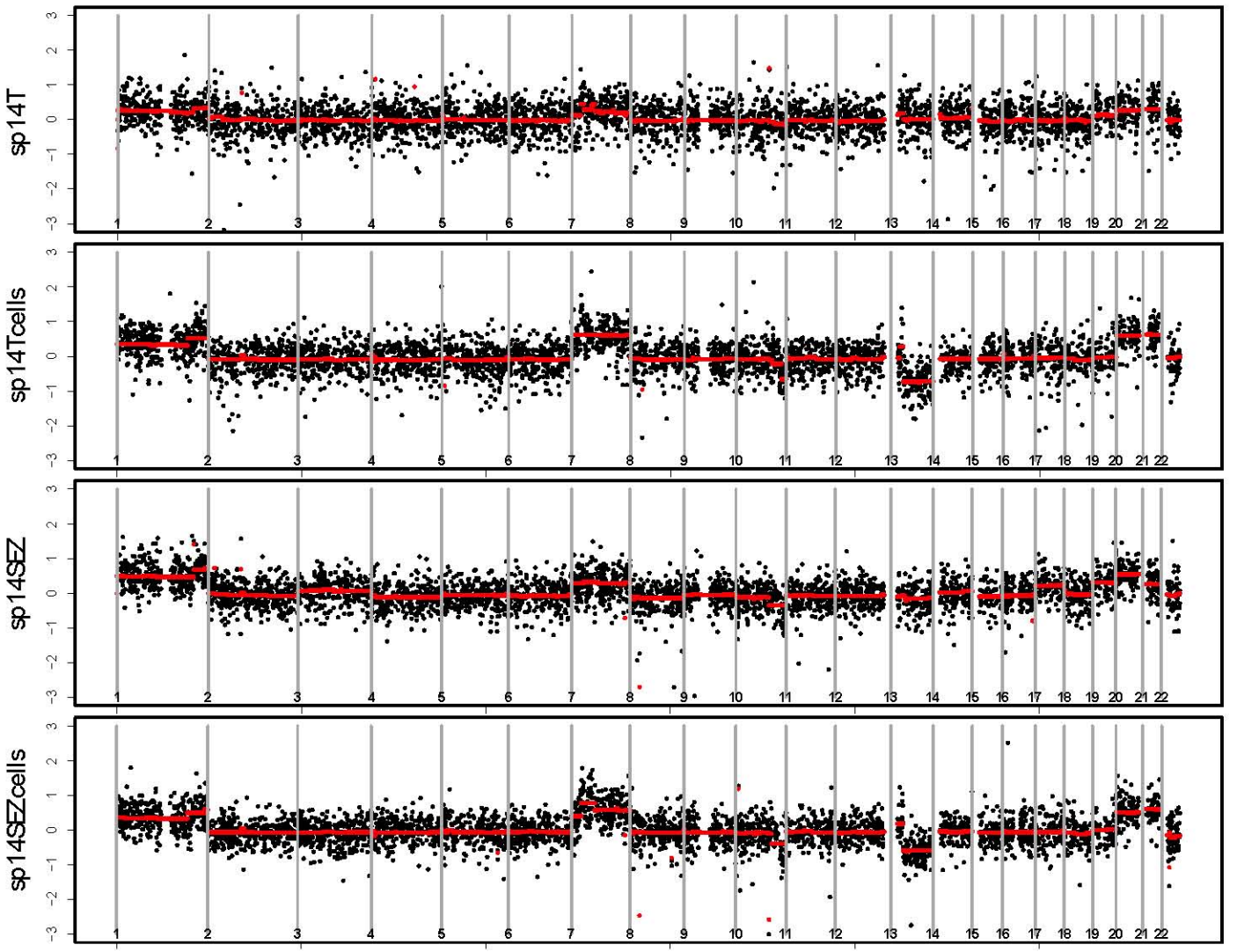

Supplementary Figure S7. Growth curve analysis of TICs from 5 additional GBs.

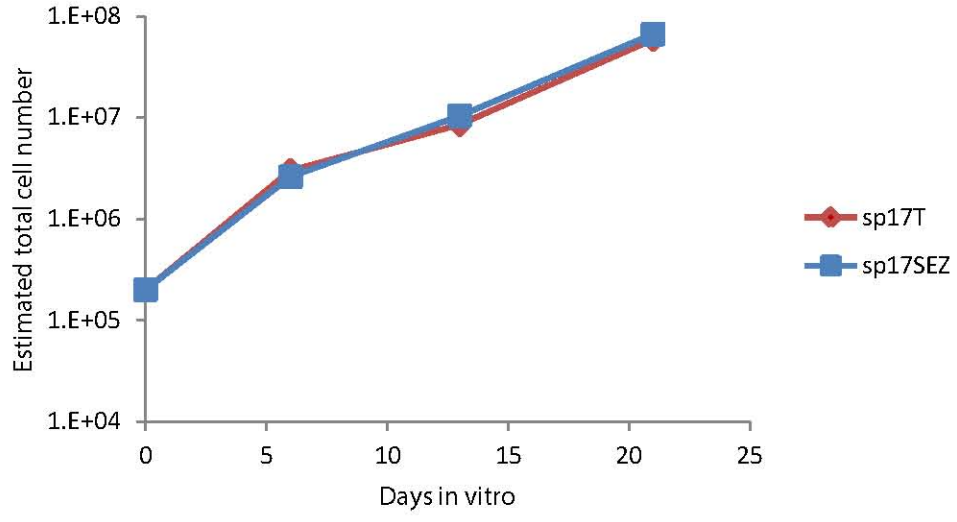

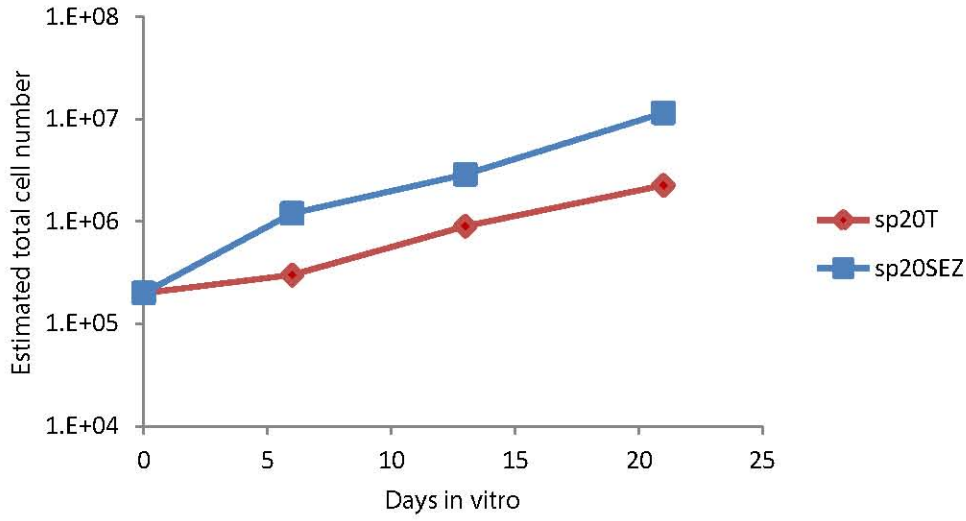

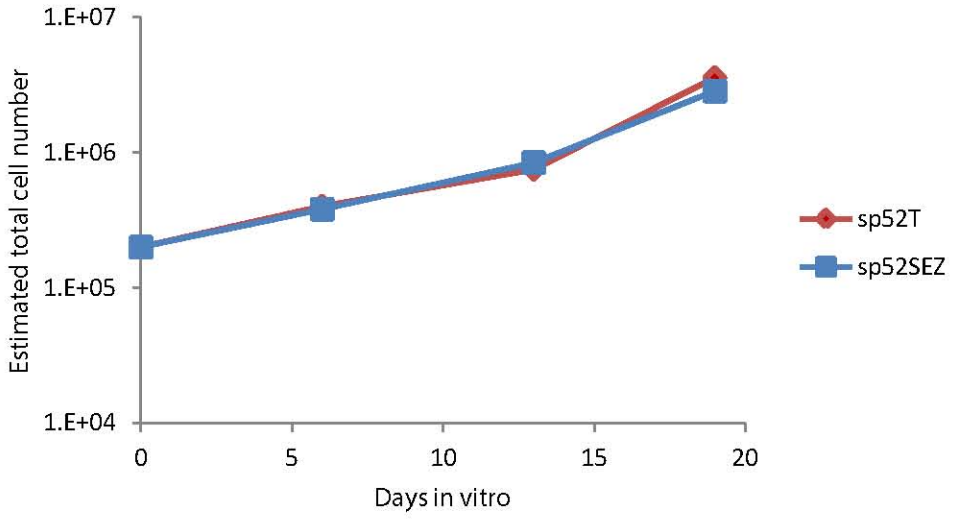

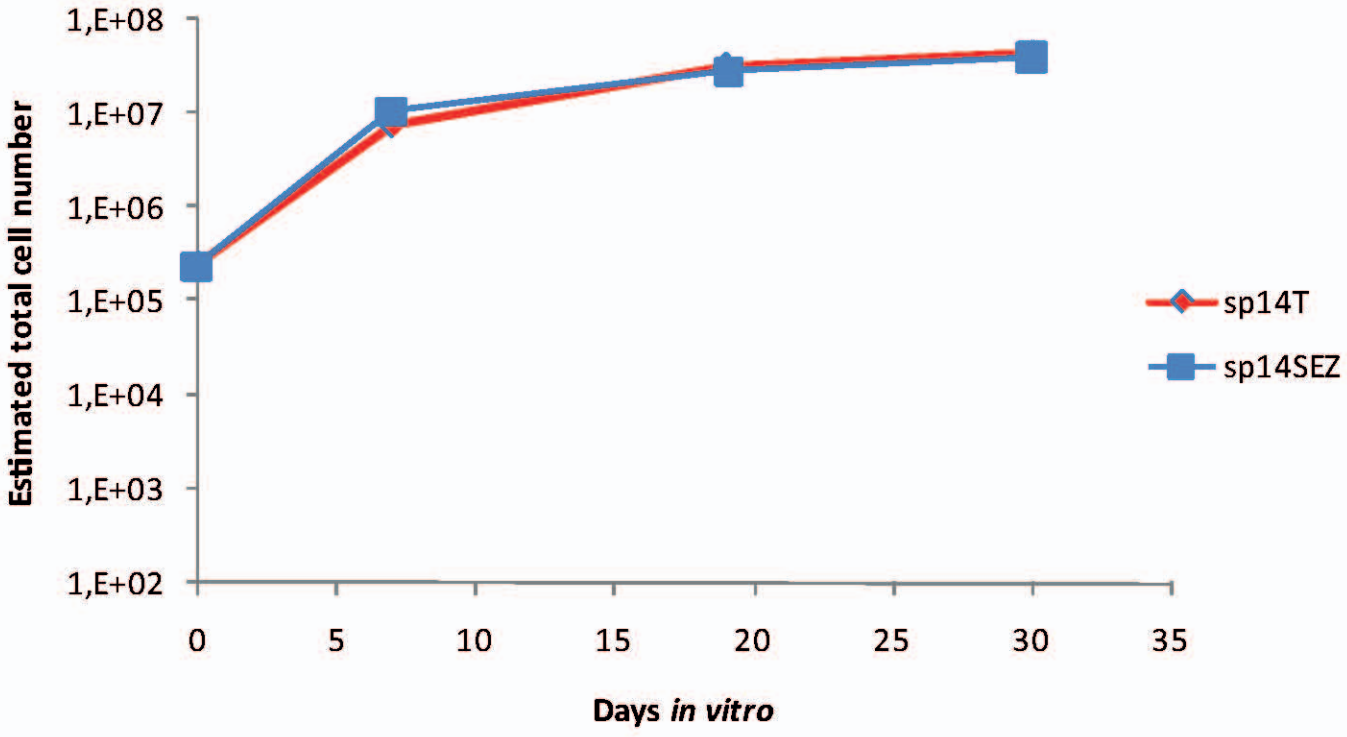
1,E+08
1,E+07
1,E+06
1,E+05
1,E+04
1,E+03
1,E+02
Estimated total cell number
0
5
10
15
20
25
30
35
Days in vitro
sp14T
sp14SEZ

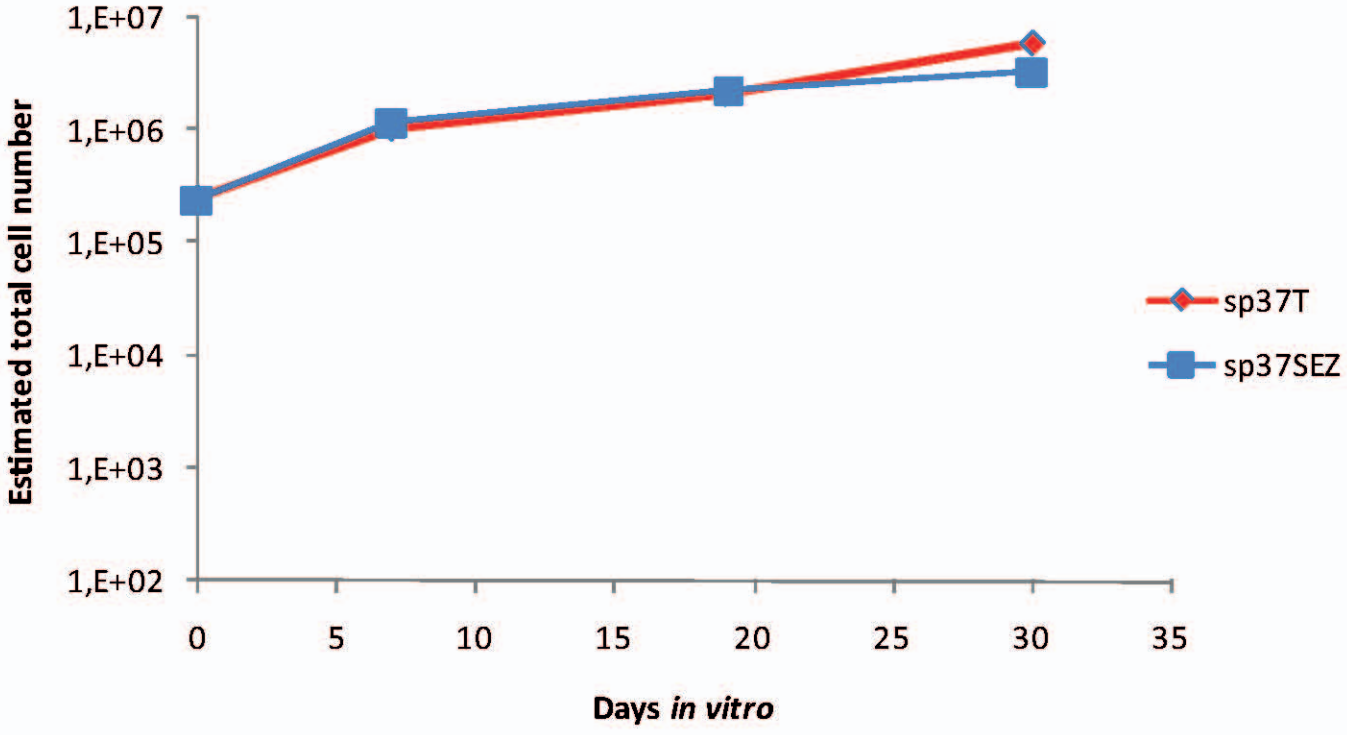
1,E+07
1,E+06
1,E+05
1,E+04
1,E+03
1,E+02
Estimated total cell number
0
5
10
15
20
25
30
35
Days in vitro
sp37T
sp37SEZ

Supplementary Figure S8. Clonogenic index and multipotency of SEZ cells.

Sample	Clonogenic index (%)
T1	16.6±3.9
T2	9.1±2.8
T3	11.5±4.6
SEZ1	14.3±5.7
SEZ2	8.7±3.5
SEZ3	9.3±1.1

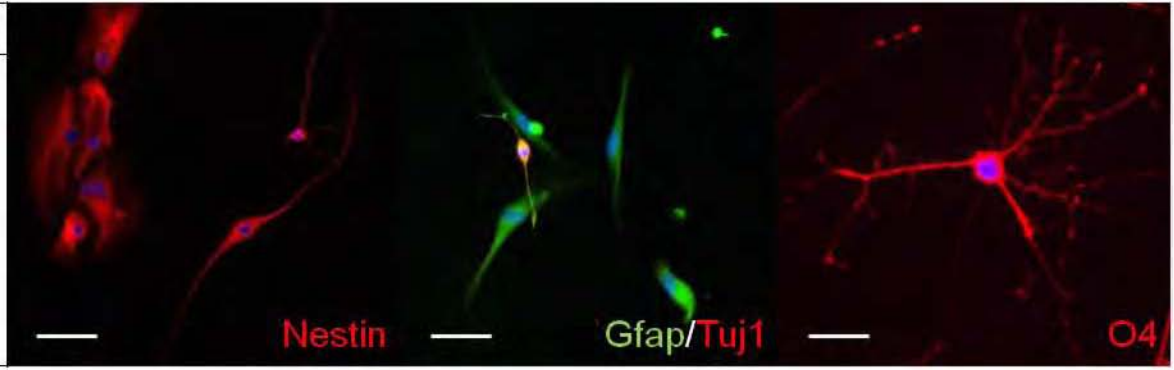

Supplementary Figure S9. Immunofluorescence analysis for "stem cell markers" on T and SEZ cells.

A

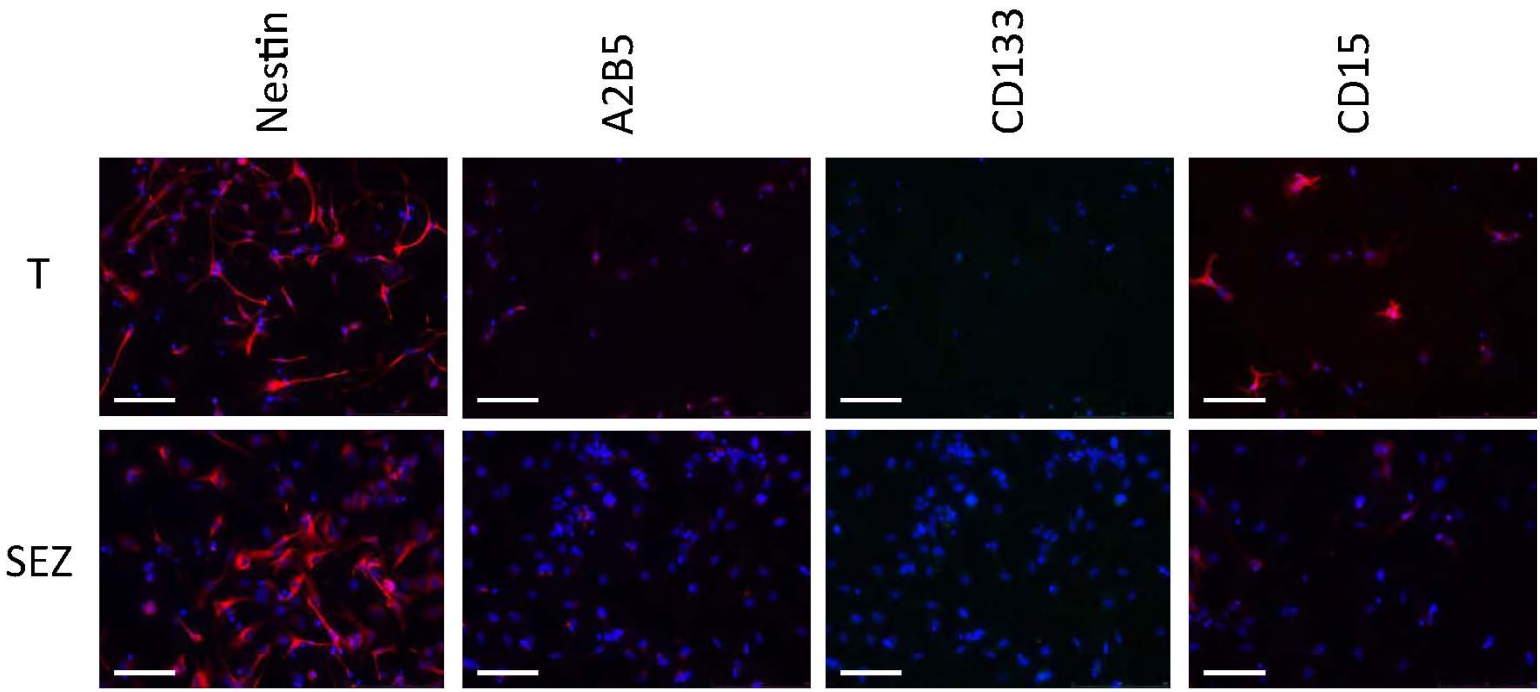

	Nestin-IR cells (%)	A2B5-IR cells (%)	CD133-IR cells (%)	CD15-IR cells (%)
T	67.0±3.7	8.8±1.4	3.2±0.9	4.1±2.2
SEZ	80.3±9.5	negative	negative	2.9±0.6

B

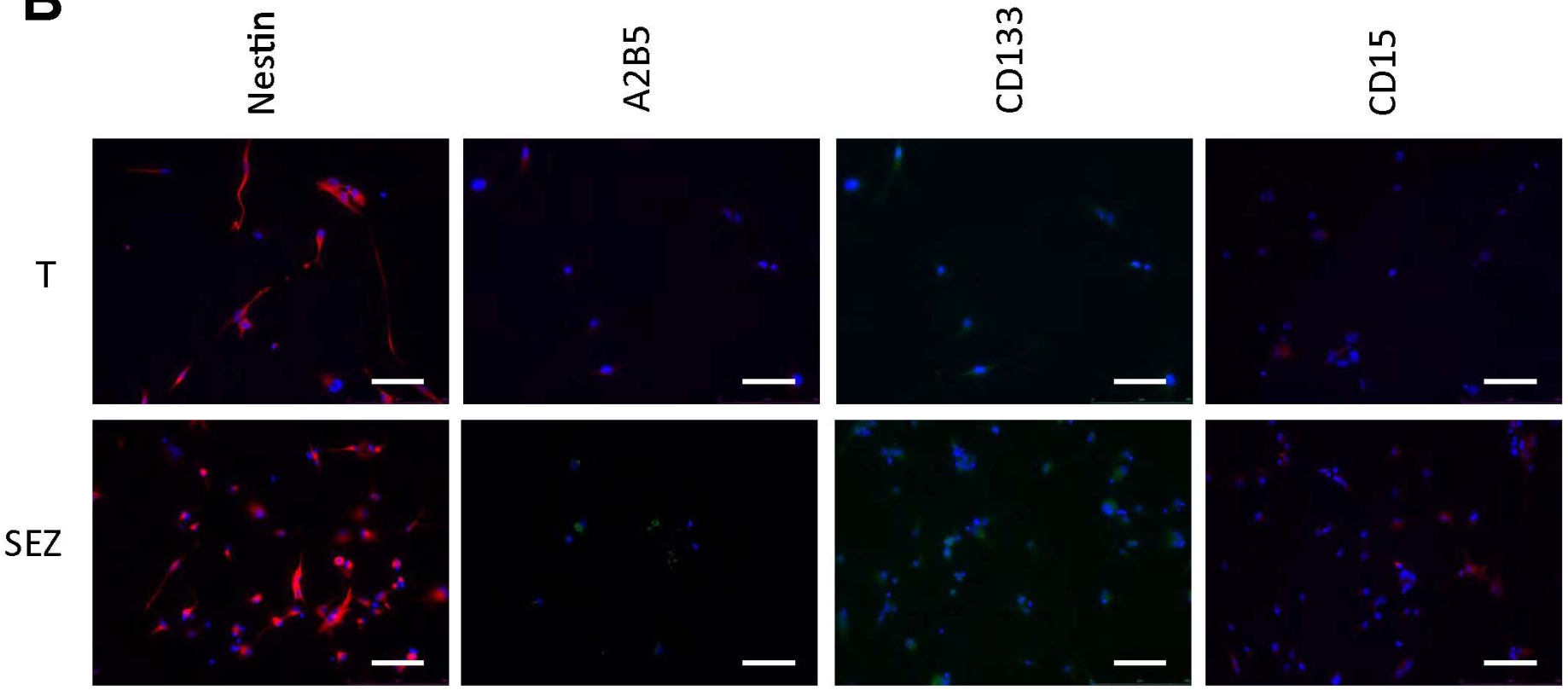

	Nestin-IR cells (%)	A2B5-IR cells (%)	Cd133-IR cells (%)	Cd15-IR cells (%)
T	48.3±2.0	3.9±0.8	negative	negative
SEZ	57.1±4.4	6.1±1.7	negative	1.0±0.5

Supplementary Figure S10. Survival analysis of 5 additional GBs.

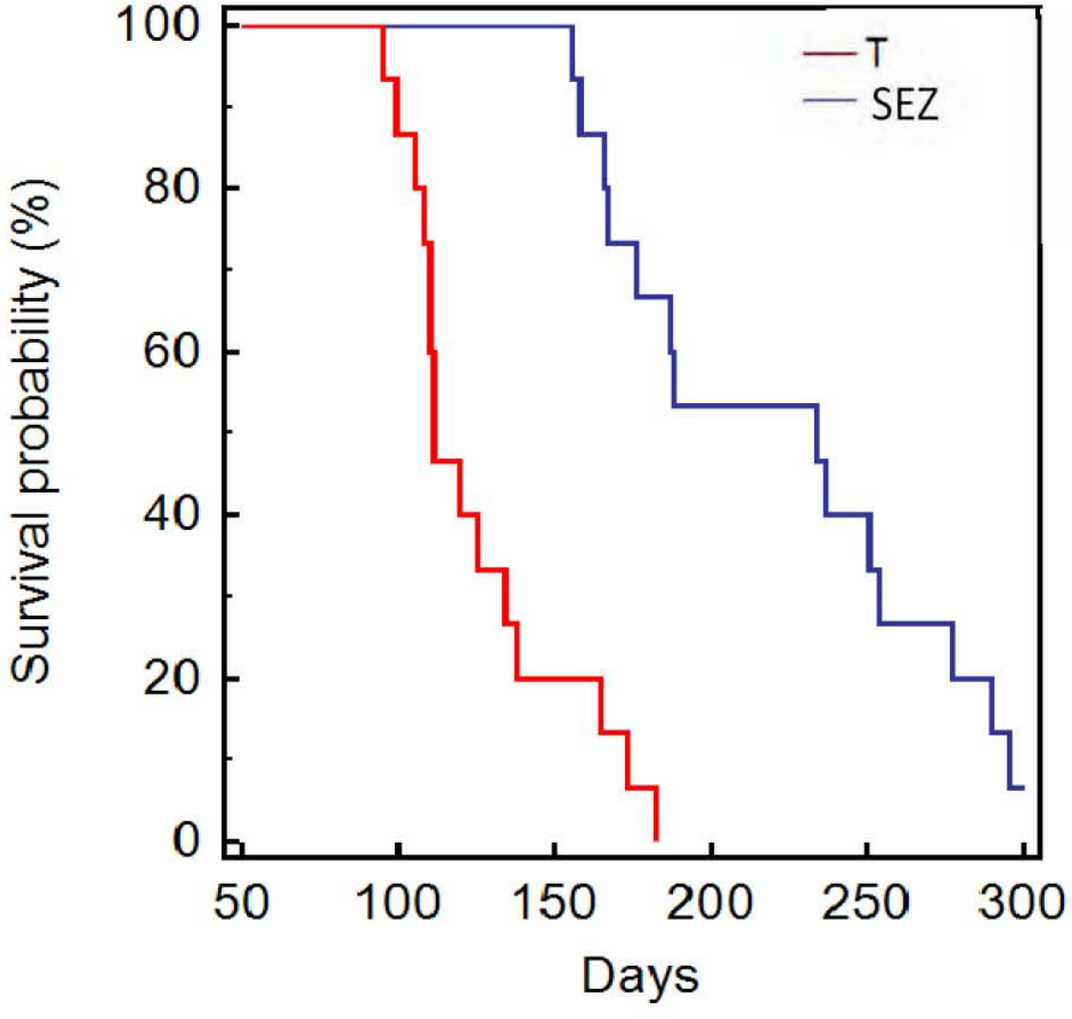

	#tumors/#injections		
	primary cells	briefly cultured cells	ALL
T	6/6	9/9	15/15 (100%)
SEZ	5/6	9/9	14/15 (93%)

Supplementary Figure S11. Analysis of *in vivo* properties of TICs from SEZ.

A

Sample	Tumor formation	Migration to SEZ	Migration to hippocampus	Migration to olfactory bulbs	Migration to cerebellum
SEZ1	yes	no	no	no	no
SEZ2	yes	no	no	no	no
SEZ3	yes	no*	no	no	no

*only contact with the SEZ due to tumor formation

B

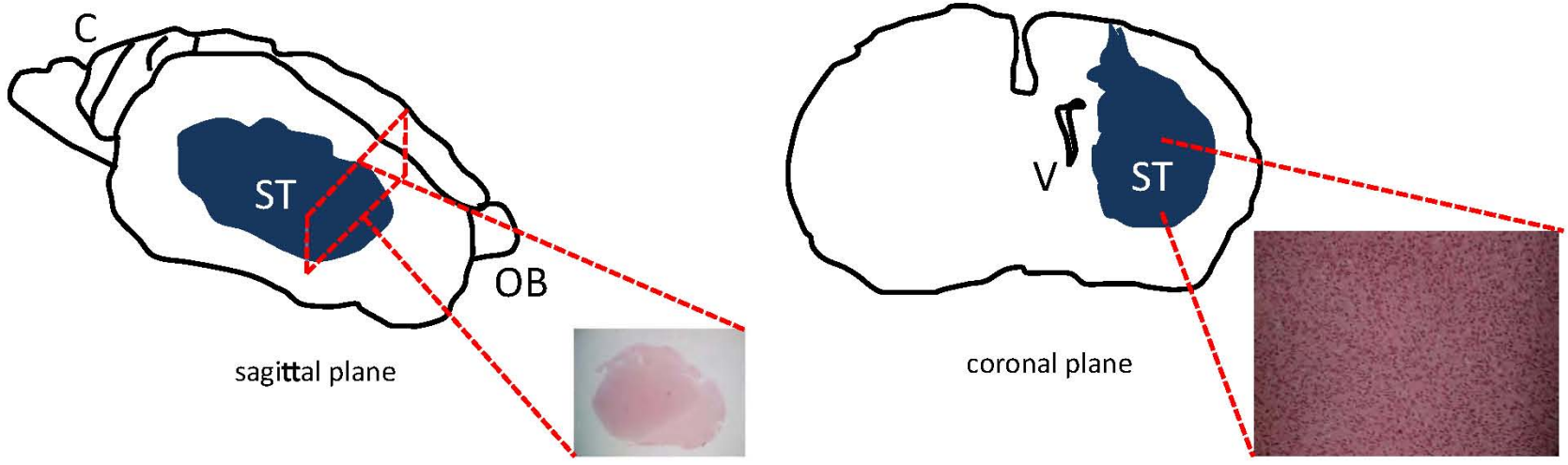

C

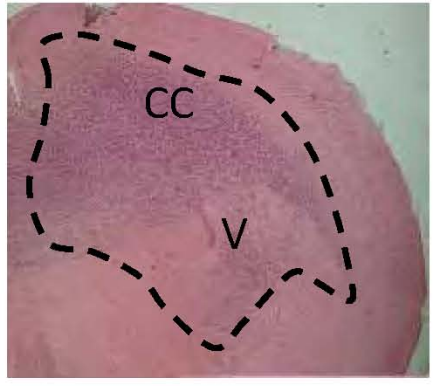

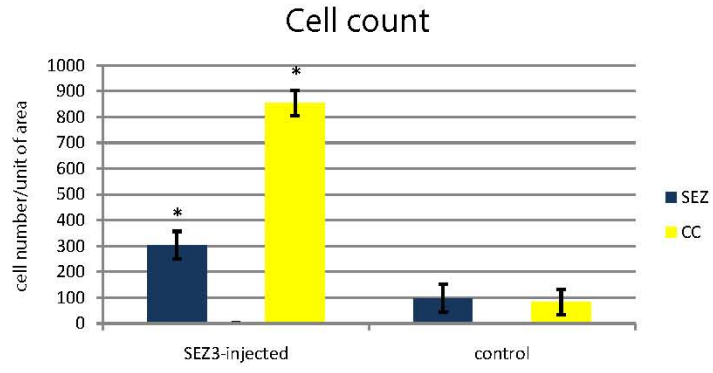

Supplementary Figure S12. BrdU cell proliferation assay of 7 paired TICs using 50μM TMZ.

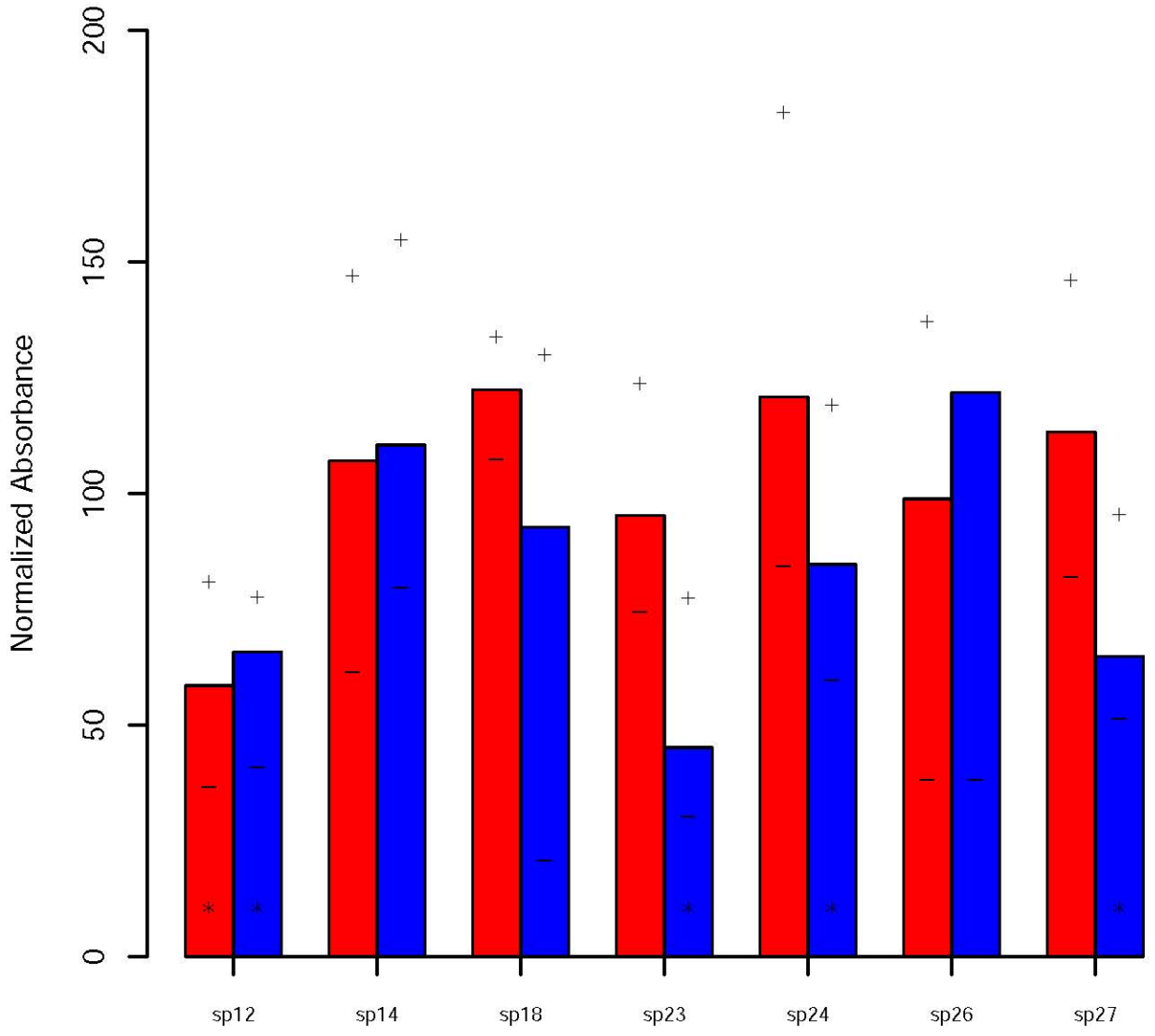

Supplementary Figure S13. BrdU cell proliferation assay of additional 20 TICs for dose escalation analysis with TMZ.

A

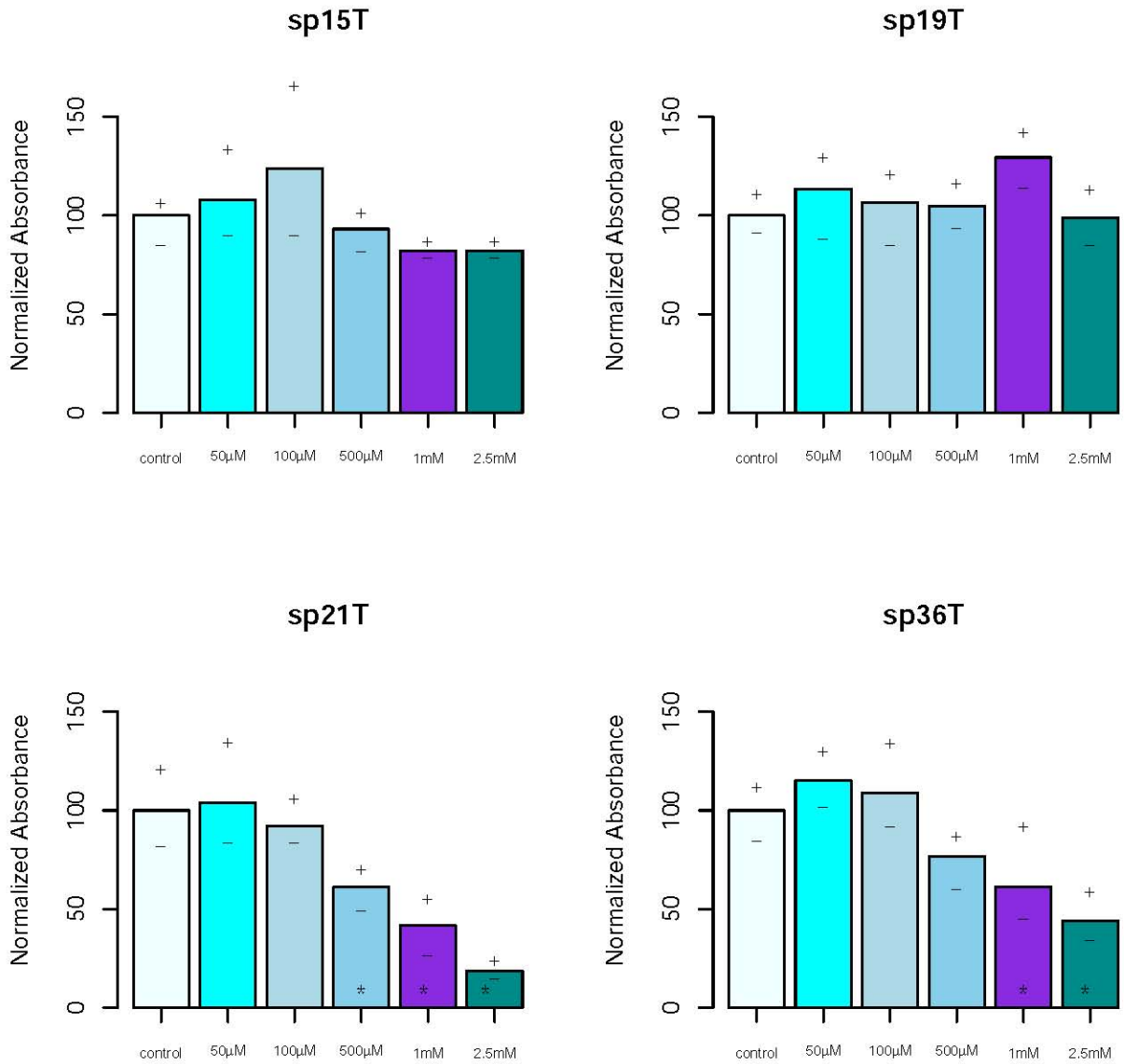

B

TICs									
sp8	sp10	sp15	sp17	sp19	sp21	sp22	sp28	sp31	sp32
sp33	sp34	sp35	sp36	sp40	sp41	sp51	sp55	sp56	sp57

Supplementary Figure S14. BrdU cell proliferation assay of additional 4 paired TICs.

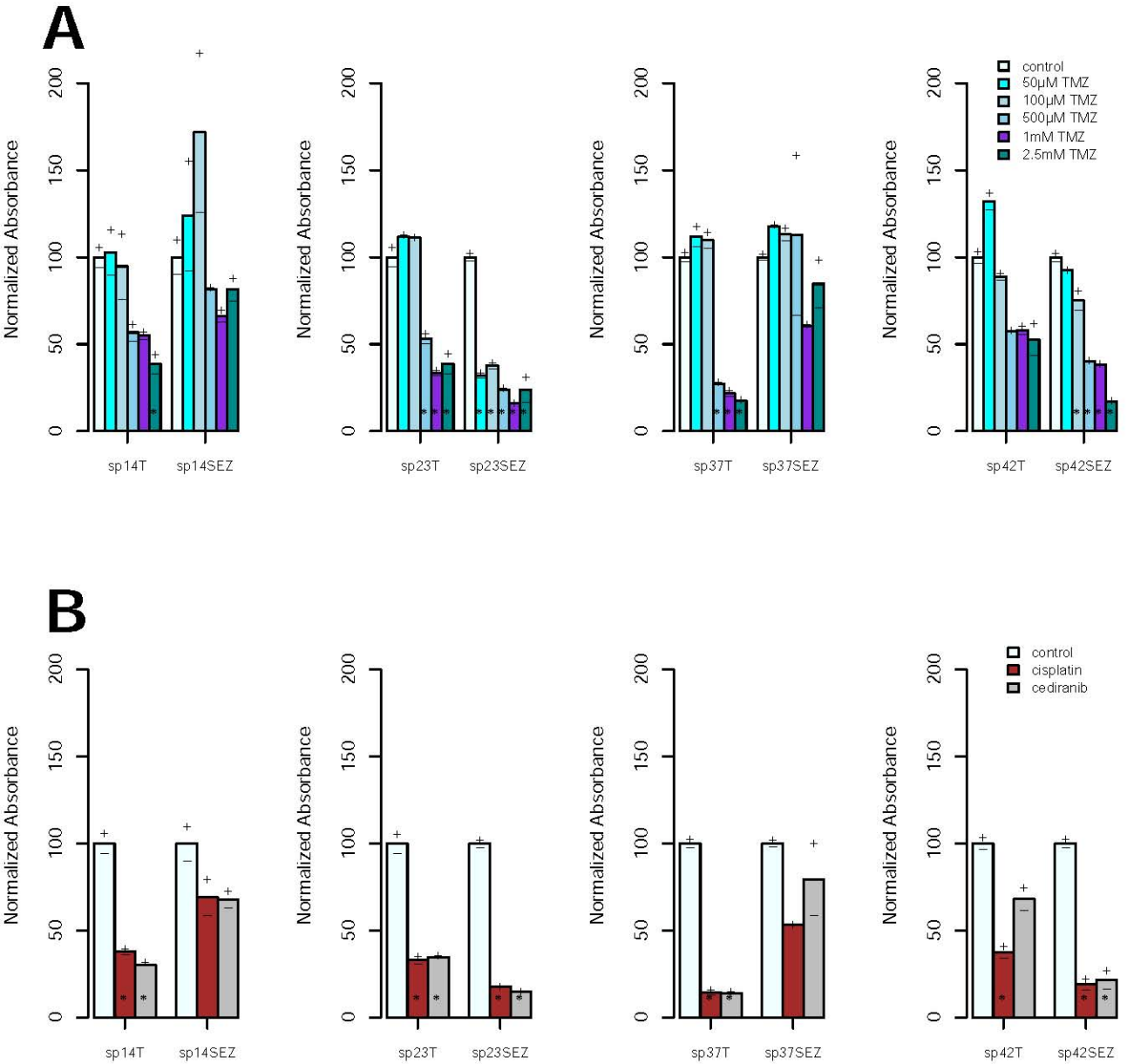

Supplementary Figure S15. MGMT promoter status for T and SEZ of the analyzed 7 paired TICs by PCR.

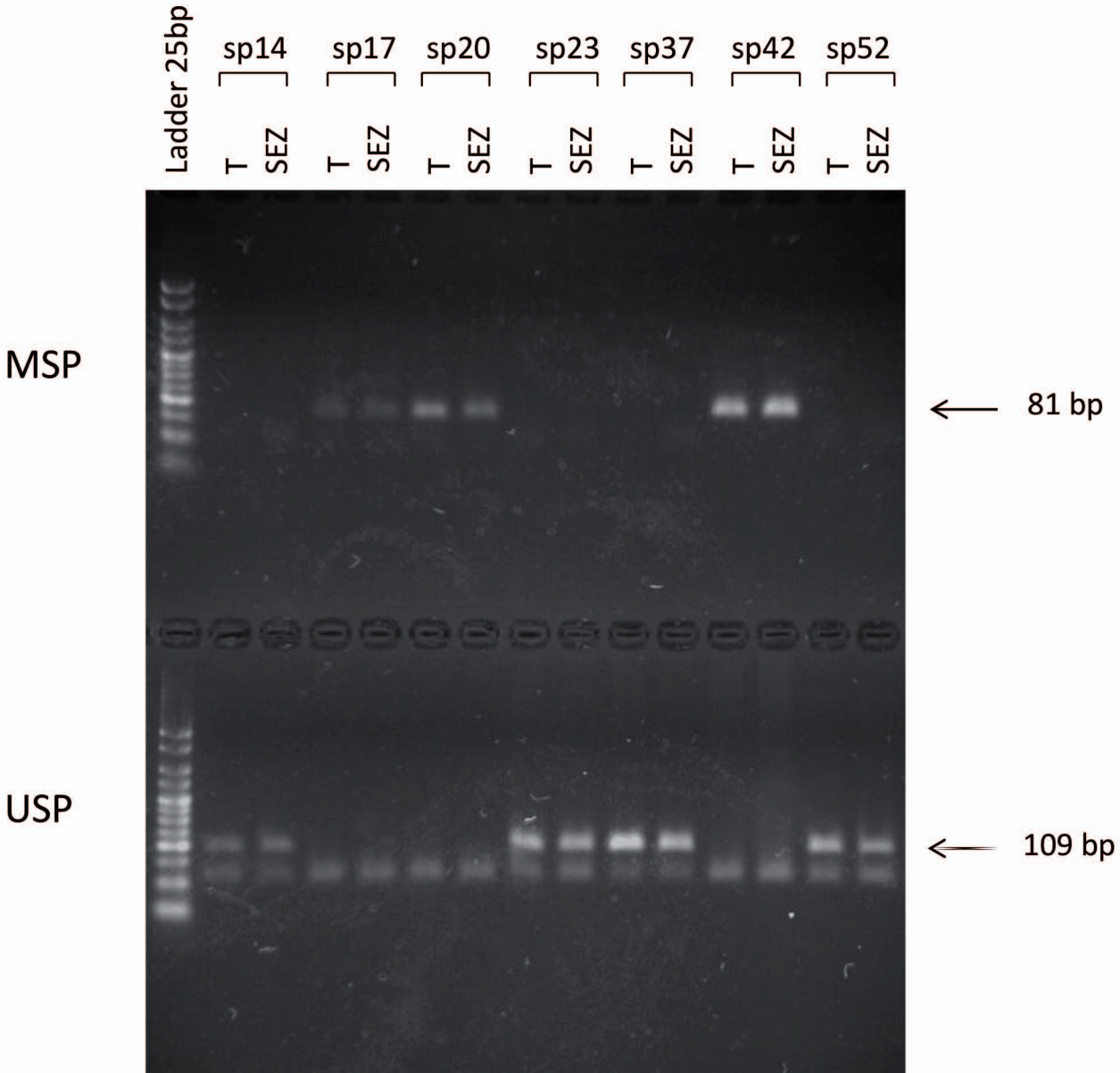

Supplementary Figure S16. Immunofluorescence analysis for Vegfr2 on T and SEZ cells.

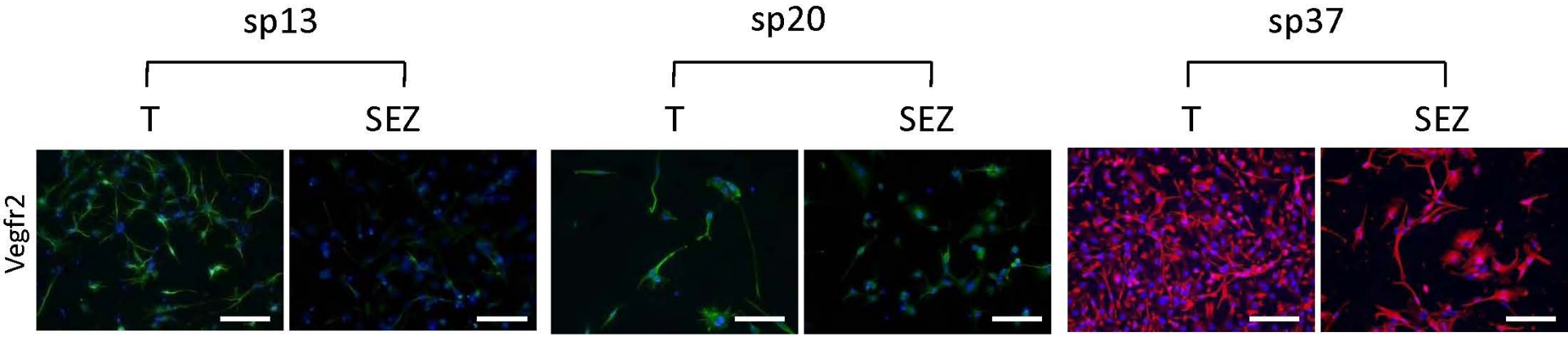

Sample	Compartment	Vegfr2-IR cells (%)
sp13	T	66.1±3.9
	SEZ	47.2±1.4
sp20	T	71.5±2.2
	SEZ	69.8±2.6
sp37	T	91.7±1.1
	SEZ	82.4±5.7

Supplementary Figure S17. BrdU cell proliferation assay of control lines.

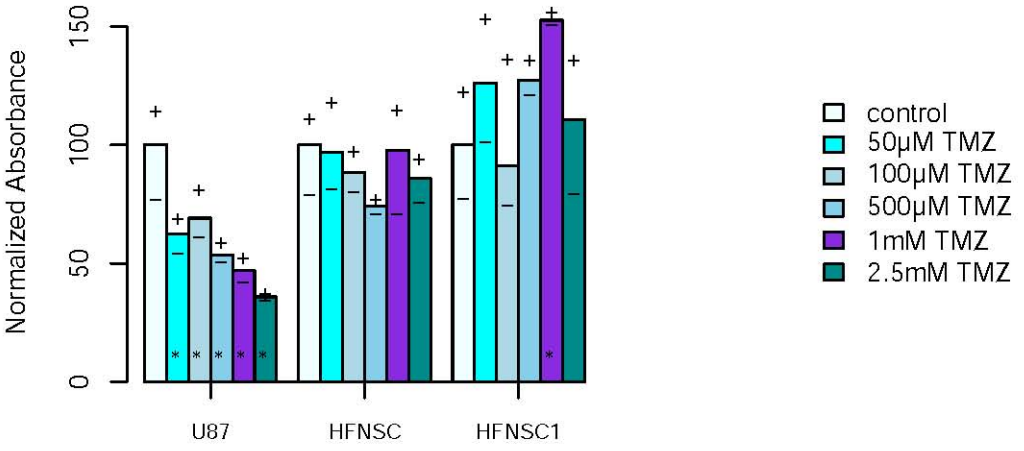

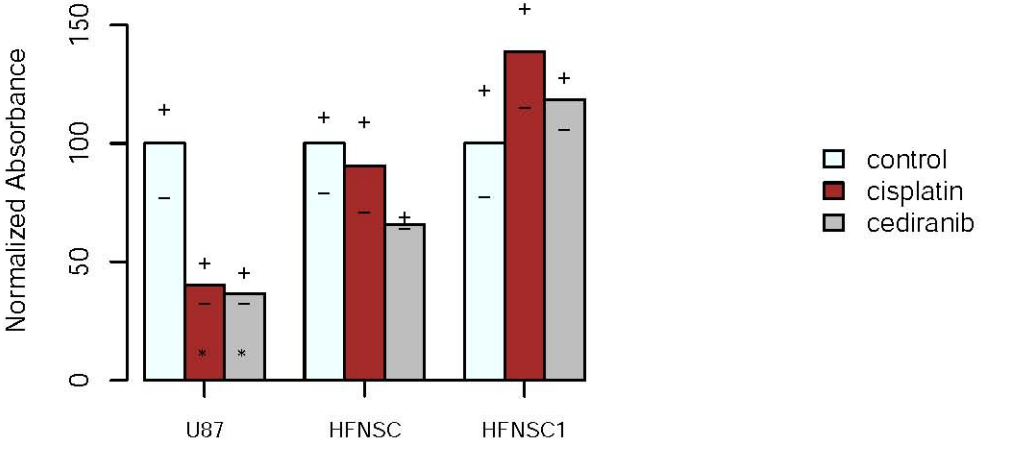

Supplementary Figure S18. A model of residual disease in human GB.

A

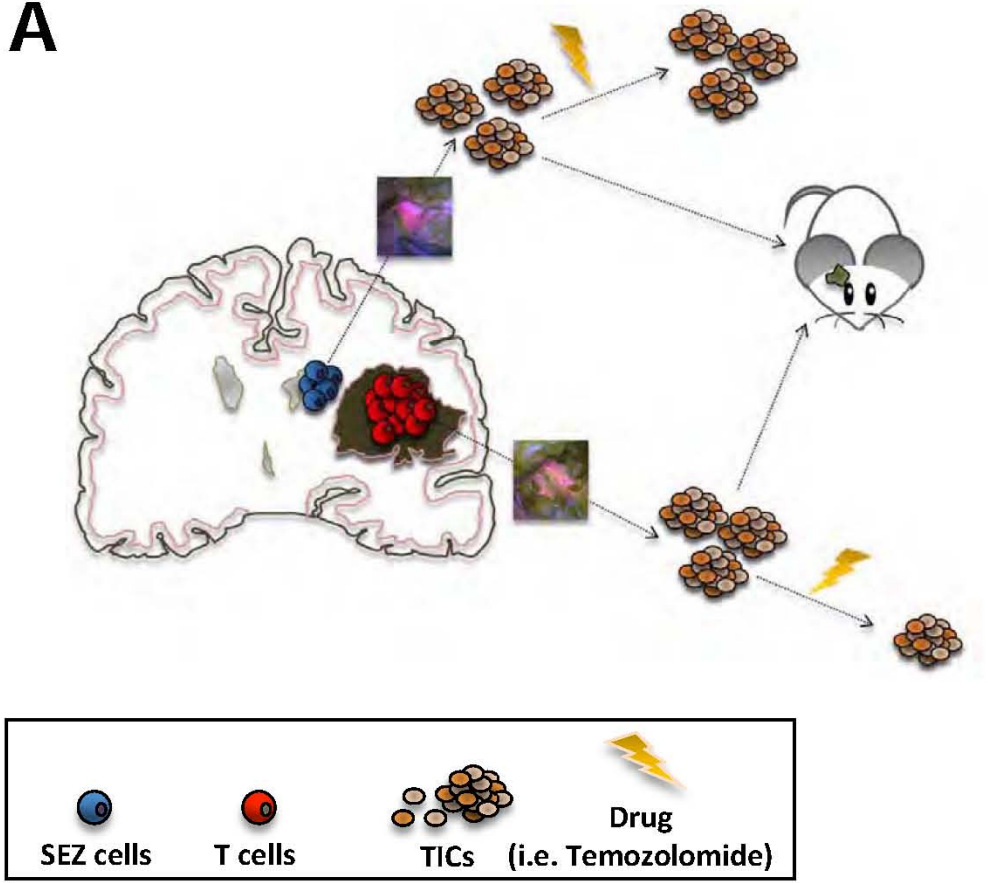

B

		GB COMPARTMENT	
		SEZ	TUMOR MASS
COMPARTMENT CHARACTERISTIC	TISSUE MORPHOLOGY	Proliferation Necrosis **Mitotic activity**	Proliferation Necrosis **Mitotic activity**
	GENOMIC CLASSIFIER	Mesenchymal/ Classical	Proneural/ Neural Mesenchymal/ Classical
	PHYLOGENY	Tumor clone(s)	Expansion of dominant sub-clones
	CELL PHENOTYPE	Self-renewal Tumorigenic	Self-renewal Tumorigenic
	DIFFERENTIAL THERAPEUTIC RESPONSE	YES	YES
	COMPARTMENT FUNCTION	Tumor cell Niche	Aggressive Tumor Growth

Supplementary Figure S19. Growth curve of cells from two SEZ in absence of fluorescence.

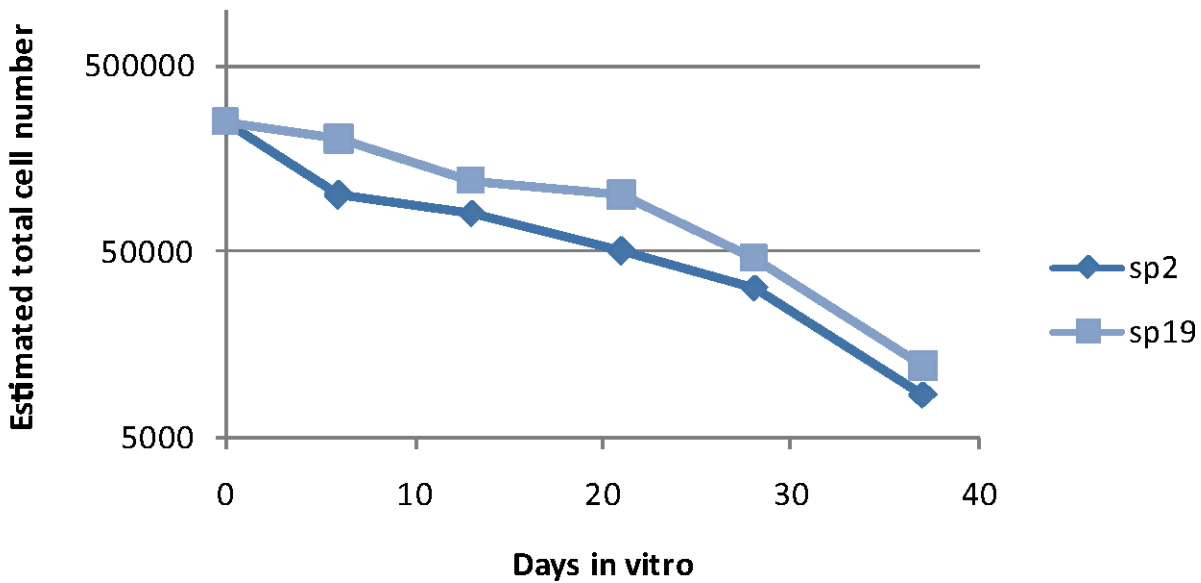

Supplementary Table S1. Histological features of T and SEZ tissues.

Patient	Sample	Necrosis	Tumor score
sp14	T	0	0
	SEZ	0	0
sp37	T	0	0
	SEZ	0	1
sp38	T	1	0
	SEZ	1	0
sp40	T	1	0
	SEZ	0	0
sp41	T	1	1
	SEZ	1	1
sp42	T	0	0
	SEZ	0	0
sp49	T	1	0
	SEZ	1	0
sp52	T	0	0
	SEZ	0	0
sp54	T	1	1
	SEZ	1	0
sp55	T	1	0
	SEZ	1	0
sp56	T	0	1
	SEZ	0	1
sp57	T	0	1
	SEZ	0	1
sp58	T	1	0
	SEZ	1	0
r4	T	0	0
	SEZ	0	0

Supplementary Table S2. Summary of the patients and samples used for the genomic analysis.

A

Patient	Sample	RNA	DNA
sp14	T, SEZ	NO	YES
sp37	T, SEZ	NO	NO
sp38	T, SEZ	NO	NO
sp40	T, SEZ	NO	NO
sp41	T, SEZ	YES	NO
sp42	T, SEZ	YES	YES
sp49	T, SEZ	YES	YES
sp52	T, SEZ	YES	YES
sp54	T, SEZ	YES	YES
sp55	T, SEZ	YES	YES
sp56	T, SEZ	YES	YES
sp57	T, SEZ	YES	NO
sp58	T, SEZ	NO	YES
r4	T, SEZ	YES	NO

B

Patient	Age at Diagnosis	Sex	Performance Status	Treatment at surgery	Treatment post surgery
sp14	79	F	1	5ALA only	None
sp41	61	M	0	5ALA only	ChemoRT
sp42	61	M	2	5ALA only	WBRT
sp49	62	M	0	5ALA only	SCRT
sp52	64	M	1	5ALA only	None
sp54	58	M	0	5ALA + Gliadel	ChemoRT
sp55	55	M	2	5ALA only	SCRT
sp56	60	M	2	5ALA only	None
sp57	65	F	1	5ALA + Gliadel	ChemoRT
sp58	68	F	1	5ALA + Gliadel	None
r4	69	M	0	5ALA only	SCRT

Supplementary Table S3. Gene ontology terms bearing at least one differentially expressed gene between SEZ and T.

GO identifier	GO category	Go term
GO 0003676	F	nucleic acid binding
GO 0003723	F	RNA binding
GO 0005509	F	calcium ion binding
GO 0005515	F	protein binding
GO 0005524	F	ATP binding
GO 0005576	C	extracellular region
GO 0005622	C	intracellular
GO 0005634	C	nucleus
GO 0005730	C	nucleolus
GO 0005737	C	cytoplasm
GO 0005739	C	mitochondrion
GO 0005829	C	cytosol
GO 0005840	C	ribosome
GO 0005856	C	cytoskeleton
GO 0005874	C	microtubule
GO 0005882	C	intermediate filament
GO 0005886	C	plasma membrane
GO 0005887	C	integral component of plasma membrane
GO 0005930	C	axoneme
GO 0006351	P	transcription, DNA-templated
GO 0006412	P	translation
GO 0006508	P	proteolysis
GO 0007155	P	cell adhesion
GO 0007165	P	signal transduction
GO 0007275	P	multicellular organismal development
GO 0007399	P	nervous system development
GO 0008150	P	biological_process
GO 0008168	F	methyltransferase activity
GO:0008270	F	zinc ion binding
GO 0015031	P	protein transport
GO 0016020	C	membrane
GO 0016021	C	integral component of membrane
GO 0016032	P	viral process
GO 0016567	P	protein ubiquitination
GO 0016568	P	chromatin modification
GO 0016592	C	mediator complex
GO 0016607	C	nuclear speck
GO 0016746	F	transferase activity, transferring acyl groups
GO 0016787	F	hydrolase activity
GO 0016874	F	ligase activity
GO 0019048	P	modulation by virus of host morphology or physiology
GO 0020037	F	heme binding
GO 0030036	P	actin cytoskeleton organization
GO 0030054	C	cell junction
GO 0030154	P	cell differentiation
GO 0030162	P	regulation of proteolysis
GO 0030170	F	pyridoxal phosphate binding
GO 0030198	P	extracellular matrix organization
GO 0030246	F	carbohydrate binding
GO 0031225	C	anchored component of membrane
GO 0031418	F	L-ascorbic acid binding
GO 0031424	P	keratinization
GO 0031625	F	ubiquitin protein ligase binding
GO 0031965	C	nuclear membrane
GO 0032312	P	regulation of ARF GTPase activity
GO 0032467	P	positive regulation of cytokinesis
GO 0035023	P	regulation of Rho protein signal transduction
GO 0035091	F	phosphatidylinositol binding
GO 0035556	P	intracellular signal transduction
GO 0042383	C	sarcolemma
GO 0042384	P	cilium assembly
GO 0042742	P	defense response to bacterium
GO 0042787	P	protein ubiquitination involved in ubiquitin-dependent protein catabolic process
GO 0042802	F	identical protein binding
GO 0042803	F	protein homodimerization activity
GO 0042981	P	regulation of apoptotic process
GO 0043025	C	neuronal cell body
GO 0043066	P	negative regulation of apoptotic process

GO identifier	GO category	Go term
GO 0043085	P	positive regulation of catalytic activity
GO 0043231	C	intracellular membrane-bounded organelle
GO 0043547	P	positive regulation of GTPase activity
GO 0043565	F	sequence-specific DNA binding
GO 0043687	P	post-translational protein modification
GO 0044267	P	cellular protein metabolic process
GO 0044281	P	small molecule metabolic process
GO 0045087	P	innate immune response
GO 0045095	C	keratin filament
GO 0045202	C	synapse
GO 0045211	C	postsynaptic membrane
GO 0045944	P	positive regulation of transcription from RNA polymerase II promoter
GO 0046474	P	glycerophospholipid biosynthetic process
GO 0046872	F	metal ion binding
GO 0047485	F	protein N-terminus binding
GO 0048015	P	phosphatidylinositol-mediated signaling
GO 0048306	F	calcium-dependent protein binding
GO 0048387	P	negative regulation of retinoic acid receptor signaling pathway
GO 0048471	C	perinuclear region of cytoplasm
GO 0050434	P	positive regulation of viral transcription
GO 0050776	P	regulation of immune response
GO 0050796	P	regulation of insulin secretion
GO 0050873	P	brown fat cell differentiation
GO 0050900	P	leukocyte migration
GO 0050911	P	detection of chemical stimulus involved in sensory perception of smell
GO 0051015	F	actin filament binding
GO 0051028	P	mRNA transport
GO 0051056	P	regulation of small GTPase mediated signal transduction
GO 0051082	F	unfolded protein binding
GO 0051090	P	regulation of sequence-specific DNA binding transcription factor activity
GO 0051219	F	phosphoprotein binding
GO 0051260	P	protein homooligomerization
GO 0051287	F	NAD binding
GO 0051289	P	protein homotetramerization
GO 0051301	P	cell division
GO 0051539	F	4 iron, 4 sulfur cluster binding
GO 0051592	P	response to calcium ion
GO 0051607	P	defense response to virus
GO 0055072	P	iron ion homeostasis
GO 0055085	P	transmembrane transport
GO 0055114	P	oxidation-reduction process
GO 0060021	P	palate development
GO 0060041	P	retina development in camera-type eye
GO 0060070	P	canonical Wnt signaling pathway
GO 0060271	P	cilium morphogenesis
GO 0060397	P	JAK-STAT cascade involved in growth hormone signaling pathway
GO 0070059	P	intrinsic apoptotic signaling pathway in response to endoplasmic reticulum stress
GO 0070062	C	extracellular vesicular exosome
GO 0070098	P	chemokine-mediated signaling pathway
GO 0070328	P	triglyceride homeostasis
GO 0070374	P	positive regulation of ERK1 and ERK2 cascade
GO 0070830	P	tight junction assembly
GO 0071013	C	catalytic step 2 spliceosome
GO 0071108	P	protein K48-linked deubiquitination
GO 0071222	P	cellular response to lipopolysaccharide
GO 0071230	P	cellular response to amino acid stimulus
GO 0071277	P	cellular response to calcium ion
GO 0071300	P	cellular response to retinoic acid
GO 0071310	P	cellular response to organic substance
GO 0071339	C	MLL1 complex
GO 0071526	P	semaphorin-plexin signaling pathway
GO 0071773	P	cellular response to BMP stimulus
GO 0071889	F	14-3-3 protein binding
GO 0072659	P	protein localization to plasma membrane
GO 0090190	P	positive regulation of branching involved in ureteric bud morphogenesis
GO 0097110	F	scaffold protein binding
GO:2001244	P	positive regulation of intrinsic apoptotic signaling pathway

Supplementary Table S4. MGMT methylation level using pyrosequencing.

Patient	average % methylation for CpG_74-78 (Quillien *et al*)	Result based on paper by (Quillien *et al*) cut off = 8%
sp13	**73,9**	methylated
sp14	**1,5**	unmethylated
sp17	**9,9**	methylated
sp20	**12,0**	methylated
sp23	**1,1**	unmethylated
sp37	**2,1**	unmethylated
sp41	**1,2**	unmethylated
sp42	**1,3**	unmethylated
sp49	**2,4**	unmethylated
sp52	**1,4**	unmethylated
sp54	**17,6**	methylated
sp55	**1,3**	unmethylated
sp56	**1,3**	unmethylated
sp57	**1,2**	unmethylated
sp58	**45,0**	methylated
r4	**20,2**	methylated

Supplementary Table S5. Summary of the survival of 8 GB patients and response to drugs by TICs from T and SEZ.

Patient	Overall survival	MGMT methylation status	TMZ response	Cisplatin/Cediranib response	Comments
sp13	159	m	y (SEZ only)	y (SEZ only)	
sp14	51	u	n	y (T only)	Palliative care
sp17	351	m	y	y	
sp20	352	m	y (T only)	y (T only)	
sp23	879	u	y	y	
sp37	122	u	y (T only)	y (T only)	PE post-op stopped Rx
sp42	190	u	y (SEZ only)	y (T only to Cisplatin, SEZ to both)	Rapid disease progression
sp52	27	u	n	y (SEZ only)	Rapid disease progression

Supplementary Table S6. Expression of PDGF and VEGF receptors in T and SEZ.

Tyr-kinases	Gene expression
	T-SEZ
PDGFRA	No significant difference
PDGFRB	No significant difference
VEGFR2	No significant difference